Summer 8-7-2021

Development Of A Combined Feedforward-Feedback Quality Control System For Extended-Release Granules Using A Quality By Design Approach

Yuxiang Zhao

DEVELOPMENT OF A COMBINED FEEDFORWARD-FEEDBACK QUALITY CONTROL SYSTEM FOR EXTENDED-RELEASE GRANULES USING A QUALITY BY DESIGN APPROACH

A Dissertation

Submitted to the Graduate School of Pharmaceutical Sciences

Duquesne University

In partial fulfillment of the requirements for

the degree of Doctor of Philosophy

By

Yuxiang Zhao

August 2021

DEVELOPMENT OF A COMBINED FEEDFORWARD-FEEDBACK QUALITY CONTROL SYSTEM FOR EXTENDED-RELEASE GRANULES USING A QUALITY BY DESIGN APPROACH

By

Yuxiang Zhao

Approved May 20, 2021

_____ Carl A. Anderson, Ph.D. Associate Professor of Pharmaceutics, Assistant Dean for Graduate Programs and Research, (Committee Chair).	_____ James K. Drennen, III, Ph.D. Associate Professor of Pharmaceutics, Interim Dean, School of Pharmacy, (Committee Member).
_____ Peter L.D. Wildfong, Ph.D. Associate Professor of Pharmaceutics, Graduate School of Pharmaceutical Sciences, (Committee Member)	_____ Ira S. Buckner, Ph.D. Associate Professor of Pharmaceutics, Graduate School of Pharmaceutical Sciences, (Committee Member).
_____ Zhenqi (Pete) Shi, Ph.D. Senior Scientist, Genentech, (External Committee Member).	_____ David Johnson Associate Professor, Graduate School of Pharmaceutical Sciences, (School Representative).

ABSTRACT

DEVELOPMENT OF A COMBINED FEEDFORWARD-FEEDBACK QUALITY CONTROL SYSTEM FOR EXTENDED-RELEASE GRANULES USING A QUALITY BY DESIGN APPROACH

By

Yuxiang Zhao

August 2021

Dissertation supervised by Carl A. Anderson, Ph.D.

Objectives

For a fluid bed film coating process to consistently deliver quality products, its control system needs to be robust against the variability of input materials and environmental disturbances. Presently, limited studies have been reported to understand the effects and interactions of the material attributes, environmental variables, and process parameters on the product *in vitro* drug dissolution. A control system can be developed with a proper understanding of the coating process, by adjusting the process parameters in feedback and feedforward manners to compensate for the undesired effect caused by disturbances, and ensure consistent product quality.

Methods

The control system was developed and evaluated using a quality by design approach. The formulation variables, material attributes, and process parameters of the coating process were

systematically assessed using Ishikawa and failure mode and effect analysis. The risk assessment was followed by a fractional factorial design to screen the criticality of four process variables: product temperature, airflow volume, atomization air pressure, and inlet air relative humidity. The size distribution of the input granules was constrained to a narrow range in the factorial design. The information gained from the screening study was used to guide the response surface design for process modeling, in which granule size distribution, relative humidity, inlet air volume, and target coating weight gain were investigated, and the studied response was *in vitro* dissolution. Using two regression methods (partial least squares and Gaussian process regression) and two curve-fitting methods (Weibull function and principal component analysis) in conjunction, four modeling approaches were applied to analyze the experimental data and establish the process models. A control system was subsequently developed. The feedback loops relied on the real-time measurements of near-infrared spectroscopy (NIR) to stabilize the in-process moisture level and determine the process endpoint. The feedforward components were built upon the process models. The controllers modified the target weight gain and airflow volume to accommodate the undesired size distribution of input granules and relative humidity. The combined feedforward-feedback control system was evaluated by comparing the control performance with and without the feedforward elements, using Monte Carlo simulation and 12 additional test runs.

Results

The initial risk assessment and the statistical designs of experiments identified the critical material attributes and process parameters and elucidated their impacts on the coating process and final product quality. The in-process moisture level was found to play an essential role in preventing batch collapse and improving coating efficiency. The hydration of the active pharmaceutical ingredient (API), theophylline, was identified as a high-risk failure mode that

requested proper control. The in-line NIR models had 0.3% and 0.5% errors in predicting the moisture level and coating weight gain. The process models were established using different modeling algorithms including partial least squares regression, Gaussian process regression, Weibull function fitting, and principal component analysis. The partial least squares regression model coupled with the Weibull function as a dissolution curve-fitting method outperformed the other models as it had the lowest error profile and great simplicity for control application. The feedforward controllers were established by mathematically transforming the process model into an optimization problem, which searched for the best solution of process parameters given the initial condition of material attributes and environmental variables. The tolerance space of the coating process supervised by the feedforward-feedback control system was established.

Conclusion

The combined feedforward-feedback control system reduced batch failures and improved product quality consistency in both Monte Carlo simulations and test batches. The combined control system also showed robustness against the variability of incoming material attributes, which would grant pharmaceutical companies tremendous flexibility in choosing the sources of raw materials.

DEDICATION

This dissertation is dedicated to my parents and other family members.

ACKNOWLEDGEMENT

I would like to thank Duquesne University, School of Pharmacy for providing me this opportunity to pursue a doctoral degree in pharmaceutics. I am also grateful to all those who helped me directly or indirectly.

This academic experience of my life would not have been possible without my mentor and advisor, Dr. Carl A. Anderson, who always believed in me, encouraged, and supported me during my graduate studies. I would like to thank him for providing me with both scientific instruction and personal guidance in this journey. He is always open-minded and generous to share his knowledge and experience of science and life. I am very much indebted to Dr. Anderson, from whom I learned scientific, leadership, and presentation skills.

I want to express my immense gratitude to Dr. James K. Drennen, III, co-advisor, for my research work. I consider it an honor working with him and thank him for providing valuable input on the work from both scientific and regulatory viewpoints. Dr. Drennen always showed kindness and genuine care for us, creating such a warm and friendly learning and research environment.

I would like to convey my special thanks to Dr. Peter L.D. Wildfong and Dr. Ira S. Buckner, my internal committee members. They provided valuable inputs and extensive scientific guidance. They always encourage me to think critically and mechanistically about my dissertation project. I am also grateful for the excellent learning experience in my courses on the interfacial phenomenon, kinetics, solids, and pharmaceutical operations. They are always open to questions and provide me feedback promptly.

I would like to acknowledge Dr. Zhenqi (Pete) Shi, an external committee member, for providing statistical and chemometrics input, which allowed us to explore different approaches to understand

the experimental data. His suggestion from the industrial viewpoints helped me think about the application when drafting the manuscript. Besides the dissertation project, he is always there to help me in my other research and career development.

I would like to extend my sincere thanks to my colleagues in graduate school, especially to Dr. Shikhar Mohan, Dr. MD Nayeem Hossain, and Suyang Wu, for providing me with important encouragement and scientific support throughout this journey. I also enjoyed working with Dr. Anik Alam, Dr. Hanzhou Feng, Dr. Yi Li, Dr. Douglas Steinbach, Natasha Velez Rodriguez, Adam Rish, Jacob Guess, Eric Piece, and Samuel Henson in B11. My colleagues and lab mates with whom I spend the most time over the past few years working and chilling together is something that will remain in my memories forever.

I would like to thank the National Institute for Pharmaceutical Technology and Education (NIPTE) and the U.S. Food and Drug Administration (FDA) for providing funds for this research. This study was funded by the FDA Grant to NIPTE titled "The Critical Path Manufacturing Sector Research Initiative (U01)"; Grant# 5U01FD004275.

Last but not least, I thank all my family members for everything that I have achieved so far. I am most grateful to my parents for trusting me and supporting me financially and emotionally. I cannot go through graduate school and many other difficult moments without them. I want to thank Wanzhu Zhao, my fiancée, who made me not the only "Zhao". Her motivation and attitude made me strong and determined when I was frustrated. I am grateful to her for her patience and for accompanying me during the last three years.

TABLE OF CONTENTS

LIST OF TABLES

LIST OF FIGURES

LIST OF ABBREVIATIONS

ANOVA	Analysis of Variance
ANCOVA	Analysis of Covariance
API	Active Pharmaceutical Ingredient
CMA	Critical Material Attributes
CPP	Critical Process Parameters
CQA	Critical Quality Attributes
DoE	Design of Experiments
FMEA	Failure Mode Effect Analysis
GPR	Gaussian Process Regression
HPMC	Hypromellose
ICH	International Conference on Harmonization
LoD	Loss on Drying
LV	Latent Variable
MCC	Microcrystalline Cellulose
MFFT	Minimum Film Formation Temperature
NIR	Near-Infrared Reflectance
PAT	Process Analytical Technology
PCA	Principal Component Analysis
PLS	Partial Least Squares Regression
PVAc	Polyvinyl Acetate
PVP	Polyvinylpyrrolidone

QbD	Quality by Design
OPC	Open Platform Communications
QTPP	Quality Target Product Profile
RMSE	Root-Mean-Square Error
RMSEC	Root-Mean-Square Error of Calibration
RMSECV	Root-Mean-Square Error of Cross-Validation
RMSEP	Root-Mean-Square Error of Prediction
SNV	Standard Normal Variate
T_g	Glass Transition Temperature
USP	United States Pharmacopeia
UV	Ultraviolet

Chapter 1 : Introduction

1.1 Statement of Problem

Pharmaceutical Quality by Design (QbD) is a "systematic approach to pharmaceutical development that begins with predefined objectives and emphasizes product and processes understanding and process control."[1] The QbD elements[2] often include

(1) a quality target product profile (QTPP) that identifies the critical quality attributes (CQAs),

(2) product and process designs, including the identification of the critical material attributes (CMAs) and the critical process parameters (CPPs),

(3) process understanding and modeling,

(4) a control strategy that mitigates risks and ensures product quality and consistency.

Yu and coworkers[1] defined three levels of control strategies from the regulatory agents' perspective. Quality by test is the lowest level of control, ensuring quality by extensive end-product testing with tightly constrained material attributes and process parameters. The input materials and final products are rejected if they fail to meet the specifications.[1, 3] The second level of control relies on the establishment of a robust design space. It grants the pharmaceutical industry flexibility in adjusting process parameters within a validated and approved design space. Design of experiments (DoE) is often used to explore the knowledge space that reveals the impact of material and process variables on product quality.[1, 4] Design space (Figure 1-1) is a subset of the knowledge space statistically determined based on the CQA acceptance criteria.[5] It is common within the pharmaceutical industry to restrict raw material specifications, run the manufacturing process in a normal operating range (NOR), and implement a hybrid control strategy combining the first two control levels.[6] Over time, the design space will need to be modified for new

knowledge gathered in the post-approval stage. For instance, the change of a supplier for excipients or active pharmaceutical ingredient (API), lot-to-lot variability in raw materials, equipment aging, and environmental changes can significantly impact the product quality and ultimately alter clinical outcomes.[7, 8] In those cases, the robustness of the design space is challenged, and additional studies are often required to adapt to the original design space.

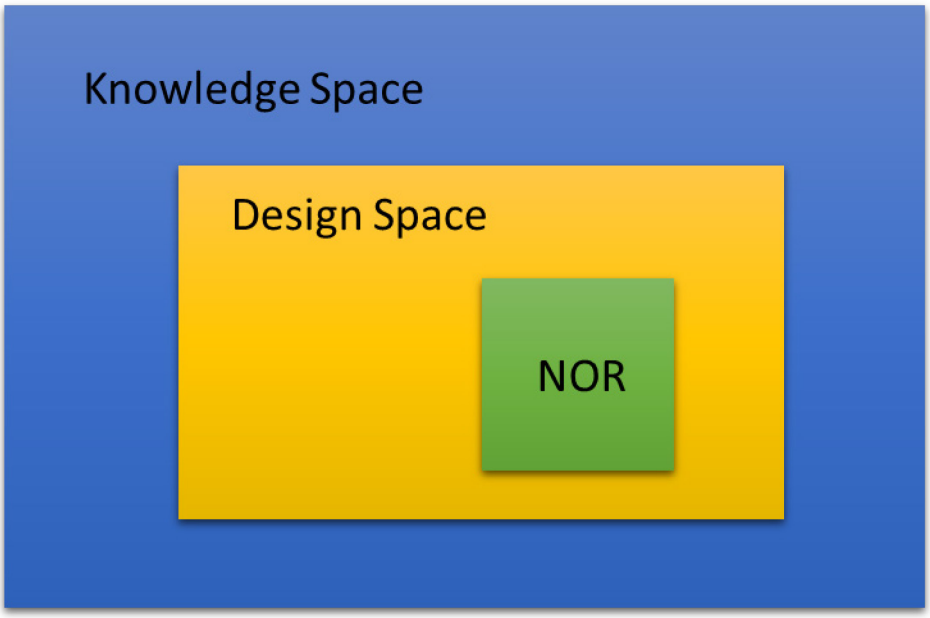

Figure 1-1: knowledge space, design space, and normal operating range (NOR).

The third and highest control level is to monitor the disturbances and adjust process parameters accordingly, which adapts the design space to material and environmental changes automatically. Process analytical technology (PAT) is often involved in this level to allow for real-time monitoring and control operations. This type of control is not entirely new since the concept has been widely adopted in chemical engineering for decades.[9, 10] Meanwhile, the regulatory agents are encouraging the pharmaceutical industry to follow this path. It is also stated in ICH Q8, "…the control of the process such that the variability (*e.g.*, of raw materials) can be compensated for in an adaptable manner to deliver consistent product quality."[11] However, pharmaceutical companies

hesitate to fulfill the highest control level because of the increased time and cost during the product development stage and potential delays of the drug approval. The pharmaceutical industry has yet to realize the strength of the systematic quality by design approach: development speed can be improved, and the robustness of the design space can be enhanced.[10] Furthermore, it is imperative to realize the benefits of incorporating the feedforward components into the quality control strategy. Well-established feedforward controllers can transfer resources from a downstream corrective mode to an upstream proactive mode.[1] Proactive controls allow the adaptation of design space to tolerate more material variability and adjust process parameters within the design space more efficiently than corrective controls.

This dissertation demonstrates the development of a combined feedforward-feedback control system for a fluid bed coating process. The feedforward components were designed [10, 12, 13] for the satisfaction of end-product CQAs. Several algorithms exist in the literature to tune feedforward controllers.[12-16] The most promising algorithm was described by Muteki and coworkers,[13] in which partial least squares regression (PLS) was applied to construct the process models, and the control output was generated using a constrained quadratic searching method.[12, 13] A non-parametrical algorithm, Gaussian process regression, was also investigated as an alternative. The feedback components were mainly built-in functions in a synTQ data management system to stabilize process variables.[17] The near-infrared (NIR) spectroscopy was integrated into the feedback loops for continuous monitoring of CQAs to allow timely adjustment of process parameters.[18-20]

1.2 Hypothesis and Specific Aims

The dissertation is based on the central hypothesis:

The combined feedforward-feedback control system, developed via the quality by design approach, will (1) improve the quality and consistency of extended-release granules produced by fluid bed coating process and (2) increase the process robustness against the input material attributes and environmental disturbance, comparing to a feedback control alone system.

Figure 1-2 illustrates the scheme of the pharmaceutical quality by design. The systematic approach is split into the following specific aims:

1. understand the fluid bed coating process:
    - define the quality target product profile (QTTP),
    - perform risk assessment,
    - use one-variable-at-a-time experiments to develop a coating formulation,
    - conduct a screening study to evaluate critical parameters related to high-risk failure modes.

2. conduct a response surface study to explore the knowledge space and develop process models that predict dissolution profiles of coated granules using two algorithms: Partial least squares regression (PLS) and Gaussian process regression (GPR), and two curve-fitting methods: Weibull function and principal component analysis (PCA).

3. establish feedback control loops based on real-time predictive models using process analytical technologies (PAT) and chemometric tools:
    - use NIR spectroscopy to monitor in-process moisture and coating weight gain,
    - use Raman spectroscopy to monitor API solid-state form.

4. construct and test the combined feedforward-feedback control system in the following steps:
   - integrate the combined feedforward-feedback control system using the process models and the real-time predictive models to control the product critical quality attributes,
   - apply Monte Carlo simulations to evaluate the process capability, and establish the design space of the control systems with and without feedforward components,
   - conduct test batches at the edge of the design space of the coating process, with and without the feedforward components.

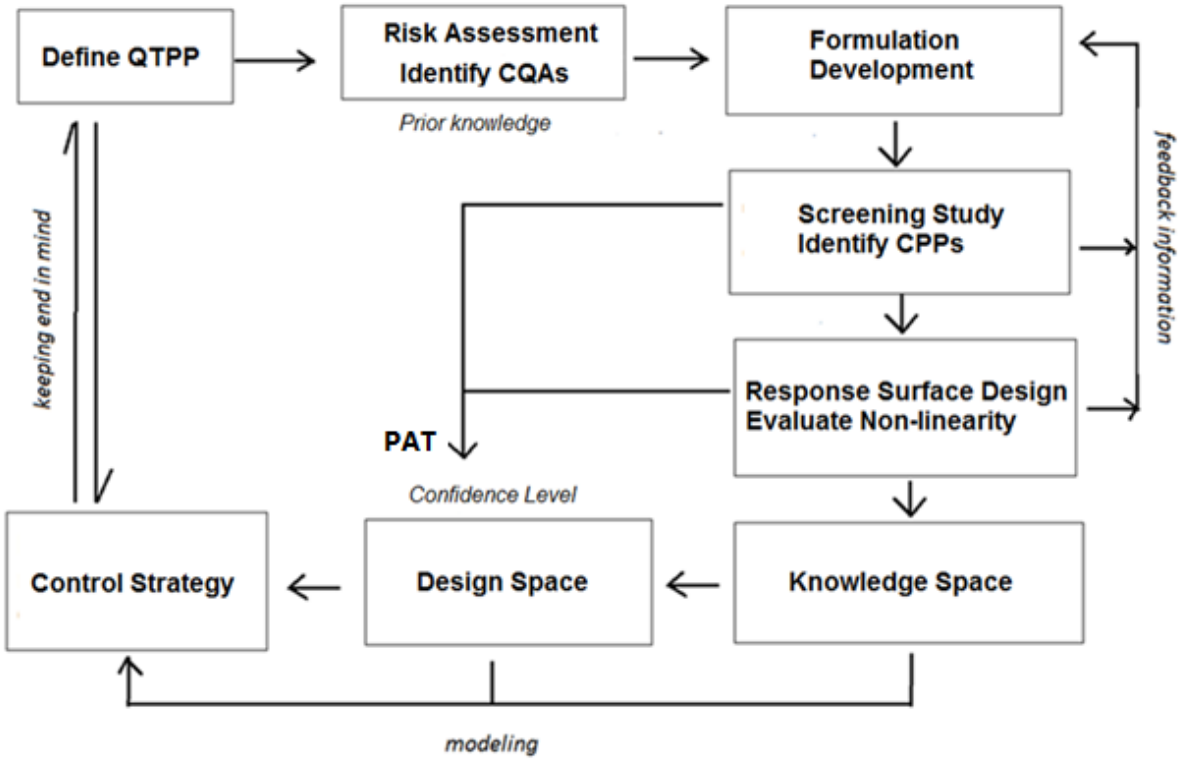

Figure 1-2: The illustration of a quality by design (QbD) approach.

1.3 Literature Survey

This work utilizes a quality by design approach to develop a combined feedforward-feedback control system. An extended-release multiparticulate dosage form and a fluid bed coating process were utilized as the model drug product and manufacturing process for this demonstration because of their inherent complexity, thus requiring advanced control to assure quality and consistency. The literature was reviewed on three subjects: (1) product and process of the aqueous fluid bed coating, (2) QbD principles, and (3) control tools.

1.3.1 Extended-Release Multiparticulates: Formulation and Process

Extended-release dosage forms provide the benefits of minimum fluctuation of plasma drug concentration, decreased probability of side effects, reduced dosing frequency, and improved patient compliance.[21, 22] The extended-release profile of the dosage form comes from the design of the formulation. In a tablet dosage form, the extended drug release is controlled by the coating around the tablet surface or achieved by forming a matrix mass consolidating the mixture of drug and polymeric excipients. An alternative is to manufacture drug-loaded multiparticulates (beads or granules) and then subject the particles to a non-enteric coating. The coated particles can be encapsulated or compressed into a tablet, depending on the target product profile. The multiparticulate drug delivery system (MDDS) has become the preferred dosage form in the pharmaceutical industry owing to its flexibility in adjusting formulation to achieve a specific release profile.[23] The major advantage of employing an MDDS is from pharmacokinetics and pharmacodynamics perspectives. Its formulation robustness yields a consistent pharmacokinetic profile with reduced variability in the in vivo performance and ensures patient safety.[24] Compared to the development of matrix compacts and film-coated tablets, the MDDS prevents dose dumping

and allows the adjustment of release profile by changing the thickness of the polymer coat while keeping the same formulation of the core. The MDDS also provides the flexibility of encapsulating/tableting different amounts of beads or granules from the same formulation to generate a series of dosage strengths, thus benefiting formulation optimization and scale up.

1.3.1.1 Coating Formulation

Film coating can be broadly classified into two types based on the application: functional and non-functional. Non-functional coating is used to improve esthetics or protect the product from dust, whereas functional coatings include drug release modification, taste masking, preventing drug degradation, and acting as a moisture barrier.[25] Along with the physicochemical properties of the drug substance and the unit operations adapted, the coating formulation is one of the three key factors contributing to the success of the coating process.

The most used modified-release coating system can be classified into pH-dependent and pH-independent. Enteric coatings use pH-dependent polymers where the pH change in the gastrointestinal tract dictates the dissolution of the polymer coating, and, therefore, the drug.[26] This dissertation focuses on non-enteric formulations where pH-independent polymers are of primary interest.[21, 27] Due to safety and environmental considerations, aqueous polymer dispersion has become more popular than organic solvent-based polymer solutions over the past decades.[28] There are three classes of aqueous polymers based on their chemical nature: Acrylic resin (*e.g.*, ammonio methacrylate copolymer), polyvinyl derivatives (*e.g.*, polyvinyl acetate), and cellulose derivatives (*e.g.,* ethylcellulose).[29] The selection of aqueous coating polymer is usually based on its solubility, permeability, mechanical properties, minimum film formation temperature (MFFT), and glass transition temperature (T_g). The minimum film formation temperature (MFFT) is defined as the

approximate temperature at which the forces driving polymer particle deformation exceed the resistance.[30] The coating temperature must be above the MFFT to obtain a continuous film. The types and ratio of monomers, particle size distribution, molecular weight, and degree of crosslinking are the major factors influencing the MFFT.[31] The film formation tends to be uniform and reproducible when the polymer is in a rubbery state and readily spreadable during the coating process.[32] Cellulose derivatives often exhibit high glass transition temperature and do not yield smooth continuous film upon spraying onto the core substrates. Hence a plasticizer is required to reduce the T_g and MFFT to facilitate film coalescence. The plasticizers are low molecular weight substances embedded into space within individual polymer strands, thus reducing the polymer-polymer interactions. The mobility of the polymer molecules increases with the addition of plasticizer, and the T_g of the formulation is decreased, ultimately leading to the transition of the polymer system from a brittle, glassy state to a flexible rubbery state.[33, 34] The plasticizers may also significantly modify the physicochemical properties of the coating with regards to water uptake, thermal behavior, and drug permeability. Aqueous soluble plasticizers mix with the coating dispersion upon preparation and may form channels in the formed film whereas insoluble plasticizers require longer mixing time to emulsify into the dispersion and decrease the film permeability.[35] The amount and type of plasticizer required for a desired coating formulation depend on the glass transition temperature of the polymer and the plasticizer, which can be calculated by the Fox equation.[36]

$$\frac{1}{T_g} = \frac{W_1}{T_{g1}} + \frac{W_2}{T_{g2}} \qquad \textit{Eq. 1.1}$$

where T_g is the desired glass transition temperature of the coating dispersion; T_{g1} and T_{g2} are the respective T_gs of the individual components; and W_1 and W_2 are weight fractions of components 1 and 2, respectively.

A subsequent process to coating, namely curing, is sometimes essential to complete the film formation. The curing temperature needs to be above the glass transition temperature to allow the coalescence of latex or pseudolatex particles. Insufficient polymer film coating or film curing can lead to erratic dissolution, which ultimately leads to sub-therapeutic drug levels or toxic levels depending on the properties of the drug molecules. The type and level of the plasticizer determine the glass transition temperature of the formulation, which at the same time governs the MFFT during coating and curing.

Acrylic resins and polyvinyl derivatives tend to have much lower T_g values than cellulose derivatives, and in general, they do not require the addition of a plasticizer to process at mild temperature (20 – 40 °C).[37] The drawback is that the low T_g and MFFT lead to tackiness and excessive particle adhesion. Anti-tacking agents, such as talc, are often necessary in those cases to prevent tablets or particulates from sticking together or adhering to the container surface during process and storage.[38] Accompany with the coating polymer, pore-forming agents (*e.g.,* hydroxypropyl methylcellulose, povidone) are sometimes used to adjust the drug release rate to achieve the desired profile.[39,40] Aqueous insoluble pigments can be added to the coating dispersion to make the film opaque or colored. However, the incorporation of pigments can induce stability problems and alter the film properties.[41] To solve the instability problem, surfactants or emulsifiers, such as sodium lauryl sulfate (SLS), help improve the wettability of polymer and pigment particles by decreasing the surface tension. The reduced surface tension improves the spreading of coating dispersion and the generation of uniform droplet distribution over the surface of the drug-loaded core.

1.3.1.2 Film Formation

An aqueous pseudolatex coating dispersion consists of discrete polymer spheres, which must coalesce to form a continuous film once sprayed onto the substrates. The commercially available polymers are usually stabilized using emulsifiers so that the polymer spheres do not agglomerate in the dispersion, however, in the film formation, the same spheres need to overcome their repulsive forces to fuse. The most accepted film formation mechanism is that the loss of solvent constrains the movement of colloidal particles to form a densely packed stack and ultimately becomes a uniform and continuous film.[42] In other words, film formation happens in three stages: (1) evaporation and particle ordering, (2) particle deformation, and (3) interdiffusion of polymer particles.[31, 43]

Stage 1: Evaporation and Particle Ordering

When the dispersion is deposited onto the surface of the substrate, evaporation of the water drives the polymer particle to come in contact as a close-packed array. The most generally accepted model assumes that transport of water occurs efficiently between water and air interface. Vanderhoff *et al*.[44] categorized the evaporation of water into three phases: (1) rapid water loss from the surface of the polymer dispersion, (2) decreased rate of water loss when the polymer particles start to assemble in an ordered manner, (3) diminished rate of water loss when the particles are fully ordered. During the evaporation, the water diffuses through the capillary space between ordered particles, impairing the stability of the pseudolatex dispersion and initiating the particle deformation.

Stage 2: Particle Deformation

Particle deformation only occurs at a temperature above the MFFT of an aqueous dispersion system. The MFFT is an experimentally determined temperature at which the film becomes

continuous and crack-free. Above the MFFT, polymer particles have adequate mobility to disrupt the repulsive forces of the polymer particles. Subsequent particle deformation results in the fragmentation of the hydrophilic layers between the polymer particles, leading to phase inversion in which the remaining water is no longer the continuous phase.[28] The negative curvature of the polymer-water droplet surface[45, 46] allows the generation of three driving forces for the deformation, including the water-polymer interfacial tension, dry sintering due to the air-polymer interfacial tension, and the capillary force from the water-air interface.[47] The driving force can be reduced with the presence of surfactant. Hence the formulators need to balance the stability of the dispersion with its propensity to overcome the energy barrier during film formation.

Stage 3: Interdiffusion of Polymer Particles

Interdiffusion of polymer chains across the interface between discrete polymer particles is the final step to form integral homogeneous films.[48] The interdiffusion requires a temperature above the T_g of the polymer system. The polymer chains have increased molecular mobility and free volume in the rubbery state.[49] They come close to each other, leading to coalescence and fusion of the particles, accompanied by surfactant exudation within the film.[50]

1.3.1.3 Fluid Bed Coating

Fluid bed coating is a unit operation in which dry solid particles are fluidized, wetted by the coating liquid, and dried simultaneously. Although employed as a pharmaceutical manufacturing process for decades, the trajectories of particles in the fluid bed are still unpredictable. The fluidized particles are susceptible to fragmentation and attrition, which can result in a significant material loss in operation. The competition between the layering of coating material on the dried particles and the agglomeration of wetted particles is always a challenge to the developers. Despite

these challenges, the fluid bed provides advantages over other coating processes: superior heat and mass transfer efficiency and the ability to process material with a broad range of size distributions.[51] With the increased demand for high-quality and efficient production in the pharmaceutical industry, a deep understanding of the fluid bed process is essential to enable process control and automation of coating operations.

Fluidization maintains the suspension of particles by blowing pressurized air into the system from the bottom of the fluid bed processor through the particle bed.[52] Particles become fluidized when the dragging force from upward air current overcomes the force of gravity. The minimum fluidization velocity is a critical parameter for a steady fluid bed. When the air velocity increases beyond the minimum fluidization velocity, bubbles start to form in the packed bed, and the particles start to behave like a liquid at the beginning of boiling. However, by its principle, fluidization is an elutriation system where the particles of different sizes or densities are readily separated, especially when the air velocity is just above the minimum fluidization velocity. As the air velocity continues to increase, the fluidized particle may transition from a bubbling regime to a turbulent regime in which the bubbles are no longer in regular shapes, the mass and heat transfer then becoming heterogeneous. Therefore, the fluidization airflow must be carefully managed to support the entire bed as a smooth and homogeneous suspension.

The point of bubble formation depends on the particle properties. Geldart[53] classified the particles into four groups based on their density (fluid and solid) and mean particle size, illustrated in Figure 1-3. Particles in Group C are cohesive and difficult to fluidize. The small particle size and strong interparticle forces (*e.g.,* electrostatic charge, liquid bridge during wetting) make them behave more like clusters than single particles. These particles are often inadequately fluidized, resulting in poor mixing and heat/mass transfer. In contrast to Group C, Group D particles are large

and dense, which require intensive airflow for fluidization. The bubbles formed in the Group D particle bed are often large and tend to grow to the diameter of the fluid bed chamber. The large bubbles are called slugs. Group A particles often exhibit an aeration property that allows them to expand significantly at low air velocity without bubbles. Group B particles have more extensive size distributions (150 -1000 μm) than group A. They tend not to form smooth fluidized beds like Group A but undergo a stable bubbling regime. Group B particles allow the formation of a large bubble so that sometimes slugging can occur. In general, both Group A and B are easily fluidized and are used in a wide range of fluid bed applications with few difficulties.[51]

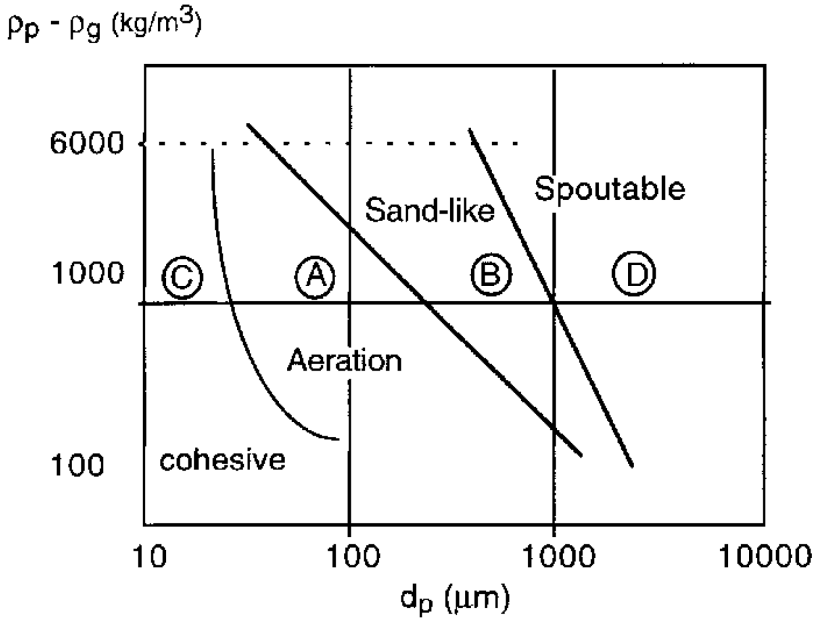

Figure 1-3： Geldart's classification of powder in fluidization. It is adapted from ref[52], permission granted.

A few phenomena among the particles, coating liquid, and fluidizing air, occur simultaneously in the fluid bed to enable a stable process. They are:

(1) interaction between air and particles. As discussed previously, the particles need to undergo fluidization in a homogeneous flow to maximize heat and mass transfer between the air and the particle surface.

(2) interaction between particles and liquid. The atomization of spraying liquid increases the probability of the collision between droplets and particles. The droplets spread on the particle surface from a liquid layer. The agglomeration between two or several particles may occur before drying the liquid causes a high risk to the coating process.

(3) interaction between air and liquid. The air helps evaporate the liquid layer on the particle surface, and the polymer coalesces into a continuous film. However, droplets can be dried before contacting with the particles, and thus no coating is formed.

Successful coating depends on the droplets spreading on the particle surface and the efficiency of the heat and mass transfer.[54]

Fluid bed processor can be roughly categorized by three configurations, which are shown in Figure 1-4, including (a) top-spray, in which the nozzle is placed at the top over the fluidized particle bed, (b) bottom-spray Wurster system, where the fluid bed contains a draft column (Wurster insert) to create a circulation particle flow (c) rotary system, in which a rotor is placed at the bed bottom and air blow through a gap between the rotor and wall, and the nozzle is positioned on the side of the chamber.

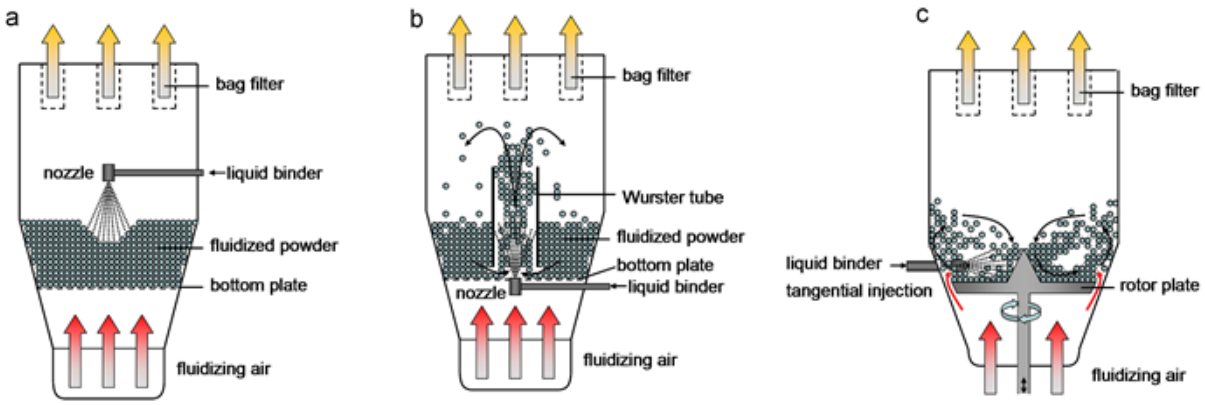

Figure 1-4： configurations of different fluid bed processors: (a) top-spray system, (b)bottom-spray Wurster system, and (c) rotary system. Figure adapted from ref[55], permission granted.

The bottom-spray Wurster system is widely acknowledged as the best design for fluid bed coating.[56] The insertion of the Wurster column divides the fluid bed chamber into four zones where the particles flow through each of them in circulation. Particles are first wetted in the spouting zone in the bottom center of the chamber, where the spray droplets and the fluidization air travel in the same upward direction. The drying process occurs in the inner column zone, where particles are pneumatically transported from the bottom to the top. After reaching the top, the particles start to fall to the bottom through the annular external column zone. When the particles return to the bottom, they move slowly from the peripheral zone to the spouting in the center. The motion trace of the particles is just like water in a vertical fountain. This mechanism of circulation limits the number of particles in the spraying zone, minimizes the droplet traveling time, and regulated the trajectory of the particles. The risk of agglomeration is reduced. The coating uniformity and efficiency are improved in this setup comparing to the other two configurations. However, the scale-up of Wurster system is difficult since some of the phenomena depend on the distance, and

the others are related to the area of the process zone. The complexity of the configuration is the main challenge in applying the Wurster system.[57-59]

In contrast, the use of a top-spray fluid bed for coating, without the additional Wurster insert, is often limited in barrier coating (against moisture, light, oxygen), ease of handling, and taste-masking, where perfect coating film is generally not required.[60-62] The challenge for coating in the top spray system is that the particle motion is unconfined and presumably random. The fluidization pattern, droplet travel distance, and drying efficiency are influenced by the mixed effects of two or more process parameters. However, the top-spray fluid bed coating has the advantages of high versatility, large batch capacity, and low capital cost.[63] It also requires less effort in scale-up than the Wurster setup due to its simplicity.[64] In addition, the top-spray feature allows the convenience of assembling a continuous horizontal fluid bed processor. Particles are charged to the fluidized chamber at one end and move slowly to the other end while the liquid is sprayed into the system from the top. This type of fluid bed exists and is used in the food industry for many years.[52]

Numerous variables are involved in top-spray coating process, and the interdependence of those parameters remains unclear. The layering of the coating does not occur during one single pass through the coating zone, but relies on many passes to allow sufficient liquid to cover the particle surface. As previously discussed, droplet formation, collision, spreading, coalescence, and evaporation are occurring simultaneously during the process. The droplet size and distribution are more relevant to the nozzle configuration and atomization of air. The fluidization air contributes the most to evaporation. However, the opposing direction of atomization air to fluidization air made the flow patterns of solid particles and liquid droplets unpredictable. Experimental study and empirical modeling are often required to provide a thorough insight into the coating operation so

that a comprehensive control may be established to produce products of consistent and desired quality, batch by batch or continuously.

The rotary coating system is a relatively new approach, often referred to as the tangential-spray coating. It utilizes a rotor disc driven by an electric motor, which generates high kinetic energy that makes it difficult to coat weak and non-spherical products (*e.g.*, granules). There is a high probability of destroying them. The rotor system is suitable for producing pallets that require spheronization and subsequent coating as a one-pot manufacturing process.[63, 65]

1.3.1.4 Drying and Curing

The coated substrate is often dried *in situ* simultaneous with the polymeric coating, and it may or may not require subsequent curing to complete the polymer coalescence fully. As discussed previously, water evaporation concentrates the polymer particles in a closely packed arrangement on the substrate surface. The capillary force, one of the main driving forces for polymer deformation, will dissipate if the polymer particles are too rigid to be deformed, or if the drying conditions are not optimized. The polymer particles are rigid if the coating temperature is below the T_g of the polymer system or if the plasticization is inadequate. Additionally, inappropriate drying conditions regarding temperature, humidity, and time may affect the rate of heat transfer, the evaporation of the water, and particle deformation. They are indirectly varying the degree of polymer coalescence. Rapid loss of water, although generally desirable, may at times diminish the capillary force action resulting in incomplete film coalescence.

The necessity of a curing step is dependent on the T_g of the dispersion system, plasticizer type and amount, and drying conditions. Curing ensures consistent drug release and physical stability. Partially coalesced films (uncured) show faster drug release and thermodynamically unstable,

resulting in a gradual decrease in drug release on long-term storage. From product development and regulatory perspective, it is imperative to demonstrate complete film coalescence for the long-term stability of the drug product. On the other hand, over-curing a polymer coating excessively at an elevated temperature can adversely affect drug release. Due to drug-polymer affinity, the drug may migrate to the coating surface, and consequently, faster drug release may be observed because of drug crystallization and the creation of a void in the coating layer. Balanced curing conditions from the coating process need to be adapted and optimized using the principles of quality by design.[66]

1.3.2 Quality by Design

Quality by design is a systematic approach initiated by regulatory bodies to enhance pharmaceutical development through proper process design and control strategies to deliver consistent quality products.[67, 68] Implementing QbD in the development phase enables formulators and process engineers to analyze reasons for batch failures based on a thorough process understanding and predict the effect of scale up on the final product, finally establishing a comprehensive control strategy. In this section, the systematic approach is discussed, starting with the definitions of quality target product profile, critical quality attributes, critical material attributes, and critical process parameters, and followed by the steps to perform a risk assessment and to design experiments using statistical principles for the construction of knowledge space and then design space and control strategy.

1.3.2.1 Key Terms for QbD

According to the International Council for Harmonization (ICH), "quality target product profile can be defined as a prospective summary of the quality characteristics of the drug product that ideally will be achieved to ensure the desired quality, taking into account safety and efficacy of the drug product."[69] In modern pharmaceutical product development, the first step is to define the quality target product profile (QTPP) from the perspectives of quality, safety, and efficacy. The attributes presented in the initial QTTP are not fixed and may be changed when additional information is obtained during the product and process development. The initial QTPP attributes are defined based on the prior knowledge of the API properties, commercially desired dosage form and strength, and target patient population. The quality attributes pertinent to the safety and efficacy of the target patient population should be listed in the QTTP. The commonly listed attributes in QTTP are administration route, dosage form, identity, strength, assay, content uniformity, impurities, stability, and dissolution.[69] The QTPP philosophy of starting with the end in mind allows a product developer to think ahead about selecting appropriate excipients and unit operation, identifying risks, planning experimental design, and ultimately developing a control strategy to ensure consistent drug product quality. All these elements in conjunction fulfill the target of quality by design: building quality into the product instead of testing at the end.

The critical quality attributes of a drug product are identified from QTTP, which directly affect the safety and efficacy of the target patients.[4] They are defined as "a physical, chemical, biological or microbiological property or characteristic that should be maintained within an appropriate limit, range or distribution to ensure the desired product quality."[67] The CQAs are dynamic elements that are updated during the product development phases. From the product developer's perspective, the CQAs need to be met to yield reproducible quality pharmaceutical products. They are

dependent on the formulation, raw material, and process parameters since these attributes can drive the manufacturing process outside the established design space and change the CQAs significantly. Identifying the CQAs in the early stage helps guide product development, including selecting appropriate excipients, choosing unit operations, and establishing control strategies. Typically, an initial risk assessment is conducted using prior knowledge to plot out a list of potentially critical quality attributes that have direct clinical impacts. The risk assessment enables the CQAs as a link between product quality and clinical performance. The list of CQAs should be updated once additional information is obtained from experimental data. The variety of dosage forms requires different types of CQAs, *i.e.*, product purity, drug release, and stability for most dosage forms; aerodynamic properties for inhalation dosage form; sterility for parenteral drug delivery system; adhesion for a transdermal patch.

Critical material attributes are the physicochemical properties of raw materials or intermediate drug products that can significantly impact the performance of the final drug product or cause a substantial issue in the manufacturing process. They should be identified from both drug substances and excipients using risk assessment tools, and their criticalities should be confirmed along with the design of experiments in the following studies. Process parameters include the type of equipment, batch setting, and process conditions. Critical process parameters are process inputs that significantly impact the critical quality attribute of the drug product. Roy[70] created a compiled list of potential critical process parameters (CPP) for various unit operations related to a solid dosage form in his review article. The list is based on theoretical assumptions on strength, dosage form, selection of excipient, and related critical material attributes (CMA). In practice, the criticality of process parameters can be determined systematically using risk assessment tools and

statistical designs of experiments. The CPPs and CMAs of fluid bed coating are discussed and justified in detail in Chapter 2.

1.3.2.2 Risk Assessment

Quality risk management in ICH Q9 indicates that "the evaluation of the risk to quality should be based on scientific knowledge and ultimately link to the protection of the patient and the level of effort, formality, and documentation of the quality risk management process should be commensurate with the level of risk."[71] The risk assessment tools in the ICH Q9 are applicable to risk assessment in the product development phase. As one of the early steps in a QbD project, the purpose of risk assessment is to identify potential high-risk formulation and process variables that have the potential to have a substantial impact on the final product quality. The risk assessment outcome prioritizes the critical parameters and determines the experimental design for the following studies. A poor risk assessment that mistakenly identified a critical parameter as non-critical at the early stage may result in extra cost and delay of the new product launch. Therefore, the risk assessment should be performed periodically throughout the entire circle of product development.[72]

Initial risk assessment is often performed using an Ishikawa diagram and a failure mode and effect analysis (FMEA) to classify the risk modes as low, medium, and high. The low-level risk modes are deemed acceptable risks since they do not significantly impact the clinical performance of the drug product. The medium risks are deemed acceptable, but require close monitoring. The high-level risks are unacceptable and need further investigation. The Ishikawa diagram, sometimes referred to as the fishbone diagram, is a theoretical evaluation of all possible attributes that may significantly impact the final product quality. Those attributes could be from raw material (drug

substance and excipients), process, analytical method, environment, *etc*. The Ishikawa diagram for the fluid bed coating process has been developed for this work and is presented in section 2.3.2.1. The extensive list of potential parameters from the initial evaluation can be narrowed based on subsequent FMEA and preliminary experiments.[73] To assign risk level in FMEA, usually, a team of experts from different fields like pre-formulation, formulation, process, and analytical method development participates in brainstorming to determine the scores of severity (S), occurrence (O), and detection (D) for every attribute. The scores can be assigned on a scale of 1-5, 1- 10, or any user-defined range. The numbers may be linearly (*e.g.*, 1, 2, 3,…) or non-linearly ordered (*e.g.*, 1, 3, 6,…).[74] The severity is evaluated on the seriousness of failure and its impact on the clinical performance of the product. The occurrence measures the frequency of failure during the manufacturing, especially for operating outside the proven range. The detection represents the probability of timely detection of the failure before the release of final products. The three scores are multiplied (S×O×D) to generate a risk priority number (RPN), which are then utilized to classify the risk levels of the failure modes as low, medium, and high. The risk levels are indicators that determine the criticality of material attributes and process parameters. RPN is the most commonly used technique in the food and pharmaceutical industry, while an alternative, called military standard method, is often used by the Department of Defense to rank potential failure modes in the defense, aerospace, and nuclear power generation industries. The military standard method uses similar principles (occurrence, severity) to RPN and includes an operating time index to reflect the time dependence of failure modes for complex systems.[75]

The preliminary risk assessment on the formulation, material, and process variables helps design an appropriate experimental plan to gain product and process understanding and ultimately to establish the design space. With the assistance of risk assessment, the QbD approach utilizes

the design of experiments in multiple stages during the product development to screen, identify and control the source of variability in materials and process. As the experimental plan progresses, the collected information forms the basis to re-evaluate the risk level assignment. The risk level of each identified failure mode can be reduced with the implementation of an appropriate control strategy, and the misclassified criticality of variables should be corrected based on the knowledge gained from experimental data.

1.3.2.3 Statistical Design of Experiments

Relationship between independent variables, *i.e.*, material, formulation, or process factors, and the responses, *i.e.*, process outcomes or quality attributes, can be deduced using statistical design of experiments (DoE). The design of experiments helps determine the most influential factors and the operational ranges of those factors to minimize the variability in product quality. The objectives of performing DoE include screening, process understanding, interaction, process optimization, and design space establishment. Due to the formulation complexity of multiparticulate extended-release dosage forms, the design of experiments can help decide on the selection of excipients and mass fractions based on the identified material attributes in the early stage. With a carefully designed experimental plan, the critical formulation attributes can be studied in parallel with the process conditions. This improves the overall robustness of the product formulation and manufacturing process by designing experiments.[76] However, it is often infeasible to study all material attributes and process parameters simultaneously. The developers are often required to sequentially conduct a series of experimental designs to apply the information gained from one set of experiments to subsequent experiments. Time and resources are saved by conducting small sets of experiments and building up a conclusion.

The most adapted statistical designs of experiments are factorial design (full or fractional) and response surface methodologies. Often, an extensive list of variables needs to be screened in the early stages of product development to evaluate their criticalities. The full factorial design, which tries all possible combinations to separate the main effects and two-factor interactions, generates a massive number of experiments. For instance, a two-level-six-factor full factorial design with 6 replicated center points requires $2^6 + 6 = 70$ runs. Replicates of the center point are essential for assessing curvature effect, range of linearity, experimental uncertainty, and lack of fit of the DoE results. Every increase in the factorial number doubles the total number of experiments. The full factorial design becomes inapplicable with large factorial numbers and limited resources. Using a fraction of the full factorial design is a more feasible and cost-effective approach in this scenario. The fractional factorial design lowers the resolution to reduce the number of experiments but causes confounding between certain interaction effects and main effects. There are multiple types of resolutions for the fractional factorial design that can be adapted depending on the expected outcome, *i.e.*, whether the two-factor interaction needs to be independently evaluated. Another design approach that is commonly applied is Plackett and Burman design.[77] This design uses a different algorithm from the factorial design to fractionalize the experiments to allow the total runs to be further reduced. The drawback is the decreased resolution whereby the effects of main factors are aliased with two-factor interactions. The confounding effect can result in difficulty for decision-making for further investigation.

Screening studies identify the critical material attributes and process parameters, which are then subjected to the response surface methodology for process optimization. Orthogonality and rotatability must be achieved to build a proper response surface design. A circumscribed central composite design (CCCD) is an excellent example to reveal the principle of response surface

methodology. In a CCCD, a two-level full factorial design serves as the basis, while star points and center points are added to complete the design. The star points are defined as the points having equal distance to the distance of full factorial design points from the center point. In such a way, all factors are evaluated at five different levels to map the response surface while conducting a relatively small amount of experiments. For all types of statistical design, analysis of variance (ANOVA) and least squares regression are the primary methods to understand experimental data. Thus, it is always prudent to evaluate the power of the design of experiments (*e.g.*, the change in the response over the experimental error) and to make sure that an adequate number of experiments are designed to achieve a minimum 80% chance to reveal a change in response at 95% confidence level. Other attributes to be considered are the uncertainty of estimated coefficient, multi-collinearity, the leverages of the design points, and the minimum degree of freedom to assess the lack of fit and protect the pure error.

1.3.2.4 Design Space

Design space, by the definition of ICH Q8 (R2), is "the multidimensional combination and interaction of input variables (*e.g.*, material attributes) and process parameters that have been demonstrated to provide assurance of quality."[11] Process adjustment within the design space is not considered a change and is not required to notify regulatory bodies. While moving out of the design space usually initiates a post-approval change process. Design space is the direct outcome of process development that defines the acceptable ranges of process parameters. However, design space is based on a statistical analysis of DoE data for the process, which means operating within the acceptable range does not lead to desired product quality with a 100% chance.

Process robustness enables a process to deliver acceptable drug product quality and performance while tolerating variability in the material when operated within predefined ranges.[78] A pharmaceutical company must demonstrate the robustness of the manufacturing process to yield a consistent quality product. For scientists, the approach to establish a robust design space is via a process model and related statistics based on product and process understanding. A process model is often developed from a response surface design and can be expressed in the form of a quadratic function:

$$Y = \sum_{i=1}^{n} \beta_i x_i + \sum_{j=1,i=1}^{n} \beta_{ij} x_i x_j + \beta_0 + \varepsilon \qquad \textit{Eq. 1.2}$$

where Y is the response (CQA) of the product, β_0 is the constant term, $\sum_{i=1}^{n} \beta_i x_i$ is the linear combination of material attributes and process parameters, and $\sum_{j=1,i=1}^{n} \beta_{ij} x_i x_j$ represents the sum of the quadratic and interaction terms. The uncertainty of the model parameters ($\beta_0, \beta_i, \beta_{ij}$) and the error term ε are the keys to define a statistic tolerance interval that ensures a level of confidence (say 95%) that a target proportion (say 99%) of batches meets the specification. The calculation of the confidence level is based on the model uncertainty, while the proportion of batches depends on the intrinsic variability of the material and manufacturing process. Thus, the more demanding the confidence or the requirement for the nearer to 100% successful batch, the smaller the design space becomes. A proper control strategy for the known variabilities (*e.g.*, environmental disturbance, material variability) needs to be implemented to reduce the process uncertainty and allow for a feasible operational condition. It should be noted that design space is scale and equipment-dependent. Mechanistic process models based on first principles are preferred as they are more often justifiable when adapting a lab-scale design space to the commercial scale.

The model response in one process model may become a model input for the other process models. Pharmaceutical products are often manufactured by a train of unit operations. For instance, the production of the extended-release granules involves high shear wet granulation, drying, fluid bed coating, and the second drying. In this case, the intermediate product of the first unit operation (wet granulation) becomes the input material of the subsequent unit operation. The CQAs determined in the early unit operation become CMAs in the following unit operations and can be used as inputs for the process model of the subsequent unit operation.

1.3.2.5 Control strategy

A control strategy is a plan of controls for the attributes of the incoming material, intermediate product, process parameters, in-process controllers, and final product. In the scope of quality by design, the control strategy aims at reducing the risks associated with the drug product and the manufacturing process. The control strategy should be established based on the understanding of product, formulation, and process. It includes but is not limited to[79]

1. control of material attributes,
2. product specification,
3. control of process parameters for unit operations,
4. in-process monitoring and real-time release testing, and
5. continual process improvement.

A good control strategy enables real-time release testing (RTRT), which falls within the scope of QbD. The RTRT models can assess the quality of the in-process and final product during manufacturing using the real-time measure of material and process information, which reduced the turn-around time required from the traditional release testing.[80, 81] Process analytical technology

tools like near-infrared spectroscopy, Raman spectroscopy, and acoustic signaling can be utilized to develop an in-process control strategy that can help to develop a real-time release testing model.[82-86] It should be noted that adaption of PAT is not the only way to implement real-time monitoring. Predictive models built on traditional material characterization and real-time measurements of process parameters are used as soft sensors.

When the source and impact of variability are well understood, the knowledge can be utilized to constrain the attributes of material from upstream or change the process parameters for downstream in a feedforward manner. From the engineering perspective, the process capability, which is a measure of the inherent variability in an established process relevant to the acceptance criteria, can be improved by using feedforward controllers to monitor the disturbances and enable adjustment to the process as required during manufacturing to assure the target process conditions are met.

1.3.3 Control Tools

1.3.3.1 Real-Time Predictive Model for in vitro dissolution

The fluid bed coating process applies the aqueous insoluble polymer onto the surface of the drug-loaded core to achieve desired product release profile. Due to the cost, time, and need for human subjects for *in vivo* drug release tests, the *in vitro* dissolution test is commonly used as a surrogate to predict *in vivo* behavior of traditional oral solid dosage form.[87] The conventional method of a dissolution test for an extended-release dosage form is laborious and time-consuming. It often delays the batch release and provides no benefit for the improvement of batch quality.[88] Predictive dissolution modeling is an emerging methodology defined as the ability to mathematically generate a time profile of the dissolved fraction of an API using information

including material properties, dissolution method conditions, formulation, and process parameters. The *in vitro* dissolution modeling in the pharmaceutical industry is mainly used for formulation and process development. Dissolution modeling can help screen the best plausible formulation for robust operational design space and patient performance. Dissolution prediction enables a fast comparison between candidates of excipients, which speeds formulation development. For real-time release testing (RTRT),[89] the model uses process understanding and real-time data to predict *in vitro* dissolution in continuous or traditional batch process manufacturing.[90] It can minimize or eliminate destructive dissolution testing and speed product release. In addition to the applications for product understanding and RTRT, dissolution models can work as surrogates for real-time monitoring, which initiates feedback and feedforward mechanisms to improve drug product consistency. However, despite the importance of dissolution modeling in product and process development, few literature reports show examples of dissolution models in a quality control environment and even fewer in RTRT situations.

In the development of predictive dissolution models, both empirical and first principle-based approaches can be employed for various intentions. The first principle-based approaches for dissolution modeling can be traced back to Arthur Noyes and Willis Whitney's work in 1897.[91] It described dissolution as a first-order rate process depending on the API solubility and a rate parameter. The process can be further reduced to a zero-order rate if sink conditions are assumed, and the dissolution rate parameters are often modified to match the experimental data.[92] The first principle-based dissolution modeling is usually encouraged in drug product development. The dissolution model can be developed from mechanistic models using dissolution contributing parameters (*e.g.*, solubility, pKa, average particle size) before a lab dissolution test is performed. It guides dosage and formulation development without conducting frequent dissolution testing.[89]

Empirical approaches for dissolution modeling are typically data-driven methods employing statistical inferences. Empirical models are generally developed with an intention for real-time release and quality control. A successful empirical model is heavily dependent on the process and product understanding, and as feedback, it can support product and process development. During the formulation and process optimization, it is a common practice to use response surface methodology for process modeling. Multi-linear functions are often utilized to describe the processes, and the desired dissolution profiles can be achieved based on those functions for both intermediate and modified release products. For a complex process like fluid bed coating involving multiple interactions, it is imperative to study the raw material characteristics in conjunction with the process parameters. With appropriate statistical treatment, the models can also utilize spectral data from noninvasive analytical tools as additional information to obtain a precise and accurate prediction.[93]

1.3.3.2 Process Analytical Technology

As part of the QbD paradigm, process analytical technology (PAT) is often utilized to help establish control strategies for both upstream and downstream manufacturing processes. In a basic control scheme, PAT provides continuous monitoring of CPPS, CMAs, or CQAs to demonstrate that the process is maintained in the design space and detects failure online or in-line. In addition, PAT detects the variability in the input materials in an advanced control system and enables timely adjustment of the process parameters to compensate for any adverse impact on the drug product quality. In this dissertation, two spectroscopic techniques are utilized: 1) in-line monitoring of loss on drying and coating weight gain using near-infrared spectroscopy, and 2) at-line monitoring of

API solid-state form (transition between theophylline anhydrous and monohydrate) using Raman spectroscopy.

Near-infrared Spectroscopy

As a rapid and non-destructive technology, near-infrared spectroscopy (NIRS) has been used for real-time monitoring of coating weight gain/film thickness for decades.[94-97] Most of the active pharmaceutical ingredients have IR-sensitive bonds, such as O-H, C=O, C-H, *etc*. Asymmetrical molecular vibration, stretching, and rotation lead to IR absorption. The NIR region, 800 – 2500 nm, represents information from overtones and combinations of the fundamental molecular vibrations.[98] The difference in the chemical composition of the coating film and the core substance allows the change of NIR incident radiation to be detected during the coating process. The peaks of the film increase, and the peaks of the core decrease on the reflectance spectra during the film deposition onto the core surface.[99]

Despite the advantages that NIR brings to coating monitoring, the broad and overlapping peaks are difficult to resolve. Scattering effects of physical variations such as density, particle size, and particle motion complicate the data analysis. Therefore, NIR was not adopted until the data treatment methods were developed and modern computational power was advanced. Qualitative and quantitative analyses such as principal component analysis (PCA), partial least squares regression (PLS), and support vector machine (SVM) became available to extract relevant information from the NIR data.

The first application of NIR spectroscopy for pharmaceutical coating was reported by Kirsch *et al*.[100] The authors utilized an at-line diffuse reflectance NIR spectrometer to monitor the film thickness of a tablet-coating process. A quantitative model was built on the correlation ($R^2 = 0.90$) between the NIR signal and the coating thickness. The NIR spectral increase was found in the

wavelength region of 1750-1850 nm, corresponding to the coating thickness. On the contrary, the 1500-1650 and 1950-2250 nm regions, which were related to the tablet core, showed decreasing trends of absorbance.

Andersson *et al.*[99] reported the first NIR in-line application for the pharmaceutical particle coating process in a fluid bed. This group mounted a fiber-optic probe at the sapphire window of the fluid bed to collect data every 0.25 seconds. The in-line collected NIR spectra required data filtration and smoothing to minimize the undesired signal caused by the particle motion. In the work of Andersson, eleven coating batches were conducted to capture the inter-batch variability to advance the model robustness to ensure the model accuracy in future batches. Bogomolov *et al.*[101] reported similar works using in-line NIR data for model calibration and test in a pilot-scale fluid bed coating process for pharmaceutical particles. The calibrated NIR model successfully predicted the coating thickness of the test batch. The successful in-line applications indicate that the NIR spectroscopy is suitable for coating monitoring but requires proper calibration and data treatment to build a robust predictive model.

Raman spectroscopy

Raman spectroscopy is one of the widely used techniques for detecting solid-state transformation.[102] In the application of Raman spectroscopy, a monochromatic laser interacts with molecular vibration, phonos, and other excitations in the sample, resulting in the energy change of the laser photons.[103] The energy change causes a frequency shift of the incident light and shows on a Raman spectrum. Molecules in crystal material are arranged in a repetitive structure, and the vibrational change of the long-range ordered structure is Raman sensitive. Comparing to NIR techniques, Raman spectra are usually less complicated and present well-resolved peaks. The

Raman data interpretation is, therefore, more straightforward and requires less chemometric analysis than NIR.

The application of Raman spectroscopy to detect solid-state transformation has been increasing in the past decades. Taylor *et al.*[104] reported a successful off-line application of Fourier transform (FT)-Raman spectroscopy to probe the solid-state form of active substances present in tablets and capsules containing enalapril maleate, prednisolone, Form I and Form II polymorphs of ranitidine, anhydrous and monohydrate theophylline, and warfarin sodium clathrate. Their work showed that Raman spectroscopy was a useful tool to determine the presence of different drug solid-state forms in intact tablets qualitatively.

Wikström *et al.*[105] utilized Raman spectroscopy for the in-line monitoring of process-induced hydrate formation. The Raman spectroscopy was successfully used to monitor the transformation of theophylline anhydrous to theophylline monohydrate during high-shear wet granulation. Raman spectroscopy is insensitive to water, making it attractive for pharmaceutical applications involving hydrate from characterization. The work of Wikström showed that Raman spectroscopy monitored the transformation kinetics of theophylline during the wet granulation, while NIR spectroscopy had strongly interfered with the presence of water. However, using a high-intensity laser can induce sample heating during Raman spectral scanning, potentially degrading the sample or converting the drug crystal to another solid-state form. The Raman heating effect on compressed theophylline monohydrate powder was studied by Johansson *et al.*[106] that the extent of heating depended on both the compactness of the powder and the laser power. Raman signal can be influenced by fluorescence which leads to a shape change of the entire Raman spectrum. A robust experimental design with proper data pretreatment is necessary for robust calibration development in such a situation.

1.3.3.3 Feedforward Control

Feedforward control measures the input variability and proactively adjusts the manipulated parameters before the process output changes.[107] The drug product quality is influenced by complex effects from monitored variables (*e.g.*, material attribute, environmental disturbances, or equipment drift) and manipulatable process parameters. Feedforward control provides an opportunity to account for the complex effects simultaneously and fulfills the requirements of control strategy in pharmaceutical product development (ICH Q8): "…the control of the process such that the variability (*e.g.*, of raw materials) can be compensated for in an adaptable manner to deliver consistent product quality."[108] The implementation of feedforward controllers falls along a spectrum of complexity. A simple feedforward controller detects the disturbance and gates the products to the waste,[109] while advanced feedforward controllers involve multivariate regression and global searching algorithms.[12, 13] Most publications discussed the simple or advanced feedforward control algorithms, but a few works were on when and how to apply feedforward control, especially in pharmaceutical manufacturing.

Igne *et al*.[2] demonstrated an approach that adapted the design space to raw material variability, equipment aging, and environmental changes in a feedforward manner. The feedforward component enabled a flexible manufacturing paradigm where the input materials could be less tightly constrained. Close *et al*.[110] provided an example of adaptive design space in the chromatographic purification process using a first-principle model combined with stochastic simulation methods.

Within the scope of QbD, the combined feedforward-feedback control system is often designed using a two-layer structure (Figure 1-5). The stabilizing layer stabilizes process variables at the

setpoints. A fast and straightforward feedback control loop, such as proportional-differential-integral controller (PID)[17] and fuzzy controller[111], is preferred at this layer. The optimizing control layer works in a feedforward manner[10, 12, 13] for the satisfaction of product CQAs. The key to building a successful feedforward controller is to gain adequate process and product understanding and identify sources of variability. Understanding sources of variability and their impact on the downstream process, in-process materials, and drug products provide the basis for process modeling, which allows us to predict the behavior of a manufacturing process and final product quality.

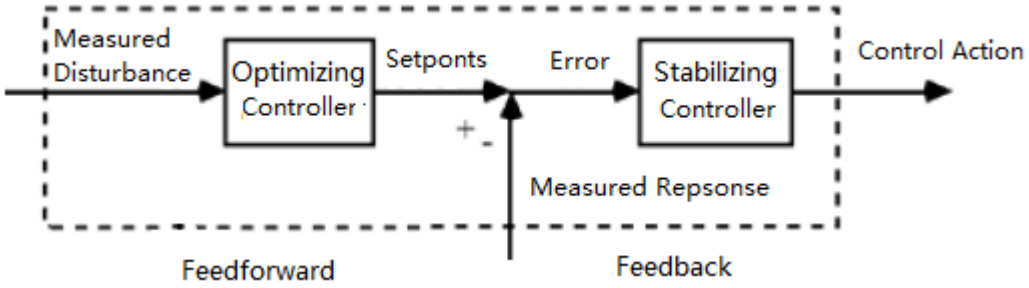

Figure 1-5: The cascade structure of a combined feedforward/feedback control, including an optimizing control layer and a stabilizing control layer.

The first attempt of developing the structured feedforward control strategy in the pharmaceutical industrial application was presented by Westerhuis *et al*. for a two-step batch process in 1997.[15] The powder mixture was granulated using wet granulation in the first step and the granules were compressed into tablets in the second step. An in-process control scheme was proposed to monitor the granule properties and adjust the compression settings of the process variables accordingly. The feedforward controller was built on the correlations between the CQAs and the process variables, the formulation variables of the powder blend, and the physical properties of the intermediate granules. Partial least squares regression (PLS) algorithm was

applied to overcome the overfitting problem caused by the collinearity of granule properties. Compared with ordinary least squares (OLS), the PLS regression had the advantage of reducing the high dimensionality space of the total variables into a lower dimensionality subspace of PLS components, called latent variables. Therefore, the value of the degrees of freedom required to estimate the model parameters was small enough that a limited number of experiments was sufficient.[13, 14] In the literature example (Figure 1-6), Batch B had a smaller mean granule size, higher bulk/tapped volumes than Batch A, although they were manufactured using the same settings of process parameters. The result revealed crushing strength and disintegration time of tablets from batch B were higher than the tablets from Batch A at the same moisture level and compression force. Therefore, a feedforward controller was developed to accommodate the impacts by adjusting the setting values of compression process parameters based on granule properties. The feedforward control scheme was built by constructing a contour plot including two variables: compression force and % moisture, to reflect the level of critical responses for each granulation batch. Near-infrared spectroscopy was used for real-time data collection in a similar study by the same authors.[112] The NIR spectra were subjected to a principal component analysis (PCA) and the scores of principal components of NIR were used instead of the physical (particle size) and physicochemical (API solid-state form) material attributes for the feedforward model calibration and implementation. The employment of NIR reduced the time, labor, and cost associated with material characterization but demonstrated similar model performance and control capability.

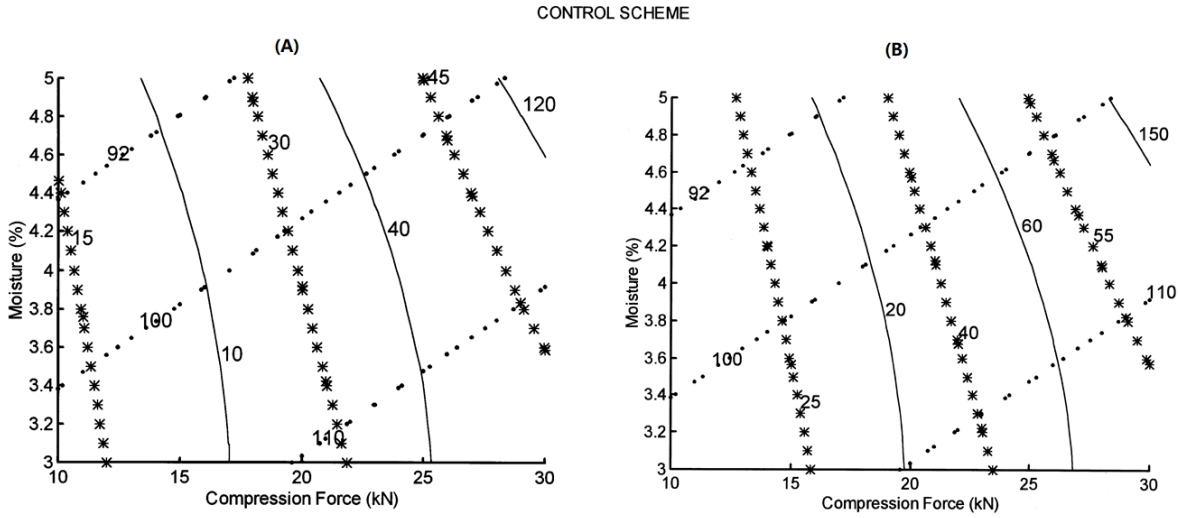

Figure 1-6：Contour plot of the control scheme for two batches of granules: A and B. Predictions for the ejection force (dashed line, unit: N), crushing force (stars, unit: N), and disintegration time (solid line, unit: s) are given for different setpoints of compression force (kN) and moisture in the granules (%). The plots are adapted from reference [15], permission granted.

Westerhuis's method relied on the contour plots for all critical responses, which required information from an extensive database of manufactured batches and intensive computational power. There was no optimization algorithm involved in the control application. The operators manually adjusted the parameter settings based on information from the contour plots and their prior experience, which introduced human error and undermined the control performance. Muteki *et al.* extended the work of Westerhuis[12, 13, 113] by integrating a sequential quadratic programming function to solve for the set values of process parameters, shown as Figure 1-7. The feedforward controller was applied on a blending – roller compaction – milling – compression manufacturing chain.[13] Four raw material attributes and six process parameters were evaluated in 11 experimental runs. PLS-2 regression models were independently established to correlate process parameters and material attributes with three tablet attributes: hardness profile, dissolution profile, and disintegration time (Array Y). The six process parameters (Array Z) and the material attributes

(Array X) of three excipients were arrayed in one matrix, experimental batches being rows and variables being columns. When implementing the controller, sequential quadratic programming was applied to solve the process parameters (Array Z).

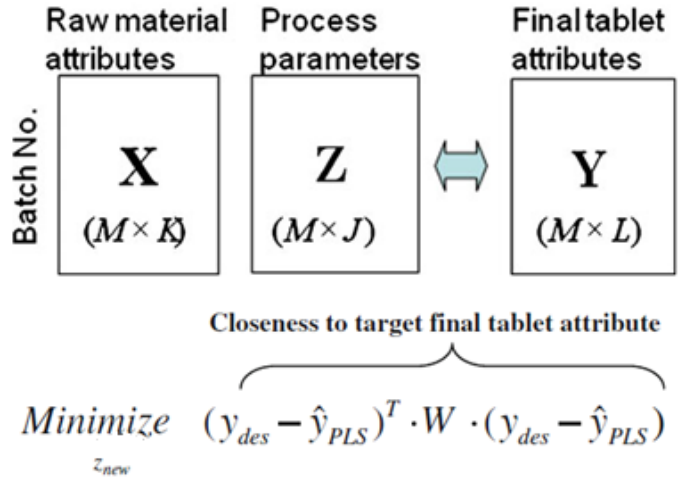

Figure 1-7: The structure of the feedforward controller. y_{des}: desired product quality profile, $\hat{y}_{PLS}$: model predicted quality profile, W: weight matrix, M: number of batches, K: number of raw material attributes, J: number of process parameters, and L: number of final tablet attributes, adapted and modified from reference [13], permission granted.

The optimization criterion was to minimize the difference between the PLS-2 model predicted and the target product attribute. The weight matrix W assigned different weights to the quality attributes based on their criticality. The model performance was examined by simulation, indicating a significant improvement in reducing the product failure. This approach offered several advantages over Westerhuis's method:

(1) it provided the specific solution of process parameters for a given raw material,

(2) it allowed for the simulation of the process to assess the impact of raw material and process variable on product quality to form an operating space,

(3) it provided information for setting meaningful specifications in incoming materials and in assessing excipients from new sources.

The models provided additional benefits in detecting changes in excipient characteristics over time and tracking the impact on product quality. However, there were certain limitations of this method, including

(1) the control performance heavily relied on the accuracy of the process model, and the feedback component cannot always mitigate the impact of uncertainty,

(2) the regression method modeled the responses separately and ignored the inherent correlation between the quality attributes, and

(3) the model development consumed substantial resources (material, time, and labor), and the controller was specific to one system and difficult to transfer between plants or across scales.

In his most recent study, Muteki *et al*. integrated near-infrared spectroscopy into the control system to improve the model accuracy and robustness. In the same publication, the researchers also demonstrated the scale-up of the feedforward control for wet granulation.[12]

Hattori *et al*.[16] proposed a similar control system using another form of regression. Process parameters instead of quality attributes were used as dependent variables and regressed on the linear combination of material attributes, in-process measurements, and quality attributes. Instead of minimizing a cost function, the solution of this controller could be obtained by direct projection. This approach significantly decreased the required computational power and could always generate a solution. However, the process model was difficult to be interpreted, and no constraints were applied. The solution of manipulated variables sometimes fell outside the operating range.

1.4 Summary

This dissertation aims to demonstrate a control strategy, including feedforward and feedback components, to reduce product batch-to-batch variability and grant flexibility based on incoming

materials. A systematic QbD approach is essential to establish a clinically relevant specification and design a robust formulation and manufacturing process. The QbD approach includes several key steps: establishing QTPP, product and process understanding, and developing control strategies. In this work, an extended-release multiparticulate oral dosage form was used as an example product, and the top-spray fluid bed aqueous coating was applied as the manufacturing process to produce such product. A series of tools, including risk assessment, DoE, PAT, and process models, is available to develop product and process understanding. A comprehensive control strategy that adjusts process parameters to compensate for undesired effects caused by material variability can be established at the final stage of the process development. The control strategy should be adaptable for newly discovered material attribute change, and the design space should be continually modified to those changes. Incorporating feedforward controllers in the control strategy allows the process to be robust against known material variability and environmental disturbance. Feedforward control is also a solution to adapt the design space to newly discovered measurable variabilities.

Chapter 2 : A Systematic Approach of Employing Quality by Design Principles: Risk Assessment and Screening Design to Demonstrate Process Understanding for Fluid Bed Coating of Theophylline Loaded Granules

Abstract

The objective of this study was to utilize risk assessment tools and statistical design of experiments (DoE) to identify critical formulation variables and process parameters for the manufacture of the extended-release granules using a top-spray fluid bed process. The formulation of the coating dispersion was determined based on literature research and a one-factor-at-a-time study. The effect of formulation factors, including plasticizer concentration and total solid/liquid ratio, was evaluated. Material attributes and process parameters were systematically assessed using failure mode and effect analysis (FMEA). The high-risk process parameters were further explored using a fractional factorial design to understand the fluid bed coating process and identify the critical process parameters (CPP) that significantly impact the quality of the final drug product. Inlet air relative humidity, product temperature, fluidization air volume, atomization pressure, and theoretical coating weight gain were studied in the DoE at a constant spray rate. The responses of the study were agglomeration, in-process loss on drying, and coating deposition rate. A study on film curing was followed in which curing time, temperature, and relative humidity were varied, and their impacts on *in vitro* dissolution and API solid-state form were investigated. The study demonstrated the application of risk assessment and DoE in identifying critical formulation and process variables of the fluid bed coating process.

2.1 Introduction

To successfully design a multiparticulate extended-release dosage form, the product and process developers must carefully consider three aspects: 1) coating formulation, 2) physicochemical properties of both the dosage form and the drug, and 3) process conditions. An aqueous coating formulation often includes a pseudolatex polymer as the base. The addition of plasticizers can enhance the flexibility of the film and facilitate polymer sphere coalescence. Anti-adherents are sometimes required to prevent agglomeration during the coating process and storage. Surfactants are often added into commercially available polymer dispersions to stabilize the polymer dispersion and promote the spreading of the atomized droplets on the substrate surface. Dyes or pigments, as process indicators, can facilitate the in-process visual monitoring of the experiments. The formulation variables were subjected to risk assessment and then studied using a DoE.

Top-spray fluid bed coating has advantages of large capacity, relative simplicity, and low capital cost.[114] Despite being used and developed for decades, fluid bed coating is a complicated process since many operating parameters can impact the coating quality. In practice, the fluid bed is operated at high fluidization air velocity to obtain adequate heat and mass transfer rate, high particle mixing rate, and bed expansion. The drug-loaded core should be strong enough to withstand fragmentation and attrition during fluidization. The drug itself must be stable to the elevated coating temperatures and the moisture challenge of aqueous film coating. The evaporation rate of the solvent is determined by the temperature, air velocity, and inlet air humidity. The coating process needs careful optimization since a high evaporation rate may cause undesired product attributes, such as cracks of coating layer[115] and the fissure of core particles.[116]

In contrast, low evaporation capability may lead to agglomeration of coated particles, and the bed of fluidized particles may be collapsed.[117] Coating efficiency is another challenge since the coating dispersion is sprayed in the counter direction to the fluidization air, resulting in losing coating droplets due to premature droplet evaporation or being carried over to the filter surface. Low coating efficiency leads to prolonged coating time, which costs time and resources and increases the risks of nozzle and filter failure. In addition to fluidization air, coating efficiency can be impacted by the interaction between atomization air pressure and spray rate, affecting the size and distribution of the coating droplets. It may alter the collision probability between droplets and core particles and may influence the spreading of the liquid on the particle surface, leading to variation in coating uniformity and ultimately change dissolution behavior.[118]

This chapter was to fulfill Specific Aim 1, defining TQPP, understanding the product and process, and identifying CPPs. A screening study utilized a full factorial design to investigate the impact of four factors, product temperature, air volume, atomization air pressure, and inlet air relative humidity, on process stability and efficiency. Theophylline anhydrous was the model drug, and the drug-loaded granules were prepared via high shear wet granulation. The film-coated products were subjected to a curing study. The effects of curing conditions and time on *in vitro* dissolution were investigated.

2.2 Materials and Methods

2.2.1 Materials and Coating Equipment

The theophylline-loaded granules (granule size range 355 – 710 μm) were obtained from Purdue University, West Lafayette, IN. The polyvinyl acetate aqueous polymer dispersion (Kollicoat SR 30D), lot nos 57675147G0/58378447G0, were obtained from BASF, Ludwigshafen,

Germany. Triethyl citrate 99% (TEC), used as a hydrophilic plasticizer, lot no. C09Y001 was obtained from Alfa Aesar, Ward Hill, WA. Talc, USP Grade, used as an anti-tacking agent, lot no. iEF0433 was obtained from Spectrum, New Brunswick, NJ. The FD&C blue 1 lake, lot no. A992, obtained from Warner Jenkison Company, St Louis, MO, was used as a color marker to monitor the progress of the coating process. All reagents utilized for assay and dissolution testing were HPLC grade.

A 7-liter top-spray fluid bed processor (Minilab, Diosna Dierks & Söhne GmbH, Osnabruck, Germany) was used for granular coating. The processor was coupled with an EGE-Electronik series LN/LG airflow sensor (Spezial-Sensoren GmbH, Gettorf, Germany) and two temperature/humidity transmitters (series RHL, Dwyer Instruments Inc., Michigan City, IN). The coating suspension was delivered into the system by a peristaltic pump (Series 120U, Watson-Marlow Inc., Wilmington, MA), and the weight change was monitored using a lab-scale precision balance (Mettler Toledo PL602E, Columbus, OH). The coating process was controlled by an integrated system where an open platform communication system (DeltaV V9.7, Emerson, MO) received analog signal and delivered digital tags to a real-time data management system (SynTQ V3.5, Optimal, UK) for control implementation.

2.2.2 Formulation Development Methods

The granule core was produced at Purdue University using high shear wet granulation, comprised of 60% w/w theophylline anhydrous, 18.5% w/w microcrystalline cellulose, 19.5% w/w lactose monohydrate, and 2% w/w hydroxypropyl methylcellulose. Theophylline is a BCS class I drug substance mainly used for the treatment of asthma. A few known anhydrous forms of theophylline include Form I, II, III, and IV, where Form IV was reported as the most

thermodynamically stable.[119] Theophylline also exists as a crystalline monohydrate. Conditions that introduce an aqueous solvent can promote pseudo-polymorphic change. The hydration and dehydration of theophylline are reversible, *i.e.*, the critical relative humidity (RH) for hydration was found to be at ca. 79%, while the critical RH for dehydration was *ca.* 30%.[120] The dehydration kinetics of theophylline monohydrate was investigated in several studies.[119, 121, 122] The most recent study revealed the dehydration occurred in two steps: (1) the monohydrate form transited to the metastable anhydrate (Form III) after losing water, and (2) the metastable polymorph (Form III) converted to the more stable form (Form II) during storage.[123] The aqueous solubility of theophylline monohydrate increases with a pH decrease, shown in Table 2-1. The solubility of the anhydrous Form II is not readily measurable, but it can be approximated by comparing its initial dissolution rate (5 folds higher) to the monohydrate form.[124]

Table 2-1: Solubility of theophylline monohydrate at different pH values, data adapted from ref. [125]

pH	Solubility (mg/mL)
7.4	6.92
5.5	7.03
4.3	7.76
3.5	9.48

The coating film formulation was designed based on process requirements and a literature survey.[126-128] Polyvinyl acetate (PVAc) was the coating polymer, triethyl citrate (TEC) was the plasticizer, and talc was the anti-tacking agent. A proper parameter to consider in evaluating various polymers was the minimum film forming temperature (MFFT). Literature suggests that during manufacturing, the process temperature needs to be at least 10 °C above the MFFT to achieve good film quality.[129] Polyvinyl acetate provided the process advantage that the low MFFT (18 °C without plasticizer) of PVAc allowed for a flexible coating temperature and had no

requirement for further thermal treatment (curing).[128, 130] Polyvinyl acetate was an atactic, non-crystalline, thermoplastic, and water-insoluble polymer synthesized from the corresponding vinyl acetate monomers. The acetate groups were not ionizable, resulting in a pH-independent film coating.[131] Kollicoat SR 30D was a commercial PVAc product stabilized with 9% povidone and 1% sodium lauryl sulfate. PVAc formed the aqueous insoluble barrier, while povidone worked as a pore-forming agent. The lot-to-lot variability of the polymer dispersion, regarding agglomeration (<0.5%), residual monomers (<100 ppm), density (1.045 – 1.065 g/cm^3), and acetic acid (<15000 ppm), was listed in the safety data sheet. In house testing indicated the solid content ranged from 28.5-31.5 g/100g, and the apparent viscosity of the received ranged from 50-60 mPa. PVAc films tend to swell when contacting with the aqueous medium and gradually close the aqueous channels.[128] Triethyl citrate (TEC) was employed as the plasticizer. As an aqueous soluble plasticizer, TEC can migrate from the coating to the medium during dissolution testing, function as an additional pore forming agent and increasing the drug release rate.[132] As a result of low MFFT, the polymer coating film can be sticky, and the addition of an anti-tacking agent is often necessary. The commonly used anti-tacking agent, talc, was selected. Blue lake (0.15% w/w of the total weight of polymer dispersion) was also added into the formulation as a process indicator. With the excipient determined, an initial risk assessment was performed to evaluate the coating formulation and material attributes to direct further experimental investigation.

2.2.2.1 Initial Risk Assessment Methods

An initial risk assessment of the drug substance was performed to evaluate the impact of each attribute (*e.g.*, solid-state form, particle size, solubility, impurities, and chemical stability) on the drug product CQAs. Failure mode effect analysis (FMEA) was employed to perform the risk

assessment. A team of experts in regulation, pre-formulation, formulation, and manufacturing initiated the assessment with brainstorming and identified a list of failure modes. The author of the dissertation was one of the team members and independently assigned the scores of severity, occurrence, and chance of detection to the failure modes. The severity was assessed with the assumption that the failure occurred and impacted the final products. Since this study aimed to demonstrate the process development, the severity was scored on a scale of 1 - 5 as follows:

1. has no appreciable consequences to quality (root cause is well understood)
2. batch loss
3. batch loss and mild risk to the patient
4. between 3 and 5
5. batch loss and severe (potentially lethal) risk to the patient

The occurrence is the numerical presentation of the likelihood that the cause of the failure mode will occur during the product lifecycle. The initial risk assessment assumed proper control strategy was not established to reduce the likelihood. The criteria of assigning the occurrence scores were as follows:

1. failure is very unlikely to occur
2. relatively few failures
3. occasional failures
4. repeated failures
5. failure is almost inevitable

The chance of detection is the probability of detecting the outcome or the cause of a failure mode, assuming the failure already occurs but DoEs not impact any patient yet. The criteria to assign values of detection were tailored in the following list:

1. the failure and its subsequence are almost certainly detected
2. high chance to detect the cause or impact of the failure mode
3. moderate chance to detect the cause or impact of the failure mode
4. low chance to detect the cause or impact of the failure mode
5. the cause or impact of the failure mode cannot be detected, or there is a system for detection.

The risk priority number (RPN) was calculated from the product of the three parameters, and the relative risk of each drug substance attribute was ranked as high (RPN 60 -125), medium (RPN 31-59), or low (RPN 0 -30). The high risk is unacceptable and warrants further investigation, whereas the low and medium risks are acceptable and require fewer studies. It should be noted that the RPN values are not absolute measurements. The threshold values were used as references, but we did not assess risk purely based on the RPN values. The high severity failure modes were considered more critical and given high priority in experimental investigation.

2.2.2.2 Design of Experiments

A preliminary study was performed to test the selected excipients. The coating dispersion composition, shown in Table 2-2, was determined based on the literature provided formulation.[129] The amounts of anti-tacking agent and plasticizer were set at 15% and 10% of the dry polymer, respectively. The coating dispersion was prepared by diluting the commercial polymer dispersion with water. Triethyl citrate was added with continuous stirring of a magnetic stirrer. Talc and Blue Lake were then added and mixed for six hours. Before coating, the dispersion was screened through a 180 μm screen. The formulation was evaluated using a coating process of a 400 g batch size. Initial process parameters were selected based on previous experience: spray rate at 6 g/min, product temperature range at 30 - 40 °C, atomization air pressure at 1.6 bar, and air volume at 30

m^3/h. The granule size range was controlled at 500 -600 µm, and the environmental humidity range was 20% - 40% RH to exclude the interference of material and environmental disturbances. Samples were pulled at different theoretical polymer coating levels: 10%, 15%, 20%, 25%, and 30%. The samples were dried until the LoD was less than 2% and evaluated for drug release by dissolution testing. The drug release profile was too fast at 10 and 15% theoretical polymer coating and too slow at 30% theocratical polymer coating. Further optimization focused on 20% - 25% coating level. The amount of talc (15% w/w) was found adequate to prevent sticking, and thus no further optimization was performed for talc. Water in the coating dispersion served as a solvent and evaporated during the film formation. It was expected to influence the coating process and further investigated. The compatibility study of API and excipients was conducted wherein the coated granules (30% coating level) were stored at 50°C/75% RH conditions for 60 days. No significant decrease in API concentration was observed (significance level $\alpha = 0.05$).

The optimization study was performed using one-factor-at-a-time experiments. TEC concentration was evaluated at three levels: 5%, 10%, and 15% w/w of the dry film. With the optimal TEC concentration being determined, the solid content of the coating dispersion was studied at three levels: 12.9%, 18.9%, and 24.9% w/w. The coating weight gain level was targeting at 25% w/w. The responses studied were the percentage agglomeration and *in vitro* dissolution. The drug fractions released at specific time points were often taken to represent product dissolution behavior. However, the errors of drug fraction released at the sampling time points were often not homoscedastic.[133-135] Instead, the time that 50% of the drug was released was the studied response in the statistical design of experiments. The center points were replicated for both studies to evaluate the pure error and lack of fit. The experimental results were analyzed using analysis of

covariance (ANCOVA) to eliminate the variance caused by the unwanted covariate - actual coating level.

Table 2-2: Formulation of the coating dispersion at the center point. The commercial coating polymer dispersion consists of three components: 70% water, 27% PVAc, 2.7 % PVP, and 0.3 % SLS where the solid content is 30%.

Coating Dispersion Formulation		
Component	Function	Levels （% w/w）
Polyvinyl acetate (PVAc), Povidone (PVP), Sodium Lauryl Sulfate (SLS)	Commercial Coating Polymer	50% (50% ×30% = ×15% in terms of solid content)
Triethyl Citrate (TEC)	Plasticizer	1.5%
Talc	Anti-tacking agent	2.25%
Blue Lake	Color agent	0.15%
Total Solid Content		18.90%

2.2.3 Process Development Methods

The process development was conducted after the coating formulation was fixed. The entire manufacturing process included four steps: 1) sieving uncoated granules, 2) polymer coating, 3) curing, and 4) sieving coated granules. The process development mainly focused on polymer coating and curing. The first sieving was performed before the coating process to obtain desired sieve cut of the uncoated granules. Although fragmentation and attrition of the uncoated granules may occur due to the particle-particle collision, the drug assay and content uniformity of the uncoated granules were examined prior to coating. API losses (1-3% w/w) due to sieving were detected in all batches. Thus, the drug potency of uncoated and coated granules was closely monitored to reduce the risk of this procedure on assay and content uniformity. The second sieving step was performed on the coated granules to exclude agglomerates and fines generated during the coating process. There was a chance that the film coating may be damaged if excessive force was

used during sieving. Considering the high flexibility of PVAc polymer and the addition of a plasticizer, the expected occurrence rate of the film rupture was low.

Coating

The coating was performed using the fluid bed to deliver film onto the surface of the drug load granules via a 1 mm nozzle spray gun. An OPC-SynTQ control system controlled the process parameters, including fluidization air volume, inlet air temperature, and pump rotation speed. The fluctuation of fluidization air volume was within +/-0.5 m^3/h deviation from the set point. The temperatures were controlled by turning on and off the heater so that the inlet air temperature variation was from -5 °C to +10 °C relative to the set point. However, the product temperature showed relatively consistency with +/- 0.7 °C standard deviations. The pump rotation speed (rpm/min) was calibrated to the spray rate (g/min). The natural fluctuation of the spray rate was lower than 0.1 g/min. Atomization air pressure was manually controlled by adjusting the air gauge on the fluid bed. The input variables, including material attributes (*e.g.*, particle size distribution, fragmentation resistance, moisture level, granule assay, and content uniformity) and relative humidity, contribute interactively with the process parameters to the product quality. Those variables were evaluated on their effects using risk assessment and followed by a factorial design of experiments.

Curing

Although the vendor states that curing is not required for PVAc, scientific publications reported contradictory results,[128, 136] Dashevsky *et al.*[128] indicated that post coating thermal treatment was unnecessary because of the low minimum film formation temperature of Kollicoat SR 30D (18 °C). Instead, curing at an elevated temperature (60 °C) for 24 h caused ibuprofen diffusion into the polymer film due to the drug and polymer affinity, which increased drug release. In contrast, Shao

et al.[136] coated highly aqueous soluble compound (diphenhydramine hydrochloride) loaded pellets with a polymer film using premixed formulations of Kollicoat SR 30D and three different plasticizers. They observed that, at the 40 °C/75% curing condition, the dissolution rate gradually decreased over time, and the type of plasticizer influenced the change of the dissolution rate. Therefore, a curing study was performed to evaluate the effect of thermal treatment on our product, the PVAc film coated theophylline granules.

2.2.3.1 Initial Risk Assessment Methods

The initial risk assessment of the overall manufacturing process was performed in two steps. An Ishikawa fishbone diagram (shown in Figure 2-1 in Section 2.3.2.1) was first applied to list potential parameters that can significantly impact the quality of the final drug product, including manufacturing operations, environmental conditions, input material, and analytical methods. The extensive initial list of potential parameters was subsequently narrowed upon performing failure modes and effects analysis. To assign risk level, a team of experts participated in a brainstorming to determine the scores of severity, occurrence, and detection. Risk priority numbers were then calculated and ranked to identify the parameters with high (RPN 60 -125), medium (RPN 31-59), or low (RPN 0 -30) risks.

2.2.3.2 Design of Experiments

Conducting DoEs to evaluate all material and process variables of the fluid bed coating process in one study is not feasible. In the formulation studies, the actual coating level showed a significant impact on the drug release of the coated granules. The desired dissolution profile was found at the theoretical coating level of 20% - 25% w/w. The actual weight gain varied based on the coating

deposition rate. Therefore, the high-risk variables, *e.g.*, particle size distribution and spraying time, were investigated after the screening study when the coating process was better understood. Spray rate was a process parameter that could rapidly change the liquid input of the coating system. It was kept constant at 5 g/min in the screening study, and it was used as a feedback control input for in-process moisture levels in later studies (Details are described in Chapters 3 and 4).

Following the initial risk assessment, the DoE studies were split into two stages to identify and optimize critical process parameters.

1. a screening DoE study was conducted to assess the impact of process parameters on the batch loss.
2. an optimization DoE study was conducted to explore the knowledge space and establish process models to facilitate the construction of control systems.

In the screening study, a 2-level 4-factor Fractional factorial design was applied to evaluate the effects of three critical process parameters (identified from initial risk assessment) and one environmental variable. They were product temperature, atomization pressure, fluidization air volume, and inlet air relative humidity. The relative humidity was based upon the relatively consistent ambient temperature (20 -21 °C). The levels of the factors are shown in Table 2-3. The numerical values of the design levels were determined based on preliminary coating experiments, which demonstrated a successful coating run and allowed substantial changes in the experimental responses. This design aimed to verify the critical process parameters and understand their influence on the process and final drug product. The factors of the design were evaluated on main effect and interaction terms. The 2^{4-1} fractional factorial design allowed us to gain the essential information from a reduced number of experiments. The resolution of the design was IV (I=1234). In this design, two-way interactions were confounded, *e.g.*, the interaction of product temperature

and atomization pressure (12) was confounded with the interaction of air volume and relative humidity (34). The main factors were not confounded with other main factors or interaction terms. Six center points were produced to determine pure error (random batch-to-batch variability) and check for curvature effects. In total, 14 experimental runs were conducted: 8 design points and 6 center points. The experimental runs were not randomized in time sequence because the variation of inlet air relative humidity came from the seasonal change. Hence, the relative humidity level was a range instead of one value. Responses studied were agglomeration, steady-state moisture level, and coating deposition rate. The data from the screening study were analyzed by ANOVA using JMP. The significance of each term was deduced using the F-test and p-values calculated from the total sum of squares, the sum of squares of error, and the sum of squares of model.

Table 2-3: Fractional factorial design of the 2^{4-1} coating process screening study.

Relation	I=1234			
Resolution	IV			
Factor Number	Variable Name	Low (-1)	Center (0)	High (+1)
1	Product Temperature (°C)	30	33	36
2	Atomization pressure (bar)	1.4	1.6	1.8
3	Inlet air Relative humidity (% RH)	Low (20 – 30)	Medium (40-50)	High (70-80)
4	Fluidization Air Volume (m^3/h)	25	30	35
	Spray Rate (g/min)		5 (5.5 rpm)	

A narrow particle size distribution of 350 – 500 µm sieve cuts was utilized to conduct all experiments. The starting batch size was 400 g for all coating experiments. The fluid bed was preheated to 30 °C before charging the granules. The coating spray was started after the granules were equilibrated to the desired product temperature (38 °C, requiring around 5 min). Atomization air pressure and fluidization air volume (based on design points) were fixed while the inlet air

temperature was adjusted during the spray rate ramp-up to maintain the target product temperature (based on design points). The spray pump speed ramped up from 2.5 rpm to 4 rpm, and then to 5.5 rpm (approximately 3, 4, and 5 g/min spray rate) in 10 minutes and then was kept constant at 5.5 rpm. Room temperature and inlet air relative humidity (RH) were monitored for all individual batches. The coating process was terminated at 22.5% w/w theoretical weight gain, and the batch was transferred to a tray to dry at 35 °C for 48 h. The actual weight gain of every batch was measured, and the data were used to calculate the coating deposition rate.

One of the six center batches of the film-coated granules was randomly selected for the curing study. The actual coating weight gain of this batch was 19% w/w. A two-level, two-factor design and one additional condition were applied: two humidity chambers with saturated sodium chloride solution (~75% RH) at either 35 °C or room temperature (20 - 22 °C), two humidity chambers with saturated lithium chloride solution (~11% RH) at either 35°C or room temperature (20 - 22 °C), and a refrigerator condition (4 °C, ~15% RH). Data logger (EasyLog EL-USE-2 Lascar humidity and temperature USB logger, Lascar Electronics inc. Erie, PA) was used to track the temperature and relative humidity change upon the storage. Samples were taken and subjected to an *in vitro* dissolution test on Days 0, 3, 7, 14, and 21. Afterward, an additional study was conducted to understand potential solid-state form transformation and its influence on the dissolution profile of coated granules. One batch of coated granules, assumingly with the same assay and coating weight gain, was split into three parts and stored in three different humidity conditions: 11% RH, 52% RH, and 75%RH at 23 °C. After 30 days, samples were taken and subjected to 3D-Raman imaging and *in vitro* dissolution test.

2.2.4 Test Methods

The methods to characterize uncoated and coated granules are listed in this section. The quality attributes of coated granules include assay, loss on dry, weight gain, dissolution profile, and API solid-state. The characterization methods for those attributes will be described along with the evaluation method for coating deposition rate. For uncoated granules, an in-house method was developed and utilized to evaluate the fragmentation resistance of uncoated granules. fragmentation-sensitive granules tended to break apart and generate excessive fines in the fluidization process. fragmentation resistance of 97% was arbitrarily used as a threshold to select uncoated granules for formulation and process development. The batches with lower fragmentation resistance than 97% were rejected. The fines generated from the fluidization process were monitored in the process development.

2.2.4.1 Granule Fragmentation Resistance

Retsch mill (model MM200, Retsch, Inc. Newtown, PA) was used to simulate the fragmentation and attrition that granules underwent during the fluid bed coating process. The Retsch mill was used to shake a scintillation vial containing uncoated granules at 30Hz for 10 min. Two grams of granule samples were sieved through a 60-mesh sieve (250μm) before the shaking. Sieve was tapped at a frequency of 30 min^{-1} for 10 minutes (model SS-3, Gilson Company, Inc., Lewis Center, OH). Fines were removed. The granules that remained on the sieve were weighed (m_{total}) and transferred into the vial and subjected to the shaking of the Retsch mill. Since no milling ball was used in the shaking process, the low loadings (around 2 g) and high frequency (30Hz) setting allows the uncoated granules to collide against each other or against the vial wall, simulating the impact in a fluid bed. Fragmentation is the primary mechanism of size reduction.[137]

The granules were transferred back onto the 60-mesh sieve after the shaking and subjected to the same tapping procedure. The granules that remained on the sieve were weighed again (m_{remain}). The weight-based fragmentation resistance was calculated using the following equation (Eq. 2.1):

$$Fragmentation\ Resistance = \frac{m_{remain}}{m_{total}} \times 100\% \qquad Eq.\ 2.1$$

2.2.4.2 Sieve Analysis

The sieve analysis was performed to separate the fines, single coated granules, and agglomerates. The coated products were screened through the sieve stacked consisted of 850 and 250 μm screen sieves. The mechanical shave shaker (Series # 18480 CSC Scientific Co Inc. Fairfax VA) works in a throwing motion with angular momentum. The amplitude was set at level 3 and the sieving time was 15 min. The granules retained on the 850 μm screen were collected and weighed to determine the degree of agglomeration. The granules retained on the 250 μm screen were collected as the coating product for the following analyses. The granules that fell through the 250 μm screen were treated as fines and were discarded. This process was repeated until the weight change of the fines, products, and agglomerates was negligible.

2.2.4.3 Assay, Loss on Drying, % Actual Weight Gain, and Coating Deposition Rate.

The % actual weight gain and coating deposition rate were calculated based on product assay and loss on drying (LoD). The assay of uncoated and coated granules was determined using a UV/Vis spectrometer (Agilent, Santa Clara, CA). 150 mg of uncoated granules were precisely weighed and dissolved in 500 mL DI water via 60 min sonication (Branson 8510 ultrasonic cleaner, Branson Ultrasonic Corporation, Danbury, CT) to prepare the sample solution. Three replicates of samples were prepared for every batch, and three repetitions were collected for each replicate.

Reference cells that contained only DI water were collected each time the UV/Vis test started. The sample absorbance value at a single wavelength (272 nm) was recorded to predict API content by interpolating a five-point linear regression calibration model of theophylline content. The same method was applied to coated granules for API content with one additional step: the coated granules were ground before the dissolution and sonication.

Loss on drying measurement was performed using a moisture analyzer, Computrac Max-2000 (Arizona Instrument LLC, Chandler, AZ). Approximately 1 g of granules was ground using mortar and pestle. The ground powder was precisely weighed in an aluminum pan by the instrument before the test. The testing temperature ramped up from 35 to 110 °C then stabilized at 110 °C until the weight change of the powder was less than 0.01%. The percentage loss of the powder was recorded as LoD values. Actual weight gain from the coating is calculated based on assay and LoD from coated and uncoated granules, as shown in Eq. 2.2.

$$\%\ actual\ weight\ gain = \frac{\frac{API\ content_{uncoated}}{(1 - LOD_{uncoated})} - \frac{API\ content_{coated}}{(1 - LOD_{coated})}}{\frac{API\ content_{coated}}{(1 - LOD_{coated})}} \times 100 \qquad \textit{Eq. 2.2}$$

The coating deposition rate was defined as the ratio between the deposited film weight and the theoretical weight based on consumed suspension. It was calculated from the actual weight gain and theoretical weight gain (22.5%), as shown in Eq. 2.3.

$$Caoting\ deposition\ rate = \frac{\%\ actial\ weight\ gain\ (\%)}{\%\ theoretical\ weigh\ gain\ (\%)} \times 100 \qquad \textit{Eq. 2.3}$$

The coating deposition rate was used to indicate the efficiency of polymer droplet deposition and film formation. This parameter is essential to determine the process endpoint for the coating process when there is a lack of a real-time monitoring system.

2.2.4.4 3D-Raman imaging

The 3D-Raman images of the coated theophylline samples were collected using an H2Optx mPAT lab coupled with Pillerater (h2Optx, Inc. San Jose, CA). The granule samples were compressed into tablets with microcrystalline cellulose (MCC, a mixture of Avicel PH 105 and PH 101) as extragranular excipients. The weight ratio between granules and MCC powders is approximately 1:3. A 4 mm X 4mm area in the center of each tablet was scanned by the incident laser excitation (785 nm), with an operating amperage of 90 mA and exposure time of 10 ms. The Raman shift was measured from 100 to 1900 cm^{-1} wavenumber range. The spatial resolution of one image layer was 10 µm, one pixel being 10 µm X 10 µm. The tablets were sliced into 20 image layers with 20 µm third dimensional spatial resolution and scanned in sequence. The layers were assembled using Image-J to form 3D images with a voxel of 10 X 10 X 20 µm. The Raman data were processed and mapped using Meta Analyzer (h2Optx, Inc. San Jose, CA).

2.2.4.5 In vitro Dissolution

The *in vitro* drug release studies were conducted on the encapsulated coated theophylline granules (400 mg coated granules per capsule containing approximately 200 mg API) in 900 mL of DI water using a USP apparatus II – paddle-type at 75 rpm and 37 ± 3°C. The capsules were dropped into the dissolution media using spiral capsule sinkers. The samples were drawn every 10 minutes using an autosampler and measured using a UV/VIS spectrometer (Agilent 8453 UV-Visible Spectrophotometer G1103A, Agilent Technologies, Cranberry Twp, PA) at 272 nm wavelength. Phosphate buffer with pH = 4.5 was also used in the dissolution method development compared to DI water. No significant difference was found between the dissolution profiles of the capsules dissolved in phosphate buffer and DI water (F2 = 92.5). The fraction of drug released was

normalized to 100% released; the time point at 1,440 minutes was used for that purpose. Three replicates were tested for each design point.

2.3 Results and Discussion

This study aimed to gain product and process understanding and identify critical process parameters to manufacture extended-release multiparticulate drug dosage forms. Risk assessment and design of experiments were sequentially used for formulation and process development. In both cases, the high-risk formulation or process variables were qualitatively identified, and then experiments were designed to collect quantitative information.

The quality target product profile (QTPP) for the theophylline coated granules was defined to facilitate the design of the product and the associated manufacturing process. The core part of the QTPP was established based on the knowledge of the drug substance and compendial standards, shown in Table 2-4. The dosage form was selected to grant pharmacokinetics and dose flexibility. The route of administration was determined based on patient compliance. Typically, the dosage strength should be determined based on clinical studies and the target patient population. However, this study was designed to demonstrate a fluid bed coating process development so that the dosage strength was determined based on the uncoated drug-loaded granules and the target coating weight gain. The product quality attributes were identified, taking account of the patient safety and product efficacy.

Table 2-4: Quality Target Product profile of the Theophylline Coated Granules

QTPP Elements	Target
Dosage Form	Extend Release Multiparticulate granules
Route of Administration	Oral
Dosage Strength	250 mg
Drug Product Quality Attributes	Identification
	Assay
	Content Uniformity
	Drug Release
	Moisture
	Microbial Limits

After the QTPP was defined, the drug product quality attributes were listed, and the criticality of every potential attribute was evaluated using an initial risk assessment. The justification is listed in Table 2-5. The following risk assessments of product and process focused on the attributes of high criticality.

Table 2-5: Criticality and justification of the potential quality attributes for the coated granules

Critical Quality Attributes	Criticality	Justification
Identification	Low	The substance was identified and controlled upstream in the high shear wet granulation.
Assay and Content Uniformity	High	Sub potent and super potent granules will steady-state moisture level variability in dose and dissolution profile.
Drug Release	High	Various material attributes and process parameters may influence drug release. It reflects in-vivo performance: bioavailability to a certain degree.
Moisture	High	Theophylline is chemically stable but may transfer to its monohydrate form in the presence of excessive moisture. It may impact the drug release.
Microbial Limits	Low	The granules are coated with a hydrophobic polymer that does not promote microbial growth.

2.3.1 Formulation Development

For multiparticulate coating systems, the properties of the drug-loaded core and the coating formulation will have a significant impact on the critical quality attribute of the drug product. In this study, the theophylline granules were produced at Purdue University; hence the granule formulation was not included in the formulation risk assessment. Because of the independence

between formulation variables, we performed the formulation screening experiments using the one factor at a time approach to study plasticizer concentration and solid content successively.

2.3.1.1 Risk Assessment

A summary of the risk assessment of the drug substance attributes on the drug product is presented in Table 2-6. The drug-loaded granules were produced using high shear wet granulation. With intensive shear and mixing, assay and content uniformity were unlikely to deviate substantially from the label claim. The potency of the uncoated granules was monitored for each batch. The coating process does not introduce additional API into the system, and the potency of the coated granules was monitored as well. The risk of assay and content uniformity was low. The drug substance supplied by the vendor is consistently pure with <0.05% impurities, reported on the safety data sheets. The risk of the coating process introducing additional impurities is low. Solid-state form and solubility were identified as high risks that may impact drug release. Theophylline may convert to its hydrate form during wet granulation and aqueous fluid bed coating processes, and this transformation may impact drug release. Theophylline has a high intrinsic dissolution rate and a high solubility. It may migrate into the coating film and potentially impact the drug release.

Table 2-6: initial risk assessment of the drug substance attributes.

CQA	Drug Substance Attributes				
	Solid-state Form	Particle Size	Solubility	Impurities	Stability
Assay	Low	Low	Low	Low	Low
Content Uniformity	Low	Low	Low	Low	Low
Drug Release	High	Low	High	Low	Low

In the initial risk assessment of coating formulation, briefly shown in Table 2-7, the formulation variables were evaluated against drug release, and the risk level was assigned based on prior

knowledge and literature. Justification for the risk ranking is presented in Table 2-8. The high-risk variables were further studied to reduce the risk to an acceptable level.

Table 2-7: Initial risk assessment of the polymer coating formulation

CQA	Coating Formulation Variables						
	Coating Level	Polymer Aging	Lot-to-lot Variability	Pore Forming Agent Level	Plasticizer Level	Anti-tacking Agent Level	Viscosity
Drug Release	High	Low	Low	High	High	Medium	low

Table 2-8: Justification for the initial risk assessment of the formulation variables drug dissolution

Formulation Variables	Justification
Coating Level	The coated granules may have an undesired extended drug release profile if the coating level is suboptimal. The risk of the polymer coating level is high.
Polymer Aging	Polymer aging or degradation may alter the polymer properties and affect drug release, but the stability of PVAc was well studied, and the degradant of PVAc (acetic acid) will not significantly change drug release profile [129]. The risk is low.
Lot-to-lot Variability	Lot-to-lot variability is controlled by the chemical supplier (BASF) with a tight specification, and those properties are unlikely to impact the coating process. The risk is low.
Pore Forming Agent Level	A pore former in the film will dissolve in aqueous solution and form channels for drug release. The addition of a pore-forming agent will substantially impact drug release. The risk is high
Plasticizer Level	Plasticizers influence the film formation and function as a secondary pore former. The plasticizer level will substantially impact the drug release. The risk is high
Anti-tacking Agent Level	An insufficient anti-tacking agent may lead to agglomeration and twining of coated granules. However, talc may increase the hydrophobicity of the film, resulting in a change of drug release profile. Based on previous experiments, 15% w/w talc was enough to prevent tackiness and provide the desired dissolution profile. The risk is medium.
Viscosity	The viscosity of an aqueous pseudo-latex coating dispersion is low. The risk is low.

2.3.1.2 Experimental Data Analysis

Two stages of one-factor-at-a-time experiments were conducted for formulation development. In the first stage, three levels of plasticizer (TEC) concentration, 5%, 10%, and 15% w/w of the drying polymer film, were studied. The 10% w/w level was repeated three times. The second stage was designed based on the results of the first stage. The optimal plasticizer concentration (5% w/w) was employed while the solid content was studied in three levels. The detailed experimental design

and the results were listed in Table 2-9. The target coating weight gain was 25% w/w. The actual weight gains were substantially lower than the target because of the unoptimized coating efficiency. Due to the preheating loss of particle fragmentation, the actual weight gain was calculated using Eq. 2.2 and was treated as a covariate for statistical analysis. The coefficient of determination (R^2) between TEC level and actual weight gain is 0.0147, indicating a lack of collinearity between the two independent variables. Analysis of covariance was performed to adjust the values of the responses (agglomeration and drug release) based on the actual weight gain so that the error was corrected, and the focus is on the effect of TEC levels.

Table 2-9: Effect of coating formulation variables on coated granule characteristics

Order	Batch No.	Factors			Response		
		TEC level (%)	Solid Content (%)	Weight Gain (%)	Agglomeration (%)	Time of 50% drug released (h)	Comments
Study on TEC							
1	2	10	18.9	22.1	8.8	4.15	
2	3	10	18.9	19.8	9.1	3.72	
3	1	5	18.9	21.6	3.4	3.37	
4	4	10	18.9	20.8	10.7	3.81	
5	5	15	18.9	21.3	33.3	4.53	Large agglomerates formed
Study on Solid Content							
6	6	5	18.9	20.5	5.2	3.21	
7	9	5	24.9	21.6	16.1	3.98	Nozzle clogged after 91 mins
8	7	5	18.9	19.5	3.5	3.12	
9	8	5	12.9	20.1	4.1	3.33	

Stage 1: TEC level

The covariate (actual weight gain) effect was estimated on the 10% TEC batches (Batch No. 2, 3, 4). At 18.9% solid content, the actual weight gain had a minimum effect on agglomeration with

an R^2 = 0.05 and p-value = 0.86. Thus, no adjustment was needed for % agglomeration. The ANOVA model (Table 2-10) revealed that the TEC level significantly impacted the % agglomeration at a 95% confidence level. The % agglomeration decreased with decreasing amounts of TEC. In addition, large agglomerates due to film tackiness were observed during the coating process with 15% TEC as the plasticizer.

Table 2-10: ANOVA results for the effect of TEC level on % agglomeration.

ANOVA					
Source of Variation	df	SS	MS	F	p-value
Between Groups	2	540.2	270.1	258.9	0.003847
Within Groups	2	2.086	1.043		

The correlation between the covariate (actual weight gain) and the response (time of 50% drug released) was 0.969 with a p-value of 0.158. Since only three batches were included in the regression analysis to estimate two parameters, a significance level of α = 0.2 was used for the covariate. The regression equation (Eq. 2.4) was presented as follow:

$$Time\ of\ 50\%\ drug\ released = 0.1906 \times actual\ weight\ gain - 0.0902 \qquad Eq.\ 2.4$$

where 0.1906 is the slope indicating the rate of change in the dissolution time depending on the change of actual weight gain. The standard error (ε) was adjusted to 0.079 from the regression analysis (ε = 0.107 without the covariate adjustment). The mean values of the time of 50% drug released for 5%, 10%, and 15% TEC levels were adjusted to 3.24, 3.89, and 4.45, respectively. The statistical significance of the ANCOVA model was determined using an F-test, p-value < 0.05. The increased TEC level increased the time for 50% drug to release. Increased twinning granules were observed with the increase of the TEC level; the decreased surface area due to twinning was probably the primary cause of the decrease of dissolution rate. Comparing to the effect of twinning, the pore forming effect of TEC, which contributes to the increase of dissolution rate, was weak.

Considering both agglomeration propensity and drug release, 5% TEC level (w/w of the dry polymer) was used in the formulation for further investigation in the second stage.

Stage 2: Solid Content

Four runs were performed in the second stage, varying the solid contents of the coating dispersion. Batch No.1 (from the first stage) was considered as an additional center point. Thus, in total, five batches were subjected to statistical analysis. The covariate effects (actual weight gain) on agglomeration and dissolution were examined using regression analysis on the center batches (No. 1, 6, and 7). The results revealed that at a 5% TEC level, actual weight gain had little effect on the % agglomeration but a significant effect on the dissolution response - time of 50% drug released ($\alpha = 0.2$ for the covariate). Thus, a one-way ANOVA model (Table 2-11) was utilized to analyze the effect of solid content on agglomeration. The % agglomeration values were different at a significance level of $\alpha = 0.05$ amongst the three groups. The increased solid content leads to an increase in% agglomeration. During the coating process of batch No.9 (solid content = 24.9%), a nozzle clog was observed at 91 min. Thus, two additional replicates were conducted at a 24.9% solid content level. Nozzle clog was observed at 75 min and 110 min, respectively.

Table 2-11: ANOVA results for the effect of solid content on % agglomeration.

ANOVA					
Source of Variation	df	SS	MS	F	p-value
Between Groups	2	116.7	58.36	78.51	0.01257
Within Groups	2	1.486	0.7433		

Before applying ANOVA to test the dissolution parameter, the regression analysis of weight gain was used to correct the group mean and standard error. The regression equation (Eq. 2.5) is presented as follows:

$$Time\ of\ 50\%\ drug\ released = 0.1195 \times actual\ weight\ gain + 0.7799 \quad \textit{Eq. 2.5}$$

where 0.1195 is the slope that reveals the dissolution is a function of the actual weight gain. The slopes of the two regression models (Eq. 2.4 and Eq. 2.5) are different, suggesting an interaction between TEC levels and weight gain. However, the p-value of the interaction term is 0.31 from a regression analysis on the data from batches (No. 1, 2, 3, 4, 6, and 7), indicating a lack of statistical significance. It is probably due to the limited sample size and a relatively large number of parameters (for TEC levels, weight gain, and interaction) to be estimated. Since the formulation would be kept consistent in future studies, the effect of interaction between TEC level and weight gain on dissolution was deemed low risk, and thus no further investigation was pursued. The ANCOVA suggests the standard error is reduced from 0.060 to 0.024, and the mean values of the time of 50% drug released for 12.9%, 18,15%, and 24.9% solid content are 3.47, 3.16, and 4.05 hours, respectively. The F-test results are shown in Table 2-12.

Table 2-12：ANOVA results for the effect of solid content on time of 50% drug released.

ANOVA					
Source of Variation	df	SS	MS	F	p-value
Between Groups	2	0.5891	0.2945	15.73	0.05977
Within Groups	2	0.03745	0.01872		
Total	4	0.6265			

Although an insignificant effect of solid content is found at a 95% confidence level for the dissolution, it is noteworthy that the p-value = 0.06 is arguable low for a 5 sample ANOVA. However, regression analysis indicates the solid content and time of 50% drug released do not appear to have a linear correlation. The batches of 18.9% solid content had the fastest dissolution, while the batch of 24.9% solid content generated the slowest dissolution and the highest amount of agglomeration. A large portion of granular twinning was found in the batch of 24.9% solid

content, whereby the granule size distribution of this batch was shifted to the high end, potentially causing the nonlinearity. The solid content of 18.9% for the coating formulation would be used in future studies to (1) overcome the nozzle clogging issue, (2) minimize the agglomeration, and (3) minimize the coating time. The coating formulation was selected based on these results, as shown in Table 2-13 for the process development.

Table 2-13: Coating dispersion formulation for further studies.

Coating Dispersion Formulation		
Component	Levels （% w/w）	Function
Polyvinyl acetate (PVAc), Povidone (PVP), Sodium Lauryl Sulfate (SLS)	50% （50% ×30% = ×15% in terms of solid content）	Commercial Coating Polymer
Triethyl Citrate (TEC)	0.75% (5% of dry polymer content)	Plasticizer
Talc	2.25%	Anti-tacking agent
Blue Lake	0.15%	Color agent
Total Solid Content	18.15%	

The formulation development addressed the identified high risks of the coating formulation. Since the commercial polymer dispersion (Kollicoat SR 30D) included 9% PVP as a pore-forming agent, no additional pore-forming agent was used. The plasticizer level was optimized at 5% of the dry polymer content. This level resulted in adequate film quality, and the risk of plasticizer concentration to impact drug release is reduced from high to low. The polymer coating level was identified as a critical factor impacting drug release, and its risk level remained as high. Further investigation is shown and discussed in the process development.

2.3.2 Process Development

This section includes studies on polymer coating and curing. A risk assessment was initially performed to identify the critical process parameters. A fractional factorial design was followed to verify the criticalities for polymer coating. A curing study using five conditions for 21 days was conducted using a center coating batch (19% weight gain). The results were analyzed using ANOVA, and the risk assessment was updated after receiving the experimental results.

2.3.2.1 Risk Assessment

The initial risk assessment of the coating and curing was performed using prior knowledge in a two-step manner. An Ishikawa diagram was utilized to identify the high-risk factors that could affect the drug product CQAs. Subsequently, FMEA analysis was applied to determine the process variables with the highest potential to cause a CQA failure.

The Ishikawa diagram was performed to catch up on all possible causes that lead to a batch failure or patient risks. The analysis (Figure 2-1) had five main categories: materials, sieving, coating, curing, and analytical methods. Since the coating dispersion was studied and understood in the previous formulation development, the materials, in this case, refer to the drug-loaded uncoated granules. In the branch of coating, the causes were divided into manipulated variables and measured variables. The manipulated variables were controllable and could impact some of the measured variables. Most of the measured variables were under close monitoring, while the inlet air relative humidity was an environmental disturbance subjected to further investigation.

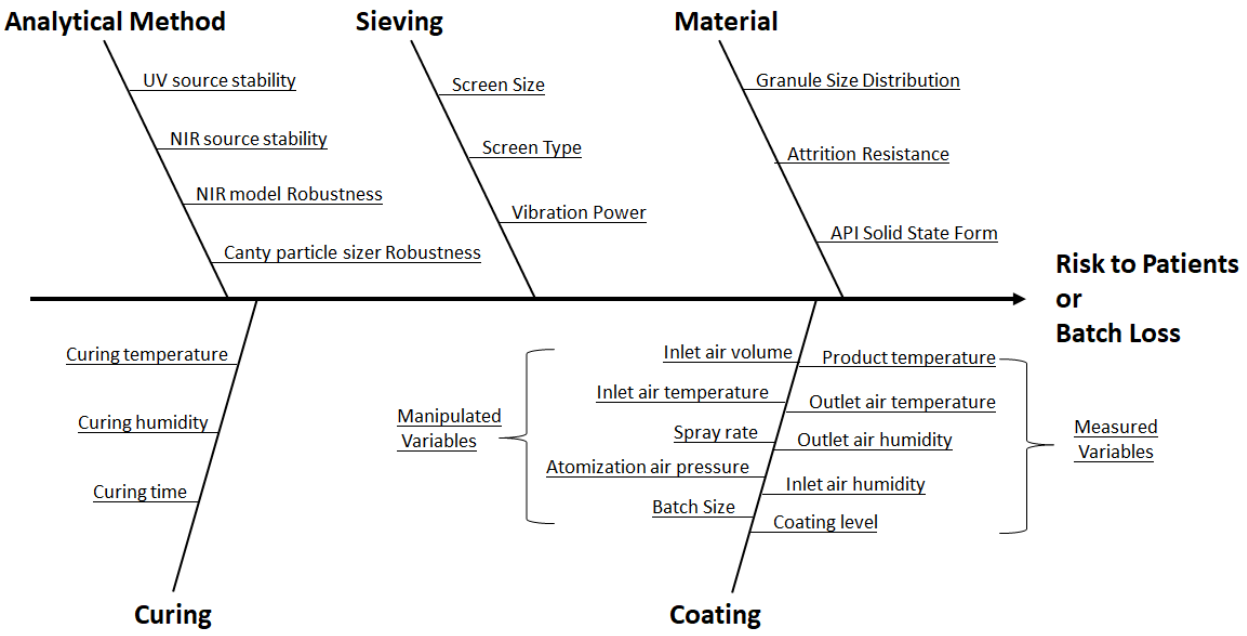

Figure 2-1: Ishikawa diagram of the manufacturing process.

Overall Risk Assessment

The FMEA analysis was performed after constructing the Ishikawa diagram. The initial risk assessment of the overall manufacturing process, presented in Table 2-14, directly links the final product CQAs to the five categories. In the deemed high-risk mode, the process variables that could impact the drug product quality or cause batch failure became the focus of the risk assessment. The variables that have the highest potential to cause a failure need to be investigated to optimize the manufacturing process and reduce the risk of failure.

Table 2-14： Initial risk assessment of the manufacturing process and justification based on Ishikawa diagram

Categories	CQAs or Batch Loss	Risk Level	Justification
Material	Assay and Content Uniformity	Low	The uncoated granules were prepared via high shear wet granulation. The product assay and content uniformity were examined before the coating process for every batch. The risk is low.
	Drug Release	Medium	The variability of granule size distribution was not negligible but controlled to an acceptable level via sieving. The risk is medium.
	Process Failure	Low	Granules with lower fragmentation resistance than 97% were rejected. The risk of batch loss is low.
Sieving	Assay and Content Uniformity	Low	The purpose of the sieving step is to screen out agglomerates and fines. The risk of this separation process to impact the drug product or cause batch loss is low.
	Drug Release	Low	
	Process Failure	Low	
Coating	Assay and Content Uniformity	Low	Assay and content uniformity are mainly determined by the granulation step and are unaffected by the coating process variables. The risk is low.
	Drug Release	High	The polymer coating is the drug release rate controlling step for the coated granules. The risk is high.
	Process Failure	High	Undesired coating conditions may lead to the formation of large agglomerates and defluidization, resulting in a batch loss. The risk is high.
Curing	Assay and Content Uniformity	Low	Assay and content uniformity are mainly determined by the granulation step and are unaffected by the curing process variables. The risk is low.
	Drug Release	High	Curing affects the coating properties and ultimately impacts the drug release. The risk is high.
	Process Failure	Medium	Excessive humidity and heat cause coated granules to interfuse with each other and form agglomerates, resulting in a batch loss. The risk is medium.
Analytical Method	Assay and Content Uniformity	Low	The UV method is standardized, and the performance of the UV instrument was routinely examined. The risk is low.
	Drug Release	Medium	The in-process coating level is determined based on the performance of in-line NIR models. The robustness of the model is a challenge. The risk is medium.
	Process Failure	Low	The analytical method is unlikely to impact the manufacturing process. The risk is low.

Risk Assessment for variables

The overall risk assessment indicated coating and curing as the high-risk steps to impact drug release and cause batch loss. Subsequently, material attributes, process variables, and associated risk on corresponding CQAs were evaluated based on prior experience and literature review. Table 2-15 summarizes the initial risk assessment of the material and process variables. The justification and initial strategy to reduce the risks are provided. The variables subjected to the DoE study are indicated.

Table 2-15: Initial risk assessment of the material and process variables based on failure mode effect analysis (FMEA).

Variables	Risk Level	Justification and initial strategy
Input Material Attributes		
Drug-loaded granule assay	Low	The assay of drug-loaded granules was monitored for every coating batch. The risk is low.
Drug substance solid-state form	High	Theophylline was known to have different apparent solubility as anhydrous or hydrate. Coating being a wet process, the risk of form conversion resulting in altered drug release is high.
Granule size distribution	High	Granule size change leads to variations in granule surface area. The received drug-loaded granules are at a fraction between 250-850 µm. The risk is high. In the screening study, the granules were restricted to the fraction of 350 - 500 µm. In the response surface study, the granule size distribution were in the range of 250 - 850 µm.
Loss on drying (LoD)	Medium	Moisture may impact film formation and API solid-state. The LoD of uncoated granules is controlled to < 5%. The risk is medium.
Uncoated granule release profile	Low	The film coating should control the drug release. The risk of drug release from uncoated granules is low.
Equipment Variables		
Nozzle tip diameter	Medium	Improper selection of nozzle tip size may impact atomization and be vulnerable to nozzle clog. The risk is medium. Based on prior experience. A nozzle with a 1.0 mm diameter is selected.
Nozzle tip/ air cap position	low	The positions of the nozzle and air cap were set constant and kept flush. The impact on atomization is low.
Coating Process Variables		
Inlet air relative humidity	High	Variation of inlet air humidity may have an impact on drying and the quality of the polymer film. The risk is high. Investigate with DoE to optimize and reduce the risk.
Preheating inlet air temperature	Low	Higher than optimal temperature may cause static charge and lead to processing problems. Preheating target product temperature was set at 38 °C
Preheating air volume	Medium	If the air volume is higher than optimal, fragmentation and attrition to the granules may lead to excessive fines. Lower than optimal air volume may cause uneven heating. The risk is medium.
Preheating time	Low	Initial drying capacity may be insufficient if the target product temperature is not reached. In practice, the preheating does not end until the target product temperature is reached. The risk is low.
Inlet air temperature (spray phase)	Medium	Inlet air temperature is adjusted to reach the desired product temperature. If it is set higher than optimal, droplet premature may occur, and if it is set lower than optimal, agglomeration may occur. The product temperature will be monitored, and the inlet air temperature is adjusted accordingly. The risk is medium.

Variables	Risk Level	Justification and initial strategy
Coating Process Variables		
Product temperature (spray phase)	High	The product temperature is impacted by inlet air temperature, air volume, and spray rate. Inlet air temperature had a much smaller effect on product temperature than air volume and spray rate. If product temperature is higher than optimal, droplet premature may occur and generate a large number of fines. If product temperature is lower than optimal, agglomeration may occur, and the film quality may be impacted. The risk is high. Investigate with DoE to optimize and reduce the risk.
Air volume (spray phase)	High	If air volume is higher than optimal, droplet premature may occur, and the granules may be coated unevenly or blown onto the filter. If air volume is lower than optimal, agglomeration may occur, leading to batch collapse. The risk is high. Investigate with DoE to optimize and reduce the risk.
Spray rate	High	If the spray rate is higher than optimal, agglomeration may occur. If the spray rate is low, spray time may be extended, and nozzle clog may occur. The risk is high. The coating process is interactively impacted by spray rate, atomization air pressure, product temperature, and volume. The spray rate is set at 5 g/min.
Atomization air pressure	High	If atomization air pressure is higher than optimal, the droplets may be too tiny and sprayed onto the inner wall of the fluid bed bowl, leading to the generation of fines. If atomization air pressure is lower than optimal, agglomeration may occur. The risk is high. Investigate with DoE to optimize and reduce the risk.
Coating time	Medium	The coating dispersion may settle because the coating time is typically 2- 3 hours. The homogeneity of the dispersion may be undermined. The risk is medium. The coating dispersion is consistently mixed using a magnetic stirrer during the manufacturing process.
Curing temperature	High	If the curing temperature is lower than optimal, the curing process may not occur. If the curing temperature is higher than optimal, the film on the granule surface may interfuse with each other, and agglomeration may occur. The risk is high. Investigate with DoE to optimize and reduce the risk.
Curing humidity	High	If curing humidity is lower than optimal, the curing process may not occur. If curing humidity is higher than optimal, the film on the granule surface may interfuse with each other, and agglomeration may occur. The risk is high. Investigate with DoE to optimize and reduce the risk.
Curing time	High	Under-curing may lead to incomplete film formation. However, unnecessary over-curing may increase the processing time. The risk is high. Investigate with DoE to optimize and reduce the risk.

2.3.2.2 Experimental Data Analysis for Screening Study.

2.3.2.2.1 *Coating Study*

The 2^{4-1} fractional factorial design for coating was designed to isolate the effects of main factors and confound two-way interactions. It serves as a screening study to verify the criticality of process parameters and environmental disturbances. The center of the design was selected based on scientific literature and previous experimental experience.

Table 2-16: Results of the screening study. The inlet temperature was adjusted during the process to maintain the desired product temperature. In the DoE, the set of process parameters were targeted at a steady state. During the coating process, the product temperature fluctuated when the spray rate was ramped up, and the air volume was adjusted accordingly.

Order	Factors				Responses		
	Atomization Pressure	Product temperature	Relative Humidity	Air Volume	Agglomeration	LoD	Coating deposition rate
	level	level	level	level	(g)	(%)	(%)
11	-1	-1	1	1	28.2	4.82	91.19
1	-1	-1	-1	-1	27.34	4.26	86.50
12	-1	1	1	-1	68.39	9.14	93.81
3	-1	1	-1	1	12.80	3.92	83.26
14	1	-1	1	-1	67.43	7.98	94.74
2	1	-1	-1	1	10.48	3.75	84.35
13	1	1	1	1	27.28	5.61	88.19
4	1	1	-1	-1	35.34	6.50	90.66
5	0	0	0	0	32.41	5.51	90.23
6	0	0	0	0	29.60	5.63	88.95
7	0	0	0	0	29.89	5.23	87.74
8	0	0	0	0	31.03	4.96	90.15
9	0	0	0	0	33.45	5.02	91.86
10	0	0	0	0	32.43	5.24	93.05

**Atomization pressure: level -1 = 1.4 bar, level 0 = 1.6 bar, and level 1 = 1.8 bar.*
** Product temperature: level -1 = 30 °C, level 0 = 33 °C, and level 1 = 36 °C.*
** Relative Humidity: level -1 = 20 – 30 %, level 0 = 40 – 47%, and level 1 = 70 – 76%.*
** Air Volume: level -1 = 25 g/m^3, level 0 = 30 g/m^3, and level 1 = 35 g/m^3.*

The design layout and results were listed in Table 2-16. The first column indicates that the experiments were conducted in a sequence from low to high humidity caused by the seasonal change. The three responses were agglomeration, steady-state moisture level, and coating

deposition rate. The results were analyzed using ANOVA. The factors, although having numeric values, were treated as categorical variables (Using numerical values did not change the results of the statistical analysis).

Significant factors for Agglomeration

Varying degrees of agglomerations were observed across all the design points. The agglomerations range from 10.48 to 68.39 g. The variation of agglomeration is attributed to either inadequate mass and heat transfer or the inherent tackiness of coating polymer at the given condition. It is beneficial to reduce agglomeration because 1) small agglomerates (twinning) that pass through the 850 μm screen may impact the drug release, and 2) excessive agglomeration may lead to defluidization and batch collapse. The ANOVA table (Table 2-17) indicates the most significant factors (at 95% confidence level) contributing to agglomeration are relative humidity and air volume. Since there was no omitted interaction term, the statistically significant lack-of-fit term reveals the non-linear effects on the generation of agglomerates.

Further optimization is necessary to gain more understanding of the non-linear effect. The p-value of the interaction between relative humidity and air volume is 0.002. While, as mentioned previously, the two-factor interaction terms are confounded in the fractional factorial design. The interaction between relative humidity and air volume is 100% confounded with the interaction between atomization pressure and product temperature. Considering that product temperature and atomization pressure have little impact on agglomeration, this interaction term is probably more relevant to relative humidity and air volume. The minimal agglomeration is generated at low relative humidity and high air volume condition. It is noteworthy that the agglomeration rate at a high temperature is not significantly different from that value at a low temperature. The formation

of agglomerates, when performing risk assessment, is proposed to have two mechanisms: 1) the polymer becomes rubbery (above T_g, which is around 30 °C [138]) and exhibits increased tackiness when exposed to an elevated product temperature, and 2) excessive moisture accumulates to form liquid bridges between granules due to low drying efficiency. The first mechanism is related to the product temperature, which is found insignificant. The second mechanism involves product temperature, relative humidity, and air volume. Increased air volume or decreased relative humidity significantly reduces the formation of agglomerates. The results suggest that insufficient drying efficiency is the predominant cause of agglomeration.

Table 2-17: ANOVA results for agglomeration at 95% confidence level. DF is the degree of freedom.

Source	Estimate	DF	F-value	p-value probability >F	Comments
Grand Mean	33.29	-	-	-	
Product Temperature	1.30	1	0.23	0.24	
Atomization pressure	0.48	1	1.72	0.65	
Relative Humidity	13.17	1	177.89	<0.0001	Significant
Air Volume	-14.97	1	229.85	<0.0001	Significant
Atomization Pressure x Product Temperature (Relative Humidity x Air Volume)	-5.12	1	26.87	0.002	Significant
Air Volume x Product Temperature (Relative Humidity x atomization Pressure)	-0.95	1	0.92	0.38	
Relative Humidity x Product Temperature (Atomization Pressure x Air Volume)	-1.28	1	1.69	0.24	
Lack of Fit		1	14.63	0.012	Significant
Pure Error		5			
Total		13			

Significant factors for Coating deposition rate

The coating deposition rate is the ratio between actual weight gain and theoretical weight gain, describing the efficiency of polymer deposition. A low deposition efficiency leads to a prolonged

process, increasing material, time, and energy consumption. The ANOVA results (Table 2-18) show that relative humidity and air volume significantly affect the coating deposition rate at a 95% confidence level. The other terms, including lack of fit, were statistically insignificant.

Mechanistically, variable drying efficiency is the primary cause of variation in coating deposition rate. The polymer dispersion is atomized into many droplets via the spray nozzle. The droplets travel in the counter direction of the fluidization airflow. The fluidization air volume determines the throughput of the air. The air conveys heat to a product to evaporate water and drives the water vapor out of the system. The level of water loading in the airstream determines the drying efficiency. High air volume leads to excessive drying capacity and promotes the premature of spray droplets before they arrive at the granule surface. An undesired fluidization pattern due to inappropriate air volume reduces collision probability between spray droplets and granules.

Relative humidity level, as another significant factor, determines the moisture level in the incoming air. The incoming air of higher relative humidity has less capacity to uptake the water vapor per unit volume, and the reduced drying capacity prevents droplets premature and decreases fines generation.

Atomization pressure, theoretically, changes the spray pattern and the droplet size. The small average droplet size increases the overall evaporation area, which promotes drying efficiency. However, in the studied range, atomization pressure had an insignificant impact on coating deposition rate.

Table 2-18: ANOVA results for Coating deposition rate at 95% confidence level. DF is the degree of freedom.

Source	Estimate	DF	F-value	p-value probability >F	Comments
Grand Mean	89.62	-	-	-	
Product Temperature	-0.11	1	0.02	0.88	
Atomization pressure	0.40	1	0.03	0.59	
Relative Humidity	2.895	1	16.98	0.006	Significant
Air Volume	-2.34	1	11.09	0.016	Significant
Atomization Pressure x Product Temperature (Relative Humidity x Air Volume)	0.048	1	0.005	0.95	
Air Volume x Product Temperature (Relative Humidity x atomization Pressure)	-0.92	1	1.70	0.24	
Relative Humidity x Product Temperature (Atomization Pressure x Air Volume)	-0.88	1	1.55	0.26	
Lack of Fit		1	1.44	0.87	
Pure Error		5			
Total		13			

Significant factors for steady-state moisture level

The steady-state moisture level is calculated by averaging the loss on drying of granules sampled during the steady-state of the coating process. The steady-state is defined as the period after the spray rate ramp-up when product temperature became stable. Samples were taken every 30 minutes during the steady state. The LoD values are averaged after first becoming stable. The result of ANOVA is listed in Table 2-19. Product temperature, relative humidity, air volume, and the interaction between air volume and relative humidity (confounded with the interaction between atomization Pressure and product temperature) are the most significant factors affecting the steady-state moisture level. The lack-of-fit term is significant, suggesting the presence of a curvature effect. The steady-state moisture is an indirect measure of the propensity of batch failure and process efficiency. Figure 2-2 shows 1) increased moisture leads to the increased agglomeration

in a linear correlation, and 2) increased moisture level increases coating deposition rate. The rate of increase in coating deposition rate drops after the moisture level exceeded 5.5% w/w. Thus, the balance point between agglomerate formation and the coating deposition rate is around 5.5% w/w steady-state moisture level. The moisture level can be monitored using PAT tools and affiliated feedback control.

Table 2-19: ANOVA results for Steady-state moisture level at 95% confidence level. DF is the degree of freedom.

Source	Estimate	DF	F-value	p-value probability >F	Comments
Grand Mean	5.54	-	-	-	
Product Temperature	0.54	1	12.40	0.013	Significant
Atomization pressure	0.22	1	1.94	0.21	
Relative Humidity	1.14	1	54.51	0.0003	Significant
Air Volume	-1.22	1	62.55	0.0002	Significant
Atomization Pressure x Product Temperature (Relative Humidity x Air Volume)	-0.45	1	8.59	0.0263	Significant
Air Volume x Product Temperature (Relative Humidity x atomization Pressure)	-0.31	1	3.93	0.095	
Relative Humidity x Product Temperature (Atomization Pressure x Air Volume)	-0.055	1	0.13	0.73	
Lack of Fit		1	11.59	0.02	Significant
Pure Error		5			
Total		13			

The screening DoE study on coating demonstrates that product temperature, air volume, and relative humidity are the critical parameters to prevent batch collapse, reduce agglomeration and improve coating deposit. The impacts of atomization air pressure on the responses are not significant within the studied range. Although the initial risk of atomization air pressure is high, it is not critical in the screening study.

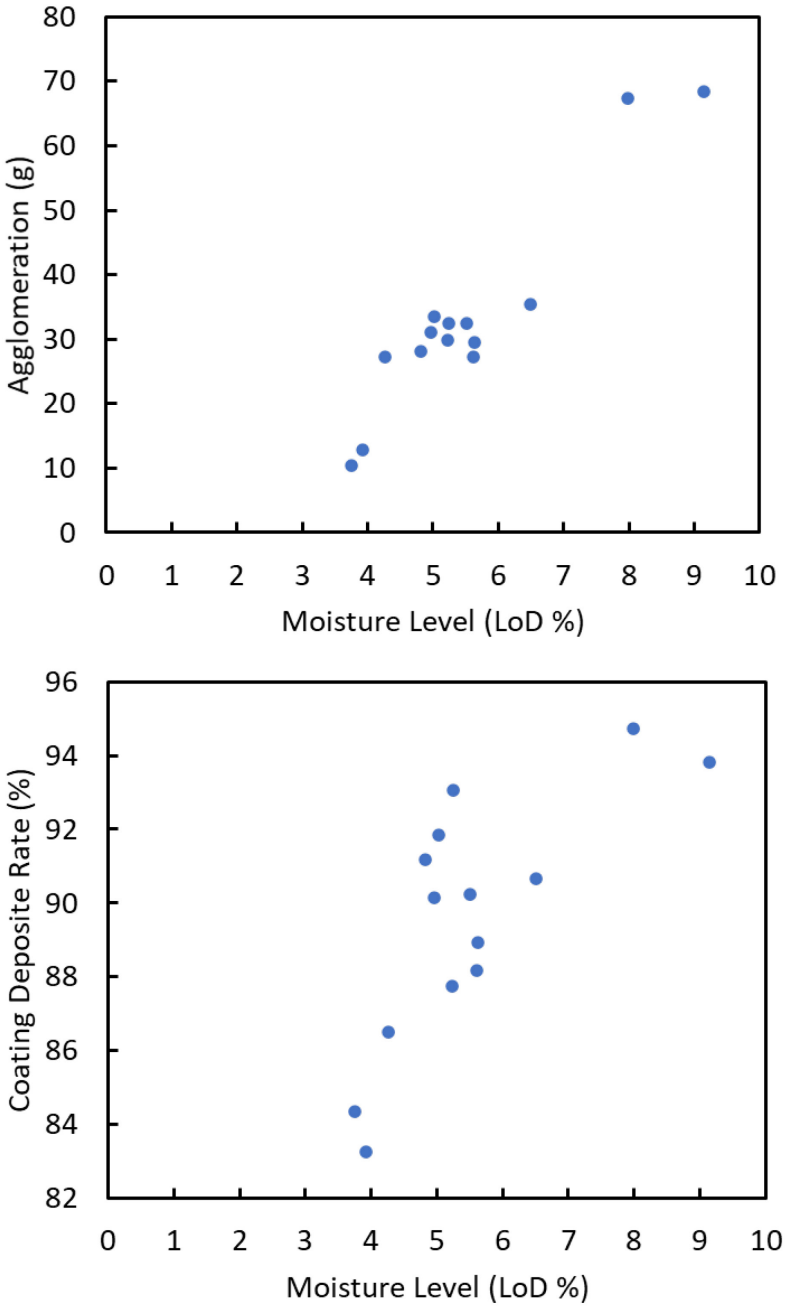

Figure 2-2: correlations between moisture level and agglomeration/coating deposition rate.

2.3.2.2.2 Curing Study

The curing study was performed using the coated granules (19% w/w actual weight gain) to understand the risks of post-coating thermal treatments. The summary of the results is depicted in

Figure 2-3. The dissolution rate increased by a small extent from Day 0 to Day 3 and stabilized from Day 3 to Day 21 in the storage condition of a refrigerator (4°C, 15% RH), shown in Figure 2-3A. The dissolution rate increased by a small extent from Day 0 to Day 3 while decreased from Day 3 to Day 14 and stabilized from Day 14 to Day 21 at room temperature and 75% relative humidity storage condition, shown in Figure 2-3B. The dissolution rate increased from Day 0 to Day 14 and stabilized from Day 14 to Day 21 at room temperature and 11% relative humidity storage condition, shown in Figure 2-3C. The dissolution rate decreased from Day 0 to Day 3 and stabilized from Day 3 to Day 21 at 35°C and 75% relative humidity storage condition, shown in Figure 2-3D. The dissolution rate increased from Day 0 to Day 3 and stabilized from Day 3 to Day 21 at 35°C and 11% relative humidity storage condition, shown in Figure 2-3E. The dissolution profiles of samples stored in 11% relative humidity but different temperatures (room temperature and 35°C) were not significantly different from each other at Day 21 ($f2 = 96$, Figure 2-3F).

Similarly, the dissolution profiles between samples stored in 75% relative humidity but different temperatures (room temperature and 35°C) were not statistically significant ($f2 = 92$, Figure 23-F). The results indicated the relative humidity was the primary cause altering the dissolution profiles of coated theophylline granules. Granules equilibrated in low relative humidity (11%) possessed fast dissolution profiles, while high relative humidity (75%) resulted in slow dissolution profiles. Temperature influenced the rate of dissolution change during the storage. Elevated temperature accelerated the coated granules to reach an equilibrium state of dissolution, but it did not impact the dissolution profile significantly at the equilibrium state. The different dissolution behaviors revealed that the stability of the dissolution profile was related to storage moisture. Two possible mechanisms could explain the dissolution changes: (1) the coalescence

degree of the coating film changed during the post-coating storage, and (2) The theophylline in the coated granule underwent a pseudo polymorphic transformation upon the storage.

A similar curing study was performed on film-coated acetaminophen granules (the same intra-granular formulation as theophylline granules except for API identity) to test the film stability. The dissolution profiles of coated acetaminophen granules did not change during the 21 days storage. Both temperature and relative humidity showed no effect on acetaminophen *in vitro* release profiles. The acetaminophen dissolution stability study indicated that the change in theophylline dissolution was probably not caused by film change.

The second mechanism assumed a portion of the theophylline transformed to its monohydrate at 75% relative humidity condition. The relatively low solubility of theophylline monohydrate resulted in a slower dissolution profile. The 11% relative humidity condition, on the other hand, allowed theophylline transform to its anhydrous form (Form II) leading to a fast dissolution profile. Figure 2-3G showed the results of an additional experiment. Samples stored at 35°C with 75% RH were taken out on Day 7 and stored at two other conditions: 35°C with 11% RH and room temperature with 75% RH until Day 21. Those samples were subjected to the dissolution test on Day 14 and Day 21. The dissolution profiles of the samples transferred to room temperature with 75% RH at Day 14 and Day 21 were not significantly different from Day 7 (F2 = 98). However, the dissolution rate of the samples transferred to 35°C with 11% RH increased over time. This indicated that the dissolution profile was reversible with the change of relative humidity. Further, it suggested temperature was kinetically impacting the transformation.

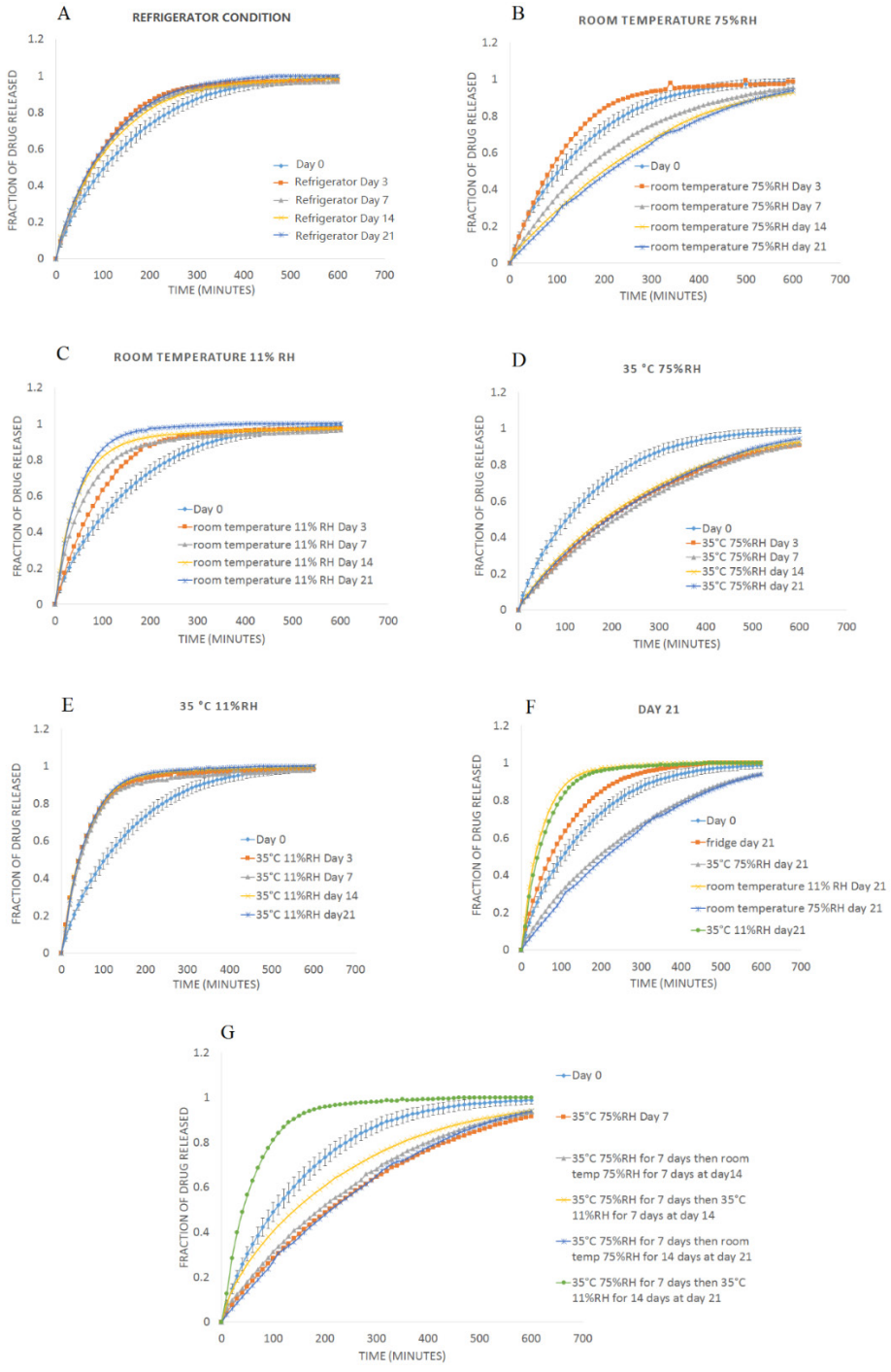

Figure 2-3: Result of the curing study A) dissolution profiles from Day 0 to Day 21 at refrigerator storage condition; B) dissolution profiles from Day 0 to Day 21 at room temperature and 75% relative humidity storage condition; C) dissolution profiles from Day 0 to Day 21 at room temperature and 11% relative humidity storage condition; D) dissolution profiles from Day 0 to Day 21 at 35°C and 75% relative humidity storage condition; E) dissolution profiles from Day 0 to Day 21 at 35°C and 11% relative humidity storage condition; F) dissolution profiles at Day 21 of all storage conditions; G) dissolution profile of samples at different storage conditions.

2.3.2.2.3 Theophylline Solid State Form and Product Dissolution

In order to better understand the theophylline monohydrate formation and the dissolution of the coated granules, samples of a center batch (19%w/w weight gain) of the screening study were stored in three humidity chambers (11%, 52%, and 75% RH) at 35 °C for 21 days. Three replicates from each humidity chamber were subjected to *in vitro* dissolution tests. The dissolution profiles of samples of the three storage conditions are depicted in Figure 2-4. The samples stored at 11% RH had the fastest dissolution rate, and the samples of 75% RH had the slowest dissolution rate.

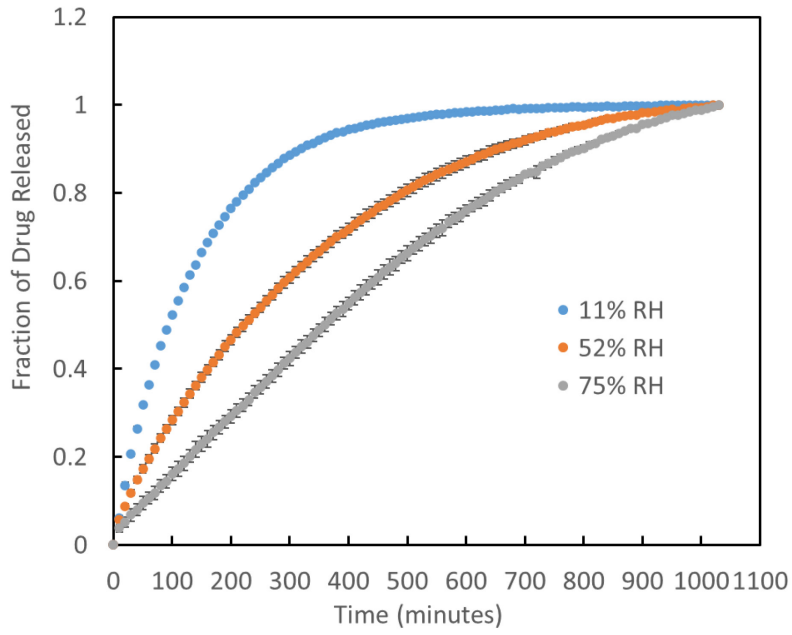

Figure 2-4: the dissolution profiles of the coated granules stored 11% RH, 53% RH, and 75% RH of 23 °C.

Raman imaging was utilized to understand the pseudo polymorphic transformation of theophylline. Figure 2-5 shows the representative layers of the granules stored at the three relative humidities. The images were analyzed using classic least squares regression based on pure component spectra from microcrystalline cellulose, theophylline anhydrous, and monohydrate. The image of granules stored at 11% RH showed 25.1% pixels of theophylline anhydrous and 0.25% monohydrate. While stored at 52% RH, a portion of theophylline (10.47% pixels) transferred to

the monohydrate form, and the majority (14.03% pixels) remained anhydrous. At the highest relative humidity condition of 75% RH, the highest ratio (16.47% pixels) of theophylline anhydrous was transferred to the monohydrate form.

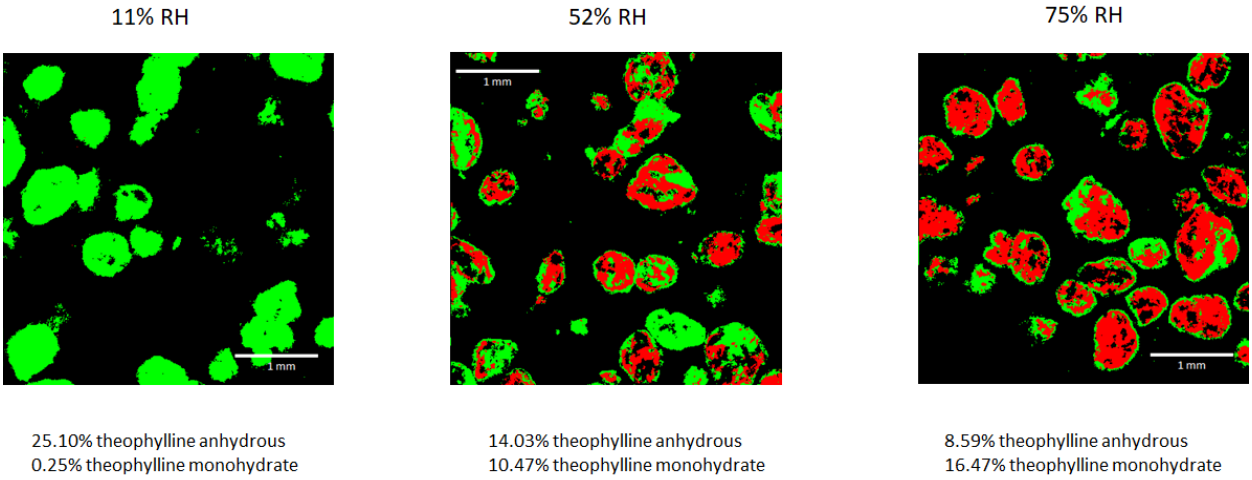

Figure 2-5: Raman images from granules stored at three relative humidity conditions: 11% RH, 53% RH, and 75% RH of 23 °C. Green indicates theophylline anhydrous; red indicates theophylline monohydrate

The study revealed that solid-state form changes due to storage RH conditions and the coated granule dissolution profiles had correlation. The dissolution of the coated theophylline granules was a complicated process. The coating film consisted of two polymers: an aqueous insoluble polymer (PVAc) which absorbs water and swells during the dissolution process, and an aqueous soluble polymer (PVP) which is a pore forming agent dissolving and leaving a channel in the film coating after exposed to the dissolution medium. The kinetics of the theophylline release from the granule core to the dissolution medium involves multiple mechanisms: (1) drug dissolution in the core, (2) drug diffusion through the film, and (3) drug diffusion through the aqueous channels formed by the pore forming agent or plasticizer. The driving forces of drug release includes the gradient of drug concentrations and the osmotic pressure between the core and the dissolution medium. The correlation between the dissolution rate and the theophylline monohydrate formation

is probably due to the difference between the solubilities of theophylline anhydrous (Form II) and monohydrate. The lower solubility of theophylline monohydrate leads to the lower gradient of drug concentrations between the core and the dissolution medium, and ultimately results in slower dissolution rate.

Literature reported that in an intrinsic dissolution test, the solvent-mediated transformation of theophylline anhydrous took about 6 minutes for the monohydrate crystals to grow and completely cover the surface of the anhydrous form, shown in Figure 2-7.[139-141] Therefore, the difference in dissolution rates was hardly observed in the dissolution tests of uncoated theophylline anhydrous and monohydrate granules. For the coated granules, theophylline and other excipients were constrained by the coating film, forming a wet mass in the initial stage of the dissolution process. Wikström *et al.* showed that the monohydrate formation could be prevented during wet granulation when 0.3% w/w of hydroxypropyl methylcellulose was added to a formulation containing 30% w/w theophylline anhydrous.[142] The same group also showed the completion of theophylline hydration took more than 60 min after the theophylline anhydrous was exposed to 1% w/w HPMC solution, shown in Figure 2-8. The alternation of hydrate morphology can be observed, comparing Figures 2-7 and 2-8. The needle-shaped theophylline monohydrate was formed in pure water (Figure 2-7), while rectangular crystals of theophylline monohydrate were produced with the presence of HPMC. Wikström *et al.* suggested that the HPMC polymer adsorbed to fast-growing faces of the hydrate crystal, thus retarded the overall transformation rate.[142] In this study, the uncoated granules contained 60% theophylline and 2% HPMC. HPMC probably detained the solvent-mediated transformation of the theophylline anhydrous. Therefore, differences in the apparent dissolution rates were observed among coated granules containing different amounts of theophylline monohydrate.

The solid-state form of theophylline was of high risk to the *in vitro* dissolution. The FMEA was updated from the outcome of the study. The moisture level of both the drying process and storage of the coated granules should be carefully controlled.

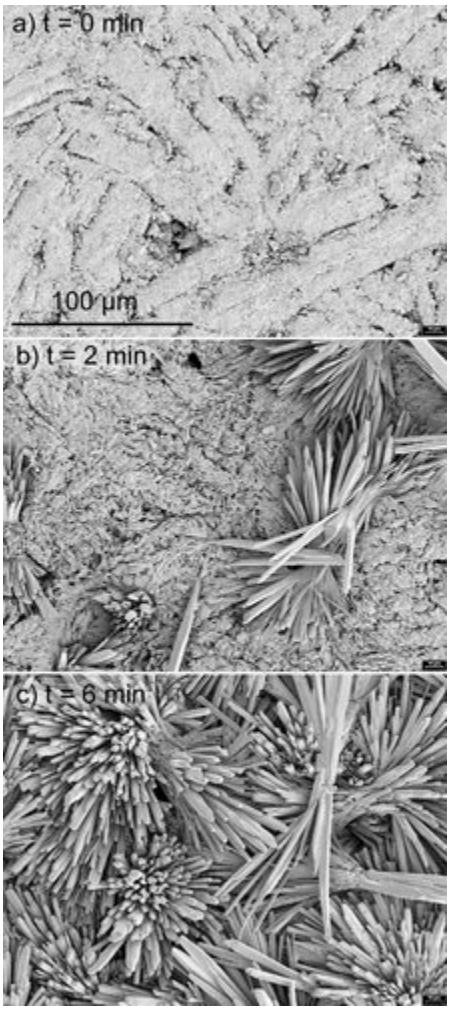

Figure 2-6: SEM scan of the surface of theophylline anhydrous during the solvent-mediated transformation. (a) t = 0 min, (b) t = 2 min, (c) t = 6 min. The figure was adapted from ref. [139] permission granted.

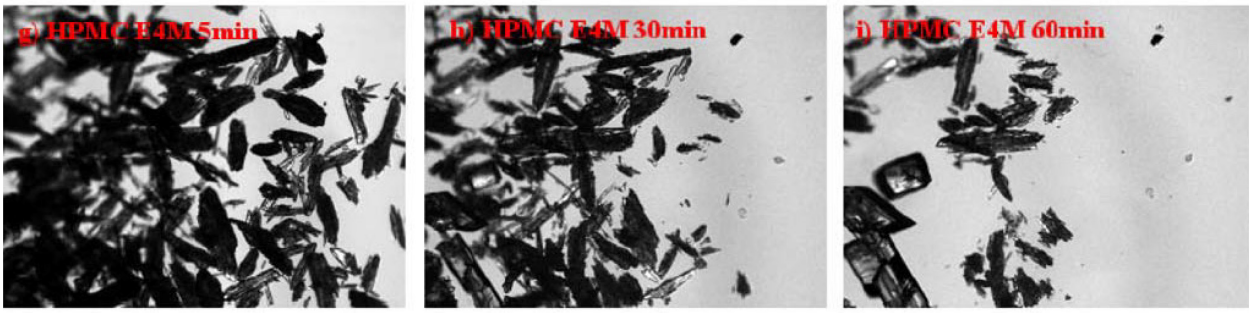

Figure 2-7: Micrographs illustrating the growth and morphology for hydrate formation in 1% w/w HPMC solution. (g) after 5 min exposure to HPMC solution, (h) after 30 min exposure to HPMC solution, (i) after 60 min exposure to HPMC solution. The figure was adapted from ref.[142] permission granted.

2.4 Conclusion

The quality target product profile of the extended-release multiparticulate dosage form was defined, and the fluid bed granular coating process was studied. The critical quality attributes, critical formulation variables, and critical process parameters were identified and confirmed using risk assessments and screening studies. A feasible coating formulation was developed and used to understand the manufacturing process. The screening studies identified that relative humidity and air volume are critical parameters to reduce agglomerates and increase the coating deposition rate. Steady-state moisture level as an in-process measurement also showed a correlation with the formation of agglomeration and coating deposition rate. Atomization air pressure was found to have insignificant impacts on the agglomeration, coating deposition, and moisture level and thus not to be investigated in the following study.

The curing study showed that the theophylline in the granules underwent solid-state form change during the coating process and storage. The dissolution tests indicated that the conversion of theophylline monohydrate was a high risk that significantly influenced the *in vitro* dissolution

of coated granules. A literature review suggested the formulation of the granule core, including a polymer binder HPMC, retarded the solvent-mediated transformation of theophylline and increased the *in vitro* dissolution rate of the coated granules.

The study of this chapter accommodated the requirements of Specific Aim 1, identifying the risks of the failure modes and narrowing down the critical parameters that needed further investigation in the following response surface study.

Chapter 3 : Utilization of Design of Experiments and Statistical Tools to Establish Process Models to Predict *in vitro* Dissolution Profiles

Abstract

This chapter utilized design of experiments (DoE) to establish process models that predict *in vitro* dissolution profiles using material attributes, environmental variables, and process parameters. The DoE consisted of two sub-designs: (1) a full factorial design and (2) a D-optimal design. In total, 19 coating experiments were conducted. The experimental response, *in vitro* dissolution profile, was empirically fitted using two algorithms: Weibull function and principal component analysis (PCA). The Weibull function had two parameters: scale factor and shape factor. The dissolution data were decomposed by PCA into scores and loadings. Thus, the responses for modeling were either Weibull parameters or scores of PCA. The predictors for modeling (*i.e.*, air volume, inlet air relative humidity, granule size distribution, and coating weight gain) were subjected to two statistical modeling methods: partial least squares regression (PLS) and Gaussian process regression (GPR). The regression methods and the curve-fitting algorithms were used in conjunction to build four sets of models (the PLS models that predicted the Weibull parameters, the GPR models that predicted the Weibull parameters, the PLS models that predicted the PCA scores, and the GPR models that predicted the PCA scores). The regression coefficients of all models were significant at a 95% confidence level. The two regression models had similar errors in predicting the Weibull parameters, while GPR predicted the PCA scores slightly better than the PLS. The error profiles between the actual and model-predicted dissolution curves suggested the PLS model combining with the Weibull function fitting outperformed the other three modeling approaches.

3.1 Introduction

Numerous studies in the literature have reported different ways to model pharmaceutical manufacturing processes.[143-146] However, there is still a lack of research that clearly illustrates the utilization of process modeling to predict critical quality attributes and enable corresponding controls. The trial-and-error approach with inadequate exploration leads to process models that are not robust and may undermine the product quality. Design of experiments (DoEs) is a statistically sound approach that systematically collects data for modeling with reduced costs. Key issues that need investigation are proper selections of (1) experimental design to produce robust process models that predict future samples with accuracy and precision and (2) modeling methodology that best fits the experimental data.

Several statistical designs are available to serve different purposes of applications.[147, 148] Under some circumstances, a model involving only main effects and interactions is adequate to describe a response surface. Nevertheless, when dealing with a complex process incorporating non-linear dynamics, the first-order linear functions are inadequate to describe the process. The full factorial designs at three or more levels are often regarded as the most comprehensive but redundant methodology to include interaction and quadratic terms to map a response surface. Investigating multiple variables at multiple levels costs a massive amount of resources, making the design infeasible to be conducted. In such instances, response surface methodology can reduce the number of experimental runs and retain the power to evaluate the non-linear quadratic effects. Several aspects need to be considered to deduce meaningful information from the response surface design and adequately map the response surface. Process ranges of the investigated variables define the underlying design structure, being of the most importance. The design levels of the variables cannot exceed their allowable range, leading to insignificant responses. Also, some variables start

to exhibit nonlinear effects when the studied ranges are increased.[149] Therefore, the levels of readily controlled variables can be set in narrower ranges to reduce their nonlinearity and decrease modeling complexity. Orthogonality and rotatability are two common features in classical response surface designs (*i.e.*, Box-Behnken design and central composite design). Orthogonality allows main effects and interaction terms to be estimated independently (no correlation) with each other. Rotatability allows the variance of the responses to be a function of the distance (not the direction) of the design points from the center. It is imperative to recognize that orthogonality and rotatability are useful in conducting an unbiased investigation for unknown matters, but they are not required for all response surface methodology.

In contrast to the classical designs, optimal designs are computer-aided designs that optimize the design structure according to a statistical criterion based on a prespecified model. For instance, A-optimality minimizes the average variance of the estimated parameters; D-optimality maximizes the geometrical volume of the design explored space; I-optimality minimizes the average prediction variance over the space of the design. As a result, the optimal designs generally do not satisfy the desirable properties such as orthogonality and rotatability that classical designs do. The optimal designs had two features that are different from classical designs: (1) the user defines the number of experiments and (2) the design allows for constraints. The features provide great flexibility to the design of experiments. It is critical to realize that the optimality criterion is model-dependent, meaning the design is only optimal for the pre-specified model using a quadratic or cubic function.

Least squares regression is the most common approach of fitting a model that maps the response surface to experimental data. In the application of ordinary least squares (OLS) regression for process modeling, the model coefficients are calculated by taking the inverse of the variance-

covariance matrix of the predictors.[150] High multicollinearity of the predictors increases the probability of the inverse being a near singular matrix. In other words, when the predictors exhibit multicollinearity or when the number of degrees of freedom of the pure error is low, OLS models have high uncertainty and tend to be statistically insignificant due to increased errors of the estimated coefficients.[151] Feature selection is a common solution, where insignificant variables and interactions are eliminated stepwise in a forward or a backward manner. In addition to feature selection, partial least squares (PLS) regression is an alternative to handle the colinearity. The PLS algorithm projects the predictors onto a latent space where the covariance between the predictors and the responses is maximized.[152] Mathematically, the predictor matrix is decomposed into an orthogonal matrix T and a near orthogonal matrix P. The matrix T, often referred to as scores, has the same number of rows as the number of samples in the predictor matrix. The matrix P, often called loadings, has the same number of rows as the number of predictors. The model can be built on the first few columns of matrix T, often referred to as latent variables. The number of latent variables can be determined based on the user's knowledge or cross-validation. The regression on the latent variables decreases the number of model parameters and, by default, increases the degrees of freedom of pure error.

As an alternative, a nonparametric Bayesian approach, namely Gaussian process regression (GPR), has been drawing a great deal of attention as a machine learning method in pharmaceutical applications.[153-156] This method does not assume the linearity of the correlation between the predictors and the responses. Instead, GPR assumes multi-dimensional normal distribution consisting of the responses from all batches and calculates the probability distributions over all admissible covariance functions that fit the data. With the covariance function built on the factors, future prediction can be made via algebra transformation. In GPR, the selection of kernel function

for the covariance is the key to a successful model. The kernel functions include constant, linear, square exponential, Matern kernel, *etc*., to accommodate potential shapes of the response surface. A linear kernel with the assumption of no stochastic error in the factors (*i.e.*, measurement error in temperature, air volume, spectral collection, *etc*.) makes GPR equivalent to ordinary least squares regression. GPR provides the benefit of flexibility in model fitting but has drawbacks, including increased computational cost (requiring simulation to tune kernel parameters), increased number of user-selected parameters, and increased risk of overfitting.

The framework of this chapter was built upon the results of the risk assessments and experiments of Chapter 2, where critical process parameters were identified in the coating and curing processes. Figure 3-1 illustrates the experimental plan and the steps for data analysis. The experimental plan included (1) a full factorial design as the calibration set to train the process models and (2) a D-optimal design as the test set to evaluate the process model on new batches. The model utilized four predictors (target weight gain, air volume, relative humidity, and uncoated granule size distribution) to predict the *in vitro* dissolution profiles of coated granules. Target weight gain, air volume, relative humidity were used as their numerical values, while uncoated granule size distribution was subjected to five curve fitting methods to reduce the number of predictors. The *in vitro* dissolution profile of coated granule consisted of fractions of drug release at different dissolution time points, which were fitted using two methods: (1) two-parameter Weibull function and (2) principal component analysis. The process models were established using two algorithms: (1) partial least squares (PLS) regression and (2) Gaussian process regression (GPR) to correlate the predictors to the response. Thus, in total, four sets of models were established:

(1) the PLS model that predicted the Weibull parameters (λ and k) of the dissolution profiles,

(2) the GPR model that predicted the Weibull parameters (λ and k) of the dissolution profiles,

(3) the PLS model that predicted the PCA scores (PC1 and PC2) of the dissolution profiles,

(4) the GPR model that predicted the PCA scores (PC1 and PC2) of the dissolution profiles.

Each set had two independent models predicting two interdependent parameters, which were from the curve fitting of coated granule dissolution profiles.

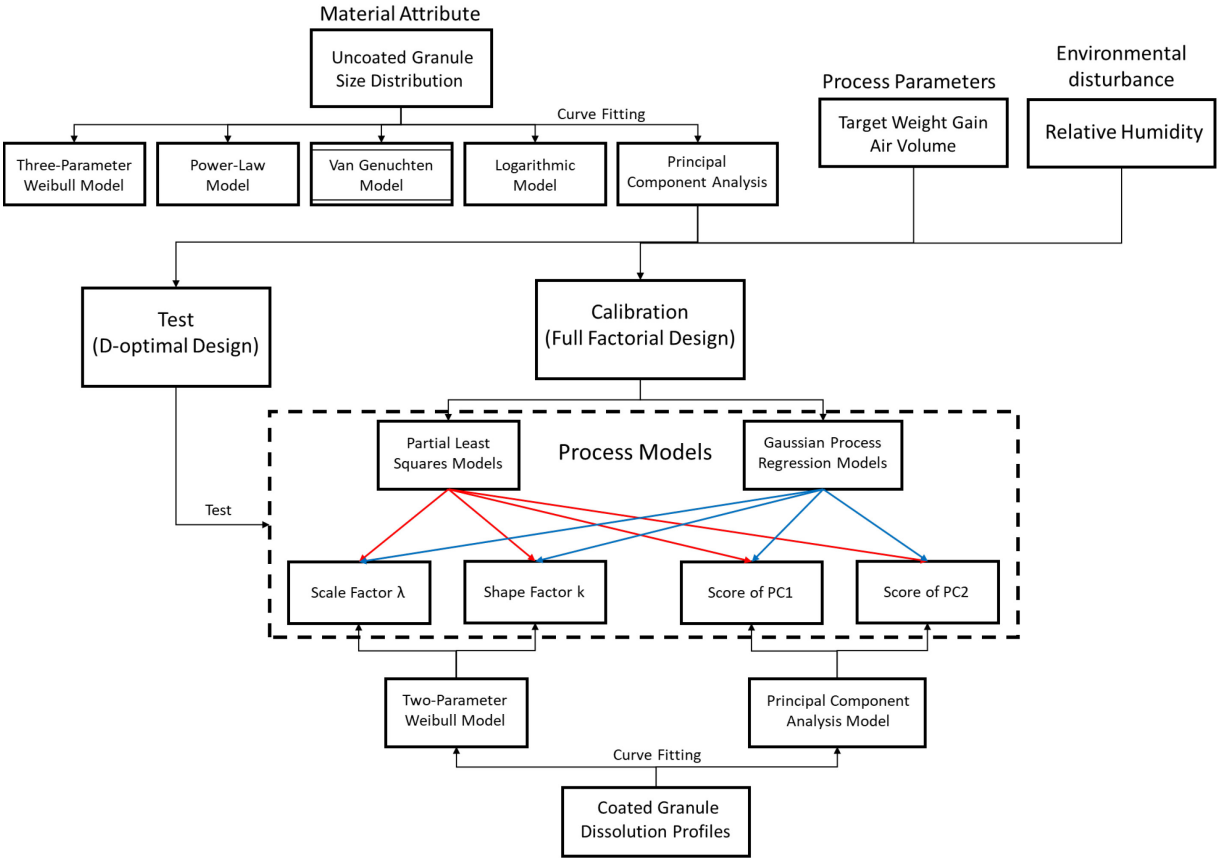

Figure 3-1: Illustration of the experimental plan and data analysis for the process modeling. The experimental plan included a full factorial design for calibration and a D-optimal design for testing.

3.2 Materials and Methods

3.2.1 Materials and Coating Processor

The theophylline-loaded granules (granule size range 250 – 850 μm) were obtained from Purdue University, West Lafayette, IN. The granules comprised 60% theophylline anhydrous, 19.5% lactose monohydrate, 18.5% microcrystalline cellulose, and 2% hydroxypropyl methylcellulose. They were produced by high shear wet granulation using a 10 L capacity granulator (Diosna P/VAC 10-60, Osnabruck, Germany) and dried in the oven at 45°C for 48 hours. The other materials and testing agents were described in Section 2.2.1.

A 7-liter top-spray fluid bed processor (Minilab, Diosna Dierks & Söhne GmbH, Osnabruck, Germany) was used for granular coating. The processor was coupled with an EGE-Electronik series LN/LG airflow sensor (Spezial-Sensoren GmbH, Gettorf, Germany) and two temperature/humidity transmitters (series RHL, Dwyer Instruments Inc., Michigan City, IN). The coating suspension was delivered into the system by a peristaltic pump (Series 120U, Watson-Marlow Inc., Wilmington, MA). The coating process was controlled by an integrated system where an open platform communication system (DeltaV V9.7, Emerson, MO) received analog signal and delivered digital tags to a real-time data management system (SynTQ V3.5, Optimal, UK) for control implementation. A near-infrared reflectance spectrometer (NIR256L-2.2T2, Control Development Inc., South Bend, IN) and a halogen light source (HL-2000, Control Development Inc., South Bend, IN) coupled with a fiber-optic probe (Ocean Optics, Dunedin, FL) were used to collect real-time signal during the coating process. The configuration of the fluid bed processor is illustrated in Figure 3-2.

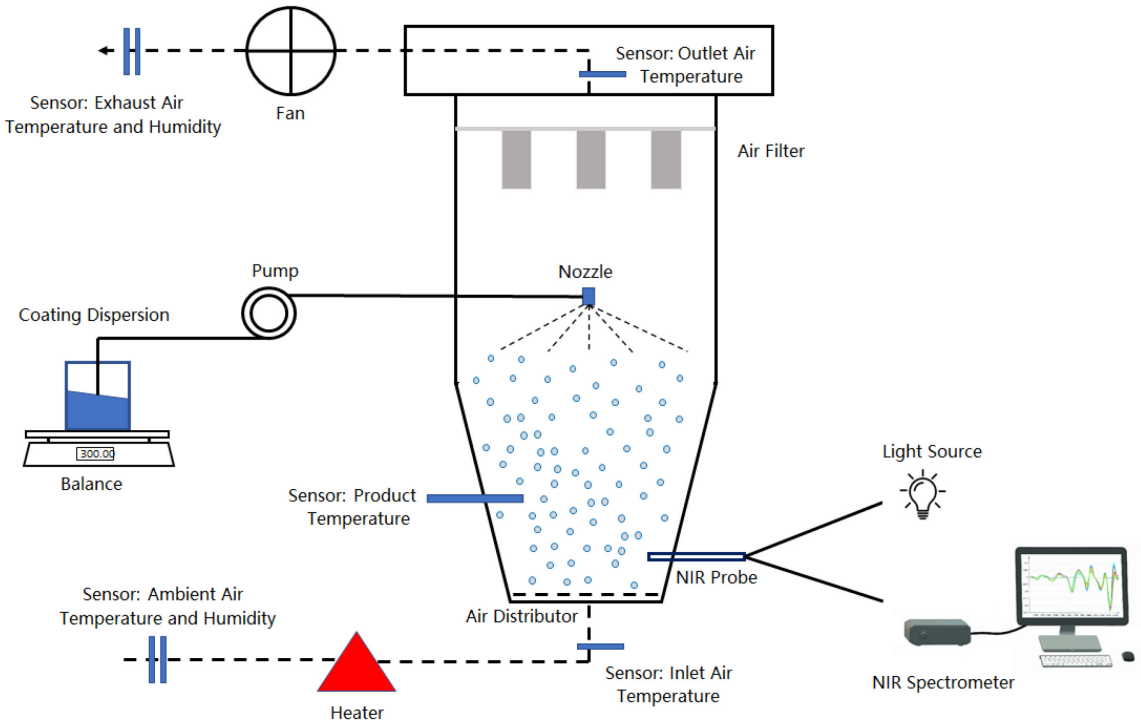

Figure 3-2: Fluid bed processor with in-line monitoring sensors and NIR spectral measurement.

3.2.2 Design of Experiments

The risk assessment outcomes and the screening study (Chapter 2) suggested that the assay and physical attributes were of low risks in the studied range of the fluid bed coating process. One of the critical quality attributes, dissolution, was not investigated as a response in the screening study when there was a lack of process understanding to prevent batch collapse. Because a large number of experimental runs (in minimum, $2^7 = 128$ runs for a 2-level full factorial design) is practically infeasible to study all disturbances (granule size distribution and inlet air relative humidity) and process conditions (product temperature, air volume, atomization air pressure, spray rate, and target weight gain) simultaneously. By dividing the study into two consecutive steps, a screening study followed by a response surface study, the total runs could be reduced to a practically feasible

number. The response surface study serves two purposes: (1) to establish process models that predict dissolution profiles with accuracy, precision, and robustness, and (2) to develop a real-time monitoring and control system for the in-process moisture and coating level using NIR spectroscopy. Chapter 3 will focus on process modeling, and Chapter 4 will discuss the real-time NIR models in detail.

The experimental design of the response surface study included a calibration set and a test set. The calibration set followed a full factorial design, and the test set adopted a D-optimal design, illustrated in Figure 3-3. The full factorial design included ten coating runs, eight corner points, and two replicated center points. The center points were reproduced to determine pure error (random batch-to-batch variability) and potential non-linear effects. The investigated factors included uncoated granule size distribution (GSD), relative humidity (RH), and fluidization air volume. A fourth factor, target weight gain, was studied at three levels of every design point. The batch size was 400g. The previously explored process parameters, including atomization air pressure and product temperature, were kept constant in all experiments to prevent agglomeration. Atomization air pressure was manually set at 1.6 bar, and the product temperature was set at 33 ± 0.7 °C. The spray rate ramped from 3, 4, to 5 g/min in 10 minutes and stayed constant in the calibration experiments, and the granule samples were taken at 0, 5, 15, 45, 80, 120, and 140 min of the spraying phase for loss on drying (LoD) measurement. Other than water, the substances in the granules and coating dispersion were not volatile. The LoD measurement was used as a surrogate indicator for the moisture level, including both bonded and unbonded water in coated granules. The NIR spectra were collected during the coating experiments of the calibration set, and they were used to develop a quantitative model to predict the moisture level.

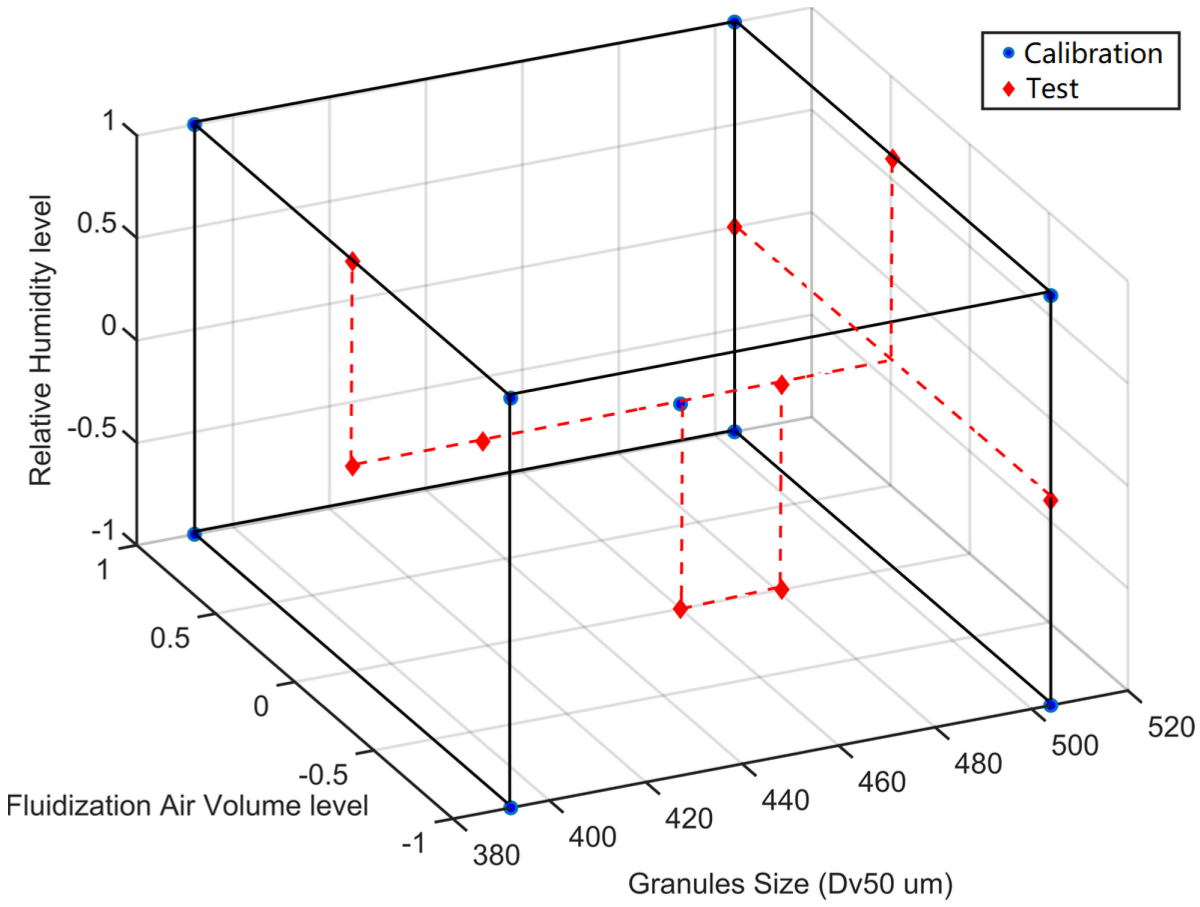

Figure 3-3: the experimental design of calibration and test in the response surface study.

The levels of the four factors are shown in Table 3-1. Five levels of granule size distributions were identified from the input uncoated granule batches. The lowest, medium, and highest levels of the five GSDs were included in the calibration design. The variability of RH was caused by operating the coating experiments at different weathers and seasons, and thus the RH levels were indicated as ranges (20-30%, 40-50%, and 70-80% RH) instead of exact values. The seasonal dependence of relative humidity constrained the randomization of experimental order for both calibration and test designs. Fluidization air volume was an experimentally controlled process parameter explored at the center and two extreme levels. The target coating weight was the fourth

factor that varied within every experiment by sampling granules after spaying for 80, 110, and 140 minutes. However, the weight gain cannot be accurately controlled without real-time monitoring due to variable polymer deposition rates between the design points. The NIR spectra collected for the moisture model were also used to develop a real-time weight gain predictive model. The target weight gain was expected to impact the dissolution of the coated granules substantially [142,143]. The sample size was 10 g per sampling time point and stored in a desiccator at 35°C to allow the granules to be dried entirely before the dissolution test.

Table 3-1: Full factorial design - design levels.

Variable Name	Lowest Level (-1)	Lower level (-0.5)	Center Point (0)	Higher level (0.5)	Highest Level (+1)
Granule Size (Dv50, µm)	392	419	460	480	504
Inlet air Relative humidity (% RH)	20 - 30	-	40 - 50	-	70 - 80
Fluidization Air Volume (m^3/h)	25	-	30	-	35
Spray Time (min)	80	-	110	-	140

A total of nine test coating runs were designed to maximize the D-optimality of a quadratic function of three factors: GSD, air volume, and RH with the constriction of granule availability. The D-optimal design included all five particle size levels of incoming granules, and the D-optimality was optimized using JMP software (Version 13, SAS Institute, Cary, NC). For the convenience of NIR model development, the sampling time points were adjusted to allow the weight gain of the samples from the D-optimal design to be within the range of the samples collected from the full factorial design: samples were taken at 85, 105, and 125 minutes after spraying for weight gain measurements, and corresponding NIR spectra were recorded. The predictive model for LoD was developed using NIR spectra collected from the calibration set. The

model was implemented in the test set to facilitate a feedback controller, adjusting the spray rate to stabilize the in-process LoD value at 5.5% w/w. The sample size was 10 g per time point. In summary, the full factorial design included 30 design points in total (10 coating experiments × 3 sampling times = 30), and the D-optimal design included 27 design points in total (9 coating experiments × 3 sampling times = 27).

The analytical measurements, including granule fragmentation resistance, assay, loss on drying, *in vitro* dissolution, followed the same procedure described in Chapter 2. The actual weight gain was calculated using Eq 2-3, presented in section 2.2.4.3. The incoming granules with lower fragmentation resistance than 97% were rejected to prevent the generation of excessive fines during preheating.

3.2.3 Granule Size Characterization and Fitting Methods

The granule size distributions of uncoated and coated granules were measured using a CANTY SolidSizer dynamic image analyzer (JM Canty, Inc., Buffalo, NY). The CANTY SolidSizer is a lab-scale image-based analyzer for dry particle size measurement. Granules were fed into a vibrating chute and precisely released in front of a bright field. A high-resolution camera continuously collected images of free-falling particles through a magnifying lens. The instrument automatically adjusted the vibrating frequency of the chute only to allow ten particles on each image. The CANTY software analyzed the 2-D images and output the granule size/shape information. Upon analyzing the images, a filter threshold was set to exclude the particles with aspect ratios greater than 2 to eliminate overlapping particles. The circular equivalent diameter from the image analysis was used to describe the granule size.

Five GSDs, corresponding to the five granule size levels in the DoE, were generated by counting the particle numbers in 12 size intervals, from 0 to 1200 μm with a resolution of 100 μm. The five distributions were then normalized by taking each interval's granule counts as a fraction of the total granule counts, namely frequency. The highly autocorrelated frequencies of a normalized GSD were not suitable as independent variables for multivariate linear regression. Thus, the normalized GSDs were fitted using five empirical curve-fitting methods to reduce the number of variables. The curve-fitting methods included:

1. Three-parameter Weibull model[157]

$$\mathrm{F(d)} = \mathrm{a}\left(1 - \mathrm{e}^{\left(-\left(\frac{\mathrm{d}}{\mathrm{b}}\right)^{\mathrm{c}}\right)}\right) + \varepsilon \qquad \textit{Eq. 3.1}$$

2. Power-law model[158]

$$\mathrm{F(d)} = \mathrm{a} \times d^{-b} + \varepsilon \qquad \textit{Eq. 3.2}$$

3. Van Genuchten model[159]

$$\mathrm{F(d)} = (1 + \left(\frac{a}{d}\right)^{b})^{-c} + \varepsilon \qquad \textit{Eq. 3.3}$$

4. Logarithmic model[160]

$$\mathrm{F(d)} = \mathrm{a} \times \ln d + \mathrm{b} + \varepsilon \qquad \textit{Eq. 3.4}$$

5. Principle component analysis[161]

$$GSD = Score_{\,pc1,\mathrm{GSD}} \times PC1_{\mathrm{GSD}} + Score_{\,pc2} \times PC2_{\mathrm{GSD}} + \cdots + \varepsilon \qquad \textit{Eq. 3.5}$$

In the first four curve-fitting models, F(d) is the cumulative frequency of granules in the interval of the median equivalent diameter d (μm), and the model parameters are a, b, and c. In the PCA modeling, GSD is the entire granule size distribution, $Score_{\,pc1,\mathrm{GSD}}$ and $Score_{\,pc1,\mathrm{GSD}}$ are the scores, and $PC1_{\mathrm{GSD}}$ and $PC2_{\mathrm{GSD}}$ are the loadings. An unconstrained non-linear optimization algorithm was applied to solve the fitting parameters using Matlab 2017a and optimization

Toolbox (function name: lsqnonlin). Two statistical measures, root-means-square error (RMSE) and coefficient of determination (R^2), were utilized to determine the model performances. The sum of squared residual (SSE) was calculated using Eq. 3.6.

$$\text{SSE} = \sum_{1}^{12} \left(F(d)_{fit} - F(d)_{measured}\right)^2 \qquad \textit{Eq. 3.6}$$

Since the numbers of model parameters were different for the five methods, it is essential to adjust the RMSE and R^2 based on their degrees of freedom to allow a fair comparison, calculation illustrated in Eq. 3.7 and 3.8,

$$\text{RMSE} = \sqrt{\frac{SSE}{12 - n - 1}} \qquad \textit{Eq. 3.7}$$

and

$$R^2 = 1 - \left(\frac{\frac{SSE}{12 - n - 1}}{\frac{SST}{12 - 1}}\right) \qquad \textit{Eq. 3.8}$$

where SST is the sum of squared total and n is the number of model parameters. The number of data points on the GSD curve is twelve. The curve-fitting method of the best adjusted RMSE and R^2 was utilized to describe the GSD as material attributes for process modeling.

3.2.4 Empirical Modeling Methods for Dissolution Curves

The *in vitro* dissolution profiles have drug concentration values every ten minutes from 10 to 600 minutes, including 60 data points. An in-house specification for *in vitro* dissolution was adapted from the USP standard drug release test #2 for theophylline extended-release capsules, illustrated in Table 3-2. The autocorrelation in the dissolution profiles could challenge the robustness of the process model if directly using the fractions of the drug released at 1, 2, 4, and 8

hours as responses. The practice may also cause stability issues in the feedforward controller (Chapter 5). Therefore, we employed two curve-fitting methods, Weibull function and principal component analysis, to fit the dissolution curves. The fitting parameters, instead of the dissolution profiles, were used as new responses for process modeling. This approach reduced the dimensionality of the responses and, at the same time, allowed independence between the responses.

Table 3-2: In-house specification of theophylline extended-release capsules: times and tolerances

Time (hours)	Fraction dissolved
1	Between 10% and 30%
2	Between 30% and 55%
4	Between 55% and 80%
8	Not less than 80%

3.2.4.1 Weibull Function Fitting

The Weibull function fitting is an empirical method that has great flexibility to fit most dissolution curves.[134, 135, 162, 163] The Weibull function can be expressed in multiple mathematical forms using two to four fitting parameters. A two-parameter Weibull function was employed in our study, represented as the following equation:

$$\phi = \left(1 - e^{\left(-\left(\frac{t}{\lambda}\right)^{k}\right)}\right) + \varepsilon \qquad \textit{Eq. 3.9}$$

where ϕ is the fraction of API dissolved at time t, λ is the scale factor, and k is the shape factor. Known ϕ and t, the Weibull parameters λ and k can be solved using logarithm transformation on both sides of Eq. 3.9 twice and then fitting a linear line. The dissolution profile can be reconstructed using the Weibull parameters λ and k, which means the degrees of freedom of multi-points dissolution profiles can be reduced to two. It is noteworthy that the Weibull function, as an

empirical fitting method, does not explain the dissolution kinetics and cannot be generalized beyond the studied range.

3.2.4.2 Principal Component Analysis

Principal component analysis (PCA) is a matrix operation for dimensionality reduction. Instead of fitting dissolution profiles using a predefined mathematic function, PCA focuses on the variance of a set of dissolution profiles and finds the shapes representing the bases of the maximum variance (PC1), second maximum variance (PC2), *etc*. This type of operation is empirical, and the PCA model is fully dependent on the studied dissolution profiles. The mathematical expression of the PCA model is presented as the following equation

$$\mathrm{C(t)} = \mathrm{Mean} + \mathrm{Score}_{\mathrm{pc1,dis}} \times PC1_{dis} + \mathrm{Score}_{\mathrm{pc2,dis}} \times PC2_{dis} + \cdots + \varepsilon \qquad \textit{Eq. 3.10}$$

where $\mathrm{C(t)}$ is the mean-centered dissolution profile, $\mathrm{Score}_{\mathrm{pc1,dis}}$ and $\mathrm{Score}_{\mathrm{pc2,dis}}$ are the scores, and $PC1_{\mathrm{dis}}$ and $PC2_{\mathrm{dis}}$ are the loadings of the dissolution profile. The PCA model was built on the variance space. The scores of PCs are the model parameters indicating the weights of the shapes (PCs). Recombination of the mean, the scored weighted shapes, and the fitting errors can return the original dissolution profiles.

3.2.5 Process Modeling Methods

The process model provides a mathematical understanding of the manufacturing process to speed development and facilitate control. Modeling a solids-based process is not as mature as the API synthesis and crystallization in the pharmaceutical industry.[164] It is partially due to the challenge associated with the continuum duality of particulate materials, which means the bulk behavior of particulates is determined by particle-level phenomena (details were discussed in

Section 1.3.1.3). The multivariate nature of material attributes and process parameters brings another challenge since no generalized equation can link those variables to process performance.[165] A mechanistic modeling approach such as discrete element method[149,166] and population balance modeling[150] are simulation methods that can accurately evaluate all particles in a system over a short period. However, the computational cost and the challenges related to robustness limit their applications for a comprehensive process model.[167] In contrast, the empirical approach assuming a quadratic function to map the response surface is widely adopted to establish process models for design space.[168-170] The complete form of a quadratic function is a linear combination of the main factors, their quadratic terms, and interaction terms expressed as the following equation.

$$Y = \sum_{i=0}^{n} X_i \beta_i + \sum_{i=1,j=1}^{n} X_i X_j \beta_{ij} + \sum_{i=1}^{n} X_i^2 \beta_{i\_2} + \varepsilon \qquad \textit{Eq. 3.11}$$

where X is the main factor, and β is the coefficient. Practically, the main factor needs to be investigated in at least three levels to have a meaningful quadratic term. In this study, the designed variability in the calibration set allowed the model to include the quadratic term of coating weight gain. We applied two regression methods to fit the model and compared their performance using the test set.

3.2.5.1 Partial Least Squares Regression

Partial least squares regression (PLS) is a statistical modeling method that reduces the number of model parameters by projecting the predictors to a latent space and thus increases the degrees of freedom of the errors. The latent space is structured based on the covariance between the predictors and the responses. Those properties make the PLS approach suitable for data sets with either more variables than samples or collinearity among the variables. In this study, the calibration

set of the DoE encompassed four main factors, including GSD, relative humidity, fluidization air volume, and coating weight gain. The predictor matrix had 11 variables (the GSDs were represented using one PC) after the addition of interactions and quadratic terms. The responses were the fitting parameters of the dissolution profiles. Four PLS models were built using Eq. 3.11 to independently predict the scale factor λ and the shape factor k from the Weibull function fitting and the scores of PC1 and PC2 from the PCA model. The PLS modeling approach was relatively straightforward, and the model statistics provided us some interpretability to better understand the coating process. However, as a linear combination of the variables, PLS was not always the optimal solution, which meant the model was sometimes underfitted.

3.2.5.2 Gaussian Process Regression

Gaussian process regression (GPR) is a non-parametric method that takes measures of the similarity between samples and generates the predicted value with the uncertainty (Gaussian distribution) for the future sample. A Gaussian process is a stochastic process assuming that every studied response (Y) follows a Gaussian distribution, and so does every linear combination of them. The predictors (X) are used to calculate the covariance between responses from different samples. The joint distribution of Y values of the calibration and test sets can be expressed using an X matrix, shown as the following distribution.

$$\begin{bmatrix} Y_{calibration} \\ Y_{test} \end{bmatrix} \sim N\left(\mu, \begin{bmatrix} K(X_{calibration}, X_{calibration}) + \sigma^2 I & K(X_{calibration}, X_{test}) \\ K(X_{test}, X_{calibration}) & K(X_{test}, X_{test}) \end{bmatrix}\right)$$

where X and Y are mean-centered data, N standards for normal distribution, K is the kernel function used to measure the similarity between samples, σ is the uncertainty of X, and I is the identity matrix. The joint distribution is essential to the GPR model. The prediction format is expressed as Eq. 3.12.

$$\widehat{Y_{test}} = K(X_{test}, X_{calibration})[K(X_{calibration}, X_{calibration}) + \sigma^2 I]^{-1} Y_{calibration} \qquad Eq.\ 3.12$$

The kernel function K is the critical component that grants GPR tremendous flexibility to fit almost any type of data but at the same time increases the risk of overfitting. A GPR model becomes equivalent to an ordinary least squares regression when a linear kernel (Euclidian distance) is used, and σ is set as zero. Four GPR models were established to predict the four responses: two Weibull parameters and two PC scores. A radial basis function was used as the kernel to allow the similarity between samples to be assessed in infinite dimensions. The kernel helped handle the nonlinearity in the response surface where the fitting of a quadratic function was insufficient.

3.3 Results and Discussion

The process models that captured the relationship between the investigated factors and their effects on *in vitro* dissolutions were established and tested in this study. The multivariate nature of the GSD and the dissolution profile made them difficult to be directly used in the process model, and thus curve-fitting methods were employed to transform them into fewer variables. After the data pretreatment, the process models were established using PLS and GPR regressions.

3.3.1 Modeling of Granule Size Distribution

There were three levels of GSDs in the calibration set and five levels in the test set. The curve fitting results of the GSDs are shown in Table 3-3, the R^2s and RMSEs being in the range of 0.843 - 0.988 and 0.029 - 0.108, respectively, calculated by comparing the fitted and original GSDs. The power-law model has the weakest prediction accuracy in comparison with other models. Weibull and Van Genuchten models have statistically similar performance ($p > 0.05$) in their R^2s and RMSEs, which outperform the power law and logarithmic models. The PCA model is a little tricky

since there are only three different distributions in the calibration set. There were only two degrees of freedom available for the PCA modeling after the mean-centering preprocessing.

Table 3-3: Results of the five curve-fitting methods on the three GSDs of the calibration set

Models	R^2		RMSE	
	mean	standard deviation	mean	standard deviation
Weibull	0.988	0.063	0.029	0.008
Power law	0.843	0.093	0.108	0.045
Van Genuchten	0.976	0.071	0.032	0.008
logarithmic	0.922	0.097	0.076	0.029
PCA (1 latent Variables)	0.996	0.003	0.008	0.006

The PCA model describes the 96.7% variance of the GSDs with only one parameter. The highest R^2 (0.996) and the lowest RMSE (0.008) indicate the PCA model is the optimal method compared to the other four ($p \leq 0.05$). Eq. 3.13 was used to calculate the scores of PC1, which were later used as predictors in process modeling.

$$GSD = Mean + Score_{pc1,\mathrm{GSD}} \times PC1_{\mathrm{GSD}} + \varepsilon \qquad \textit{Eq. 3.13}$$

The five GSDs of the uncoated granules are illustrated in Figure 3-4A, three of them being used in the calibration (level 1, 3, and 5) of the PCA model. The PCA model captured the difference between the GSDs. The term "Mean" in Eq. 3.13 means the mean shape of the three calibration batches. The loading of PC1, shown in Figure 3-4B, illustrated the primary shape of the variability of GSDs. Any GSD could be constructed by a linear combination of the mean shape and the weighted loading shape of PC1, using Eq. 3.13. The weight of the loading was "$Score_{pc1}$". With the known shapes of mean and the loading of PC1, The values of "$Score_{pc1}$" could be used to represent the GSDs. Comparing to the other four methods, the PCA model provides the advantage

of simplicity and accuracy. In this study, the R^2 and RMSE of the test data were 0.983 and 0.009, respectively.

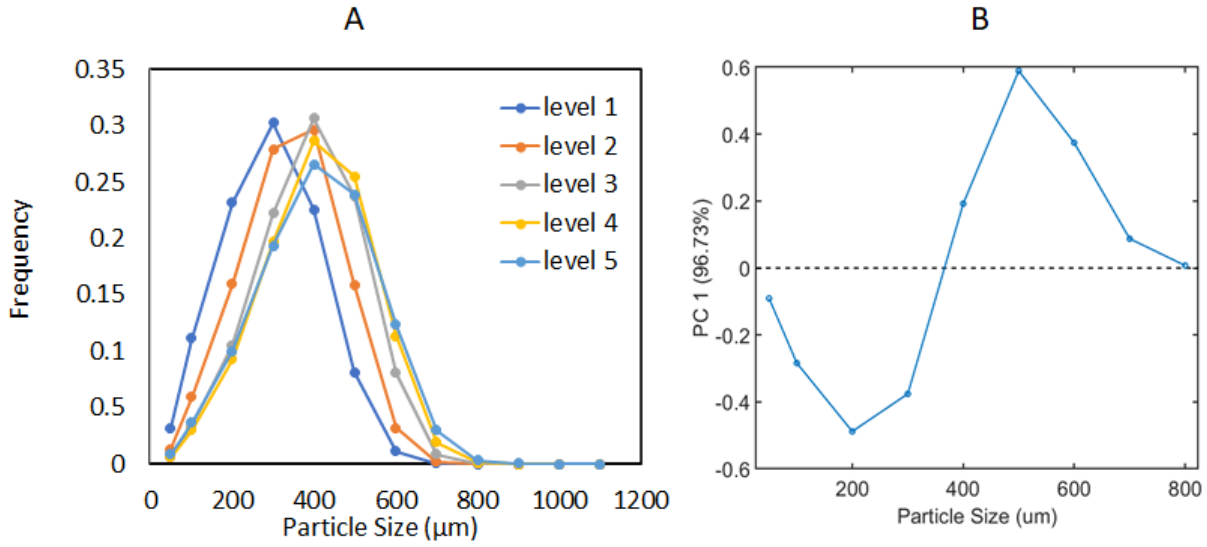

Figure 3-4: (A) the five GSDs of uncoated granules and (B) the loading of PC1 from the PCA model of GSDs.

3.3.2 Empirical Fitting Results of Dissolution Curve

The *in vitro* dissolution profiles of the calibration (30 design points) and the test (27 design points) are shown in Figure 3-5. The calibration set covers a broad range of dissolution profiles, and the test data falls within the designed range. The Weibull function and the PCA model were used to fit the dissolution profiles. The Weibull function fitting results in high R^2 values (0.975 – 0.998) for the dissolution profiles, indicating that the primary curve shapes are captured. The PCA model decomposed the variance space of the dissolution profiles. The first three PCs explain 97.32%, 2.43%, and 0.10% of the total variance, respectively. The loading shapes of the PCs are illustrated in Figure 3-6. Since the dissolution data were mean-centered before subjected to PCA modeling, the loadings represent the variability but not the mean of the dissolution profiles. The loadings of PC1 and PC2 are smoother than that of PC3, suggesting more noise is captured by PC3

than PC1 and PC2. The first two PCs were used as the best fit of the dissolution profiles to minimize the modeled noise and simplify the process models. The total variance captured by the PCA model equals the sum of PC1 and PC2, 99.75%.

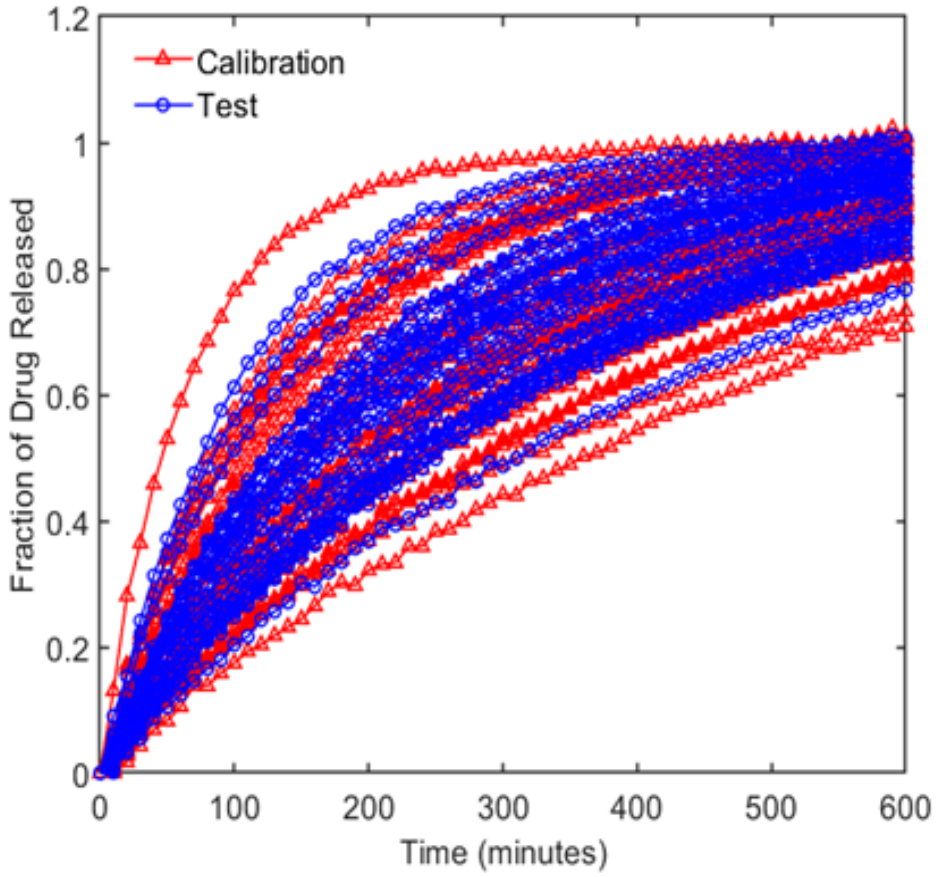

Figure 3-5: The mean dissolution profiles calculated from the three replicates of the calibration and test sets

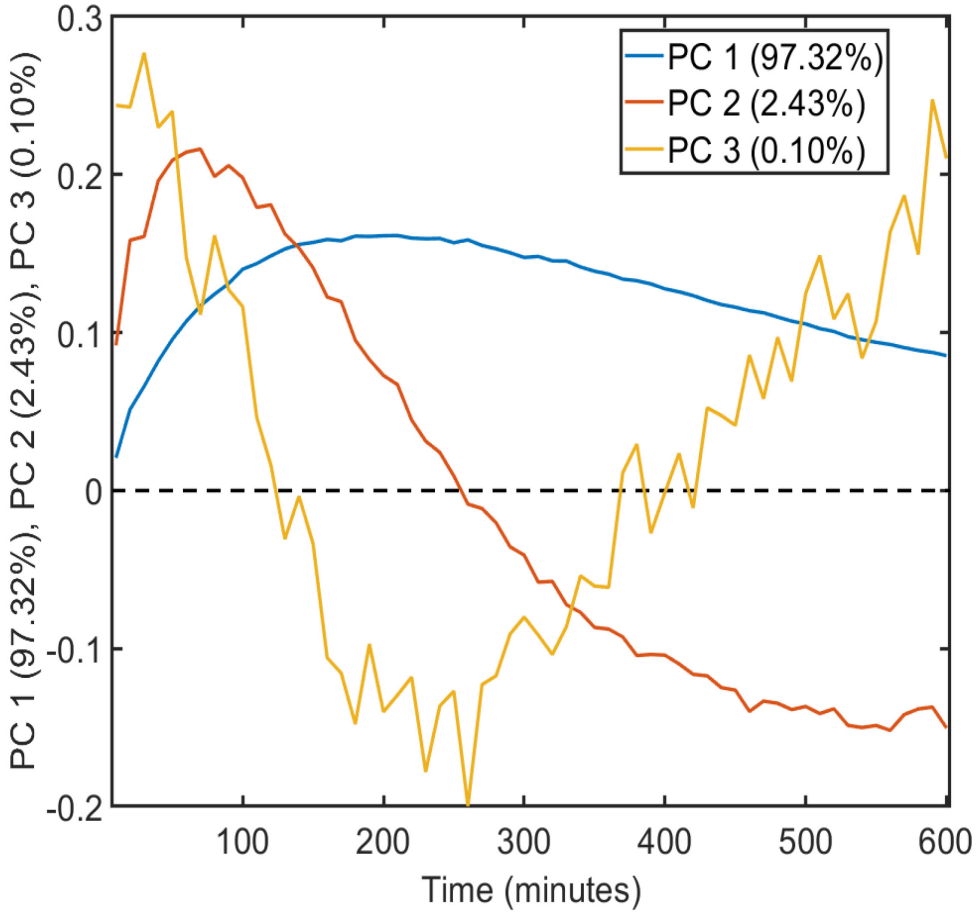

Figure 3-6: The loadings of PC1, PC2, and PC3 are calculated from the dissolution curves of the calibration set.

The two fitting residual profiles were examined, and the patterns are illustrated in Figure 3-7. The Weibull function fitting causes a bias between the measured and fitted data where the measured fractions of drug released are consistently lower than the fitted data during the initial 30 minutes. The residual pattern from 30 to 600 minutes is a continuous smooth wave shape. The error bars indicate that the pure error is more significant than the bias at most of the time points (the 95% confidence intervals included zero). In contrast, the PCA approach does not introduce any bias to the error structure due to its mean centering step. In both the Weibull function and PCA

fittings, the errors change along the time-axis in the 600 minutes interval, and the absolute values of the pure errors are around 0.005 at most time points.

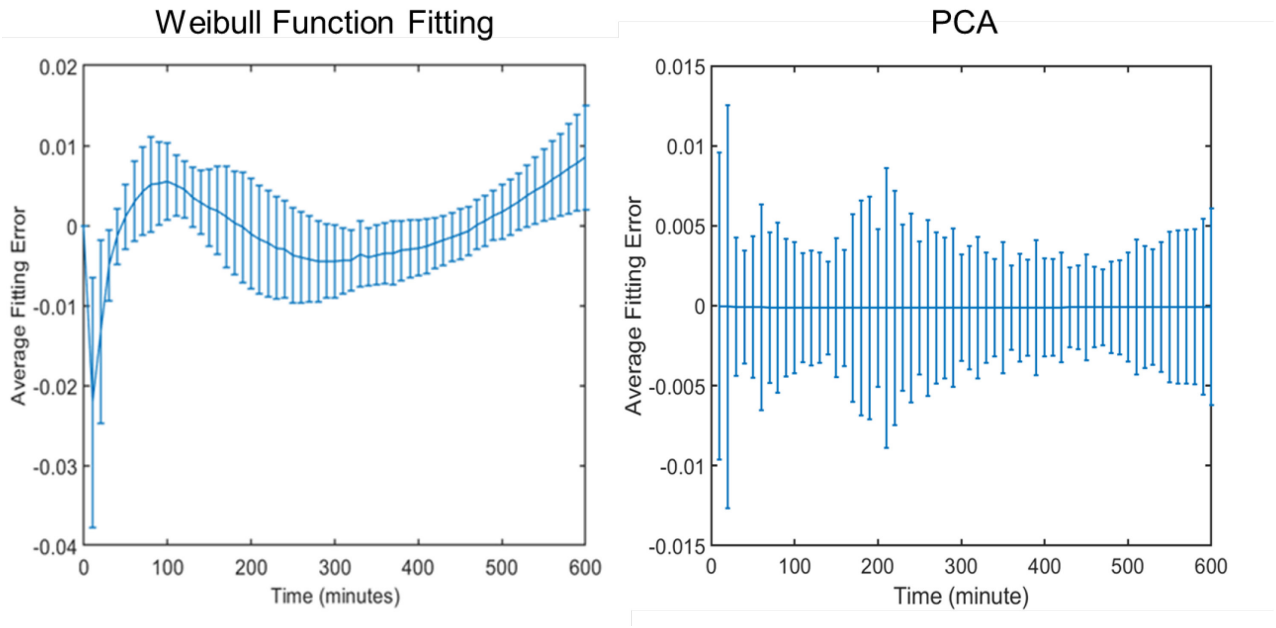

Figure 3-7: The error shapes of the Weibull function fitting and the PCA model.

3.3.3 Process Modeling Results

Four process models were established by regressing the four responses (two Weibull parameters and two PC scores) on the predictors, including fluidization air volume, weight gain, particle size distribution, and relative humidity. Fluidization air volume, weight gain, and relative humidity were continuous variables. Particle size distribution was in the form of a probability density function, which the PCA model fitted. The scores of the first two PCs (in place of the GSD) were used as the regression predictors.

3.3.3.1 Partial Least Squares Regression (PLS)

The numbers of latent variables were optimized in the PLS models using a random-subset cross-validation method with five data splits and five iterations, randomly partitioning the full calibration into five equal-sized subsets. One of the five subsets was retained as validation data for model testing, and the remaining four were used as calibration data. Five results were generated from the five subsets for one iteration and were averaged to produce a single root-mean-square error of cross-validation (RMSECV). Five iterations were applied, and the RMSECVs of all iterations were averaged. The latent variable selection minimized the cross-validation errors using a reasonable number of latent variables.

With the Weibull parameters being the model responses, three latent variables were selected in the PLS models to predict the scale (λ) and shape (k) factors. The number of chemical and physical factors is far greater than three, suggesting that the number of selected latent variables does not put the model at risk of overfitting. The coefficients of determination (R^2) and root-means-square errors of prediction (RMSEP) were calculated to evaluate the model performance using the test set. The two PLS models were mathematically expressed as the following equations:

for scale factor λ,

$$\lambda_{scaled} = -0.109X_1 - 0.033X_2 + 0.341X_3 + 0.056X_4 - 0.067X_1X_2 + 0.238X_1X_3 + 0.059X_1X_4 + 0.122X_2X_3 + 0.061X_2X_4 + 0.061X_3X_4 + 0.349X_3^2$$

and for shape factor k,

$$k_{scaled} = -0.605X_1 + 0.019X_2 + 0.204X_3 + 0.027X_4 - 0.183X_1X_2 - 0.152X_1X_3 + 0.049X_1X_4 + 0.086X_2X_3 + 0.039X_2X_4 + 0.01X_3X_4 + 0.19X_3^2$$

where λ_{scaled} and k_{scaled} = autoscaled Weibull parameters; X_1 = scaled fluidization air volume; X_2 = scaled relative humidity; X_3 = scaled weight gain; X_4 = PC1 score of GSD.

The predictors strongly correlate to the scale factor λ, with R^2 being 0.967 for calibration and 0.940 for cross-validation (Figure 3-8A). It reveals that the model explains most of the variance in the designed space. The RMSEC and RMSECV are 19.4 and 26.1 (unitless), numerically close to each other, indicating a reduced risk of overfitting. The R^2 is 0.884 for the test set, and RMSEP is 26.8, indicating that the model prediction on the test set is similar to the cross-validation. Figure 3-8B depicts the correlation between the predictors and the shape factor k. The R^2 value are 0.816 for calibration, 0.756 for cross-validation, and 0.497 for prediction. The RMSEC, RMSECV, and RMSEP are 0.0220, 0.0256, and 0.0269. Although the prediction of k is not as accurate as λ, the PLS model significantly (F-test, $P<0.05$) reduces the error from the standard deviations of k values in calibration (0.0515) and test set (0.0349).

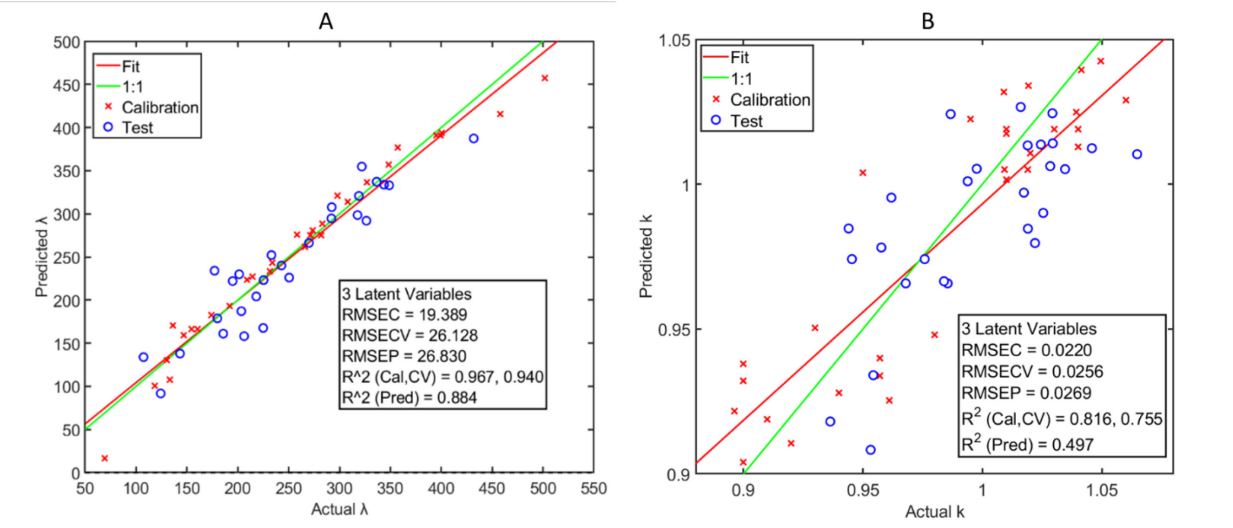

Figure 3-8: The PLS model predicting (A) the scale factor λ and (B) the shape factor k

Three latent variables were selected for the PC1 scores, and two latent variables were selected for the PC2 scores when predicting the PC scores from modeling dissolution. Figure 3-9A shows that the model predicting PC1 has good accuracy, with R^2s being 0.983 for calibration, 0.970 for cross-validation, and 0.867 for prediction. However, the RMSEP (0.278) of the PC1 model almost

doubles the values of RMSEC (0.120) and RMSECV (0.162), suggesting a potential risk of overfitting. The mathematic form of the PC1 model can be expressed as the following equation:

$$\text{PC1 Score} = 0.108X_1 + 0.038X_2 - 0.35X_3 - 0.062X_4 + 0.069X_1X_2 - 0.249X_1X_3 - 0.066X_1X_4 - 0.107X_2X_3 - 0.055X_2X_4 - 0.048X_3X_4 - 0.342X_3^2$$

where X_1 = scaled fluidization air volume; X_2 = scaled relative humidity; X_3 = scaled weight gain; X_4 = PC1 score of GSD. Since PC1 scores of the dissolution profiles are mean-centered, the model equation does not have the intercept.

Figure 3-9B reveals the correlation between the predictors and the scores of PC2 is weak, with R^2s being 0.155 for calibration, 0.092 for cross-validation, and 0.048 for prediction. The root-mean-square error of cross-validation (0.177) and prediction (0.100) are not significantly different ($p>0.05$) from the standard deviation of the calibration (0.150) and test (0.089). The PLS model cannot predict the scores of PC2 with the desired accuracy.

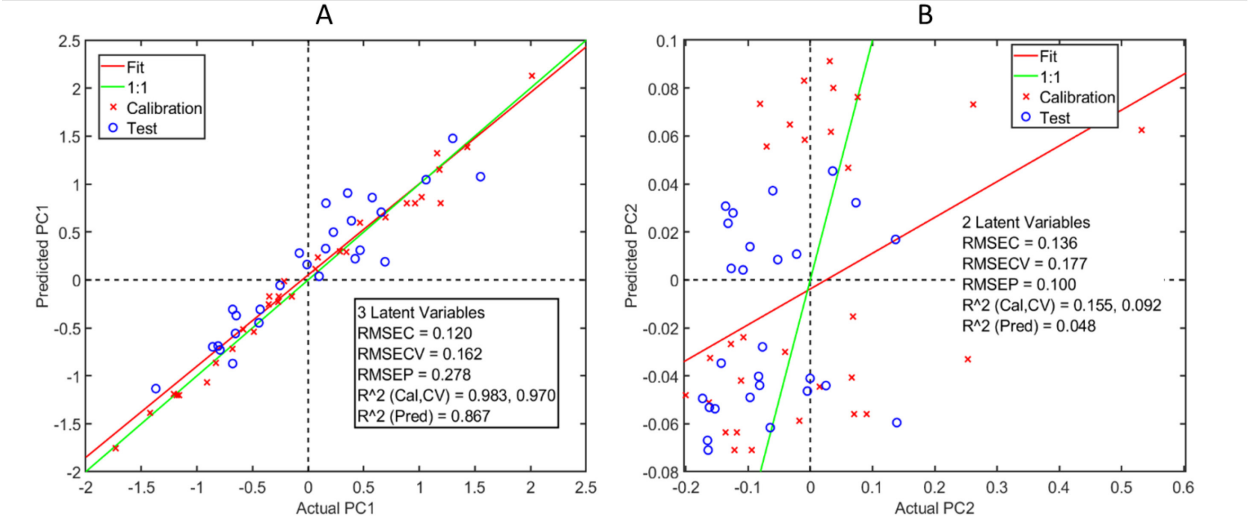

Figure 3-9: The PLS model predicting (A) the scores of PC1 and (B) the scores of PC2.

The PLS algorithm generated a few model statistics, which allowed us to gain some process understanding. The variable importance in projection (VIP) score is a ranking indicator of each

predictor, calculated using the regression coefficient b, weight vector w_j, and score vector t_j, as given in Eq. 3.14.

$$VIP\ score_k = \sqrt{n \frac{\sum_{j=1}^{a} b_j^2 t_j^T t_i (\frac{w_{kj}}{\|w_{kj}\|})^2}{\sum_{j=1}^{a} b_j^2 t_j^T t_i}} \qquad \textit{Eq. 3.14}$$

where w_{kj} is the kth element of the weight vector w_j.

A VIP score is a measure of variable contribution to predicting the response (Y), which does not reveal the statistical significance of a particular variable but indicates its importance relative to the other variables. Variables with higher VIP scores contribute the most to Y, and those with lower VIP scores have little influence on Y. However, the nature of the PLS algorithm makes the VIP calculation sensitive to collinearity. Highly collinear variables share one projection direction, which means the contributions of individual variables could appear low even if the projection direction is important. In this case, the VIP score of one variable could increase substantially after excluding the other collinear variables.

To better understand the VIP scores in our study, we adopted a "jack-knifed confidence interval" method to assess the variables with statistical measures.[171] The method repeatedly calculated the VIP scores from the PLS models using a leave-one-variable-out approach. A column of randomly generated values was added to the predictor matrix to function as a reference, no correlation between this column and the responses. Twelve PLS models were generated for one response after every variable was left out once. The confidence intervals of the VIP scores could be calculated for all variables. Figure 3-10A illustrates the VIP scores and the confidence intervals of the variables predicting the scale factor λ. The target weight gain (X3) and its quadratic term (X3^2) have significantly higher VIP scores than the other variables, including the column of random

values. Since the coating is applied to control the dissolution profile, It is anticipated that the target weight gain is the predominant variable determining the scale factor.

In contrast, the fluidization air volume (X1) and the interaction between air volume and target weight gain have significantly higher VIP scores than the others in the PLS model, predicting the shape factor k, shown in Figure 3-10B. A likely explanation is that the air volume influences the fluidization pattern and leads to uneven coating deposits on the granules of different sizes. If more coating was deposited on the smaller granules, the apparent dissolution rate tended to appear slower at the early stage and faster at the late stage. In our study, we observed the different weight gains between small granules (< 355 μm) and large granules (> 355 μm) from the same batch. Although statistically insignificant, the ratios of weight gains between small and large granules were different between experimental runs of different air volumes.

Figure 3-10C shows the VIP scores and the confidence intervals of the variables predicting the PC1 score, which has a similar pattern to the model predicting the scale factor λ (Figure 3-10A). Figure 3-10D reveals the correlation between the scale factor λ and the PC1 score, indicating a strong but nonlinear relationship ($R^2 = 0.974$). It confirms that the scale factor λ of the Weibull function captures the major variability of the dissolution profiles, and the coating weight gain is the most influential variable impacting the dissolution profiles. The PLS models for the PC2 scores were not significant, and thus the importance of the variables was not investigated.

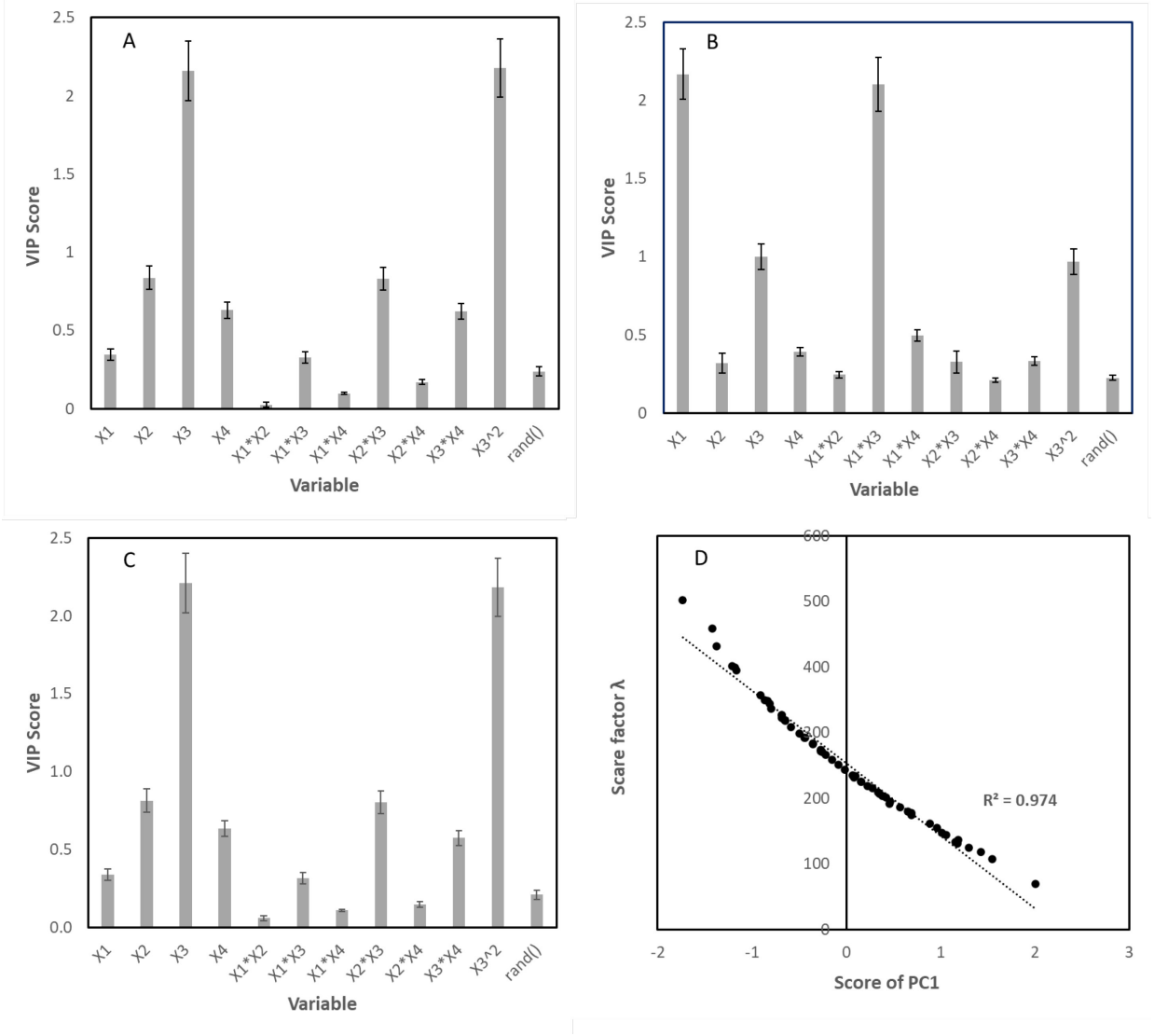

Figure 3-10: (A) VIP scores of the variables in the PLS model predicting the scale factor λ, (B) VIP scores of the variables in the PLS model predicting the shape factor k, (C) VIP scores of the variables in the PLS model predicting the score of PC1, (D) the correlation plot between the scale factor λ and the score of PC1. X_1 = scaled fluidization air volume; X_2 = scaled relative humidity; X_3 = scaled weight gain; X_4 = PC1 score of GSD; rand() =a column of random values

3.3.3.2 Gaussian Process Regression (GPR)

The GPR models were optimized using Bayesian optimization[172], which stochastically determined the hyperparameters when the objective function was not available but known to be convex. The prior GPR model was a Gaussian distribution with added Gaussian noise σ, and the

kernel was a radial basis function with a kernel parameter θ. Thus, the prior distribution has the covariance $K(X_{calibration}, X_{calibration}|\theta) + \sigma^2 I$. Fitting the GPR model to the calibration data is computationally-intensive to solve the noise σ and the kernel parameter θ. In this study, the Bayesian optimization algorithm was applied to maximize an acquisition function, called expected improvement (EI),[173, 174] instead of a clearly defined objective function. It started with a random set of (θ, σ) to obtain a series of posterior distributions of Y (the responses), and then iteratively change the values of (θ, σ) using the method suggested by Bull.[175] The optimization process stopped after 30 iterations because multiple runs from different seeds (start points) showed the optimization criteria converged before 30 iterations. The best set of (θ, σ), which had the most significant expected improvement, was selected. Figure 3-11A revealed a strong correlation between the predictors and the Weibull scale factor λ, with R^2s being 0.975 for calibration and 0.901 for prediction. The RMSEC and RMSEP of the GPR model were 18.7 and 24.6. The T-test showed there was no significant difference between the RMSEPs of the GPR and PLS models at a 95% confidence level(P>0.05).

Figure 3-11B showed the performance of the GPR model predicting the shape factor k. The R^2 of calibration is 0.825, and the R^2 of prediction is only 0.495. The RMSEC (0.0222) and RMSEP (0.0260) of the GPR model were statistically insignificantly different from the previous PLS model (P>0.05) at a 95% confidence level. The PLS and GPR models had similar performance in predicting the Weibull parameters.

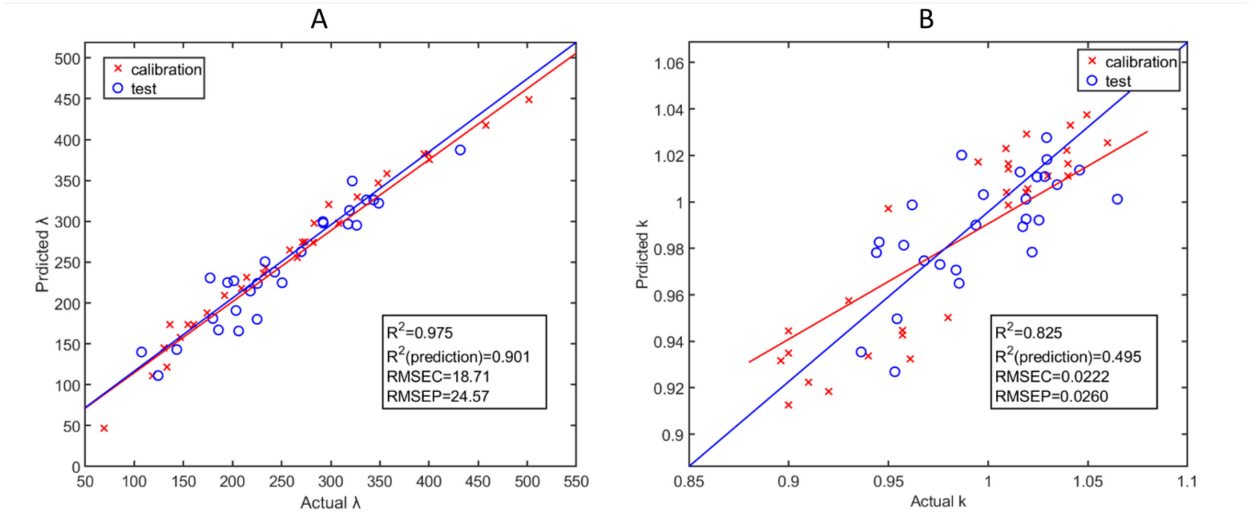

Figure 3-11: The GPR model predicting (A) the scale factor λ and (B) the shape factor k

Figures 3-12 A and B depicted the performance of the GPR model predicting the PC1 and PC2 scores of the dissolution profiles. The GPR model showed strong predictability on the PC1 scores, with R^2s being 0.987 for calibration and 0.881 for prediction. The RMSEC and RMSEP of the model predicting the PC1 score were 0.13 and 0.26, insignificantly different from the PLS model (0.12 and 0.28). In contrast, the GPR model for PC2 scores exhibited a risk of overfitting, with R^2 being 0.999 for calibration and 0.281 for prediction. The RMSEP for PC2 scores was 0.082, which was 16 folds greater than the RMSEC (0.005). Compared to the PLS algorithm, GPR is a black-box modeling method with little interpretability. Limited statistics are available to understand the contribution of each variable towards the final prediction.

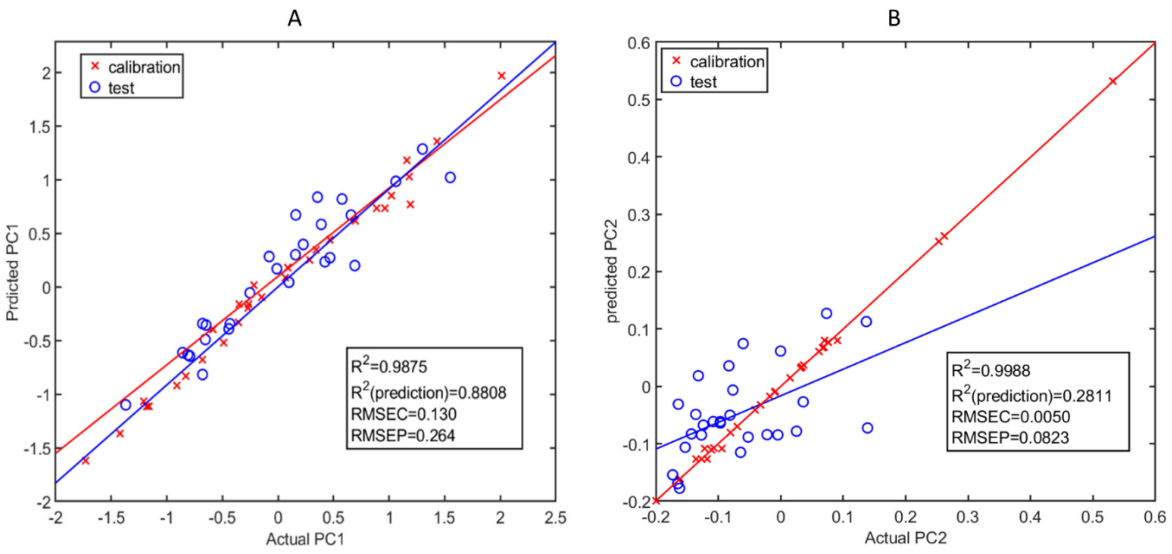

Figure 3-12: The GPR model predicting (A) the scores of PC1 and (B) the scores of PC2.

3.3.4 Reconstructed Dissolution Profiles from PLS and GPR.

The previous section (3.3.3) discussed the performance of the four modeling methods:

(1) the PLS model that predicted the Weibull parameters (λ and k) of the dissolution profiles,

(2) the GPR model that predicted the Weibull parameters of the dissolution profiles,

(3) the PLS model that predicted the PCA scores of the dissolution profiles,

(4) the GPR model that predicted the PCA scores of the dissolution profiles.

The predicted Weibull parameters and PCA scores were used to reconstruct the dissolution profiles. It should be noted that the PLS and GPR models cannot predict the PC2 scores of the dissolution profiles accurately. The dissolution curve based on the PCA fitting was reconstructed using the predicted PC1 scores and the mean dissolution profile. Since only 2.43% variance of the dissolution profiles was explained in PC2, the error caused by excluding PC2 from the model was considered acceptable.

The self-prediction, cross-validation, and test-prediction were used to estimate the accuracy of the reconstruction dissolution profiles. The RMSEC, RMSECV, and RMSEP profiles along individual time points of the dissolution profiles were calculated by subtracting reconstructed dissolution profiles from the actual dissolution profiles. Since the GPR model was optimized using Bayesian optimization instead of cross-validation, only the RMSEC and RMSEP profiles were presented.

The absolute error vs. time plot of the first modeling method (Figure 3-13A) shows that the error gradually increases from 0 to 100 minutes in all three profiles. From 100 to 200 minutes, the error remains above 0.025 for RMSEC, 0.03 for RMSECV, and 0.035 for RMSEP. After the time point of 200 minutes, all three error profiles show a decreasing trend over time. Similar trends of the absolute vs. time plots are observed in the other three methods (Figure 3-13B, C, and D). This observation is consistent with the raw dissolution profiles (Figure 3-5), where the most substantial variability is observed from the second hour to the fourth hour between the design points. Comparing Figure 3-13A and B, the RMSEC and RMSEP profiles of the PLS and GPR models are similar when the same dissolution curve-fitting method: Weibull function fitting, was applied. The critical time points of the in-house specification are identified on the RMSEP profiles: the error values are around 0.02, 0.035, 0.035, and 0.025 at Hour 1, 2, 4, and 8, respectively. The highest values of the two RMSEP profiles are below 4% in both plots. The similarity of RMSEP profiles between the PLS and GPR models is depicted in Figures 3-13C and D, where the PCA model fits the dissolution curves. The RMSEP values at the critical time points are around 0.03, 0.05, 0.045, and 0.03 at Hour 1, 2, 4, and 8, respectively. The highest RMSEP values of the two error profiles are both around 5%.

The results reveal that the PLS and GPR regressions had similar performance in terms of the errors between the actual and reconstructed dissolution profiles. It is consistent with the previous finding that the two regression methods have similar performance predicting the Weibull parameters or the PCA scores. Meanwhile, the models predicting the Weibull parameters outperform the models predicting the PCA scores. The previous discussion reveals that the pure errors of the two curve-fitting methods are similar (around 0.005 at most time points), and there is a fitting bias in the error profile of the Weibull function fitting. Therefore, the higher errors in the reconstructed dissolution profiles from the PCA model are mainly due to the higher errors of the process models, regardless of the regression methods. The process models do not accurately predict the scores of PC2 from the PCA model, which by default introduces 2.4% relative error into the reconstructed dissolution profiles.

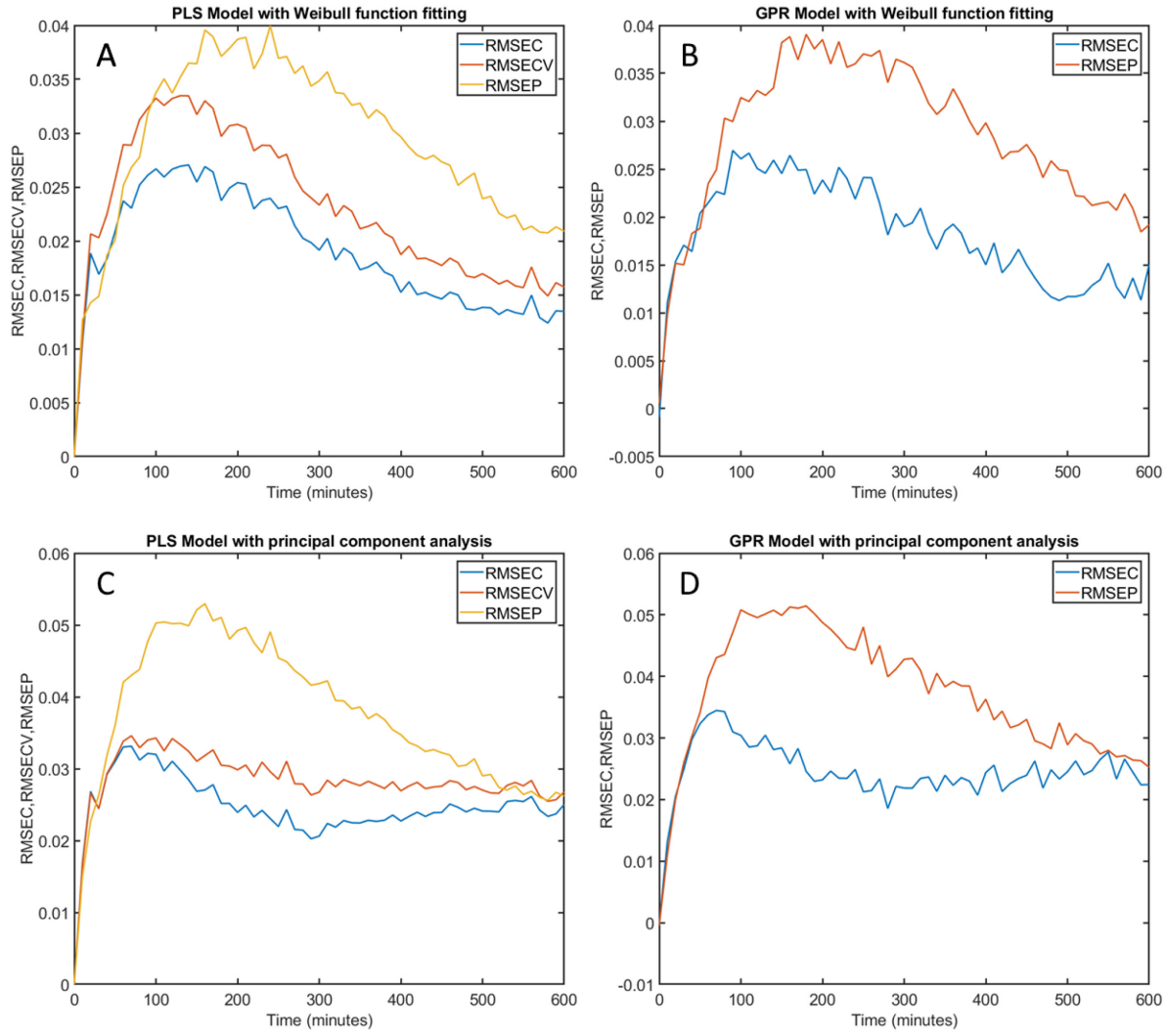

Figure 3-13: Absolute error vs. time plots from the four modeling methods in calibration, cross-validation, and prediction. (A) the PLS model that predicted the Weibull parameters of the dissolution profiles; (B) the GPR model that predicted the Weibull parameters of the dissolution profiles; (C) the PLS model that predicted the PCA scores of the dissolution profiles; (D) the GPR model that predicted the PCA scores of the dissolution profiles.

3.4 Conclusion

The impact of four predictors (fluidization air volume, coating weight gain, inlet air relative humidity, and granule size distribution (GSD)) on the *in vitro* dissolution of granules produced in a fluid bed coating process was studied using a response surface methodology. Both the GSD as a

predictor and the *in vitro* dissolution as the response had multiple variables. Principal component analysis (PCA) was used to reduce the GSD from a multivariate distribution to one variable (score of PC1). The *in vitro* dissolution profiles were fitted using two algorithms: Weibull function and PCA. Process models were established by regressing the *in vitro* dissolution on the four predictors. Two regression methods: PLS and GPR, were applied and compared. The process model using a combination of PLS regression and Weibull function showed the best performance in predicting the *in vitro* dissolution profiles.

The study of this chapter accomplished Specific Aim 2 by developing the process models of the fluid bed coating process. The process models serve as the basis of feedforward control loops in the following studies.

Chapter 4 : Development of Real-Time Predictive Models for In-Process Monitoring and Feedback Control using Near-infrared Spectroscopy and Raman Spectroscopy

Abstract

A feedback control system for a coating process must maintain the in-process moisture level, and ensure polymer deposition, and preserve theophylline monohydrate at desired levels to prevent batch collapse and obtain reproducible product dissolution profiles. This study utilized NIR and Raman spectroscopic technologies to develop in-line and at-line models that predict the values of loss on drying (LoD), coating weight gain, and theophylline monohydrate concentration in coated granules. Partial least squares regression (PLS) was utilized as the modeling method to extract information from the multivariate spectral data correlated to the analytes of interest. NIR spectroscopy was successfully applied to predict 1) the LoD values of the granules, which was a surrogate indicator for the moisture level at the steady state of the coating process, and 2) coating weight gain to indicate when the desired target was reached. The NIR models were used to maintain the steady-state moisture level and terminate the spray phase of the coating process via closed-loop feedback control. Raman spectroscopy was employed to monitor and control the concentration of theophylline monohydrate in the coated granules during the drying stage. However, the predicted concentration of theophylline monohydrate was insufficient for the control of *in vitro* dissolution profiles due to the uncertainty of the Raman model at low concentrations (RMSECV = 2.5%w/w). Thus, instead, the NIR model for LoD was utilized to determine the drying endpoint of the coating process. This study showed that the PATs enabled the real-time

monitoring and control for the coating process, and the selection of PAT should be based on the practical considerations and model uncertainty.

4.1 Introduction

Process analytical technology (PAT) has drawn a great deal of attention as a tool to optimize, monitor, and control the pharmaceutical manufacturing process to improve product quality. Adopting PAT allows the pharmaceutical industry to take in-line, on-line, or at-line measurement of the critical quality attributes (CQAs) for in-process or end products. PAT offers several advantages as a real-time analysis method, including minimal sample preparation and rapid data collection of the variability from physical and multiple chemical sources.[176]

Near-infrared (NIR) spectroscopy is a widely used PAT tool for process monitoring under the QbD paradigm. The NIR signals are the overtones of the mid-IR band caused by asymmetric molecular vibration. NIR radiation is absorbed by the chemical bonds that present a change in the dipole moment with molecular vibration. The typical low absorptivity of a chemical substance in the NIR region results in the ability to examine a sample with no or minimal sample preparation, enabling a rapid and non-destructive measurements.[177] Water is probably the most common measurement made using the NIR spectroscopy since it has four strong characteristic bands in the NIR region of 970, 1200, 1450, and 1950 nm. NIR had been reported for use in a fluid bed processor to determine the in-process product moisture level in real-time.[96, 178, 179] In addition, several studies have shown applications of NIR spectroscopy in monitoring drug potency, content uniformity, and coating weight gain for pharmaceutical unit operations, including wet granulation, blending, tableting, roller compaction, and coating.[96, 180-183]

As a complementary technique to NIR spectroscopy, Raman spectroscopy is the observation of inelastically scattered photons upon their interaction with electromagnetic radiation and molecular vibrations, phonons, or other excited vibrational states, resulting in a frequency shift of the incident light. Raman scattering is highly selective, so that it becomes an ideal alternative PAT to NIR. Raman spectroscopy has been used in characterizing coating properties,[184] in-line monitoring fluid bed coating process,[185] and detecting theophylline hydration and dehydration.[120]

Both NIR and Raman spectral data often include hundreds to thousands of variables. With advancements in computational devices and chemometrics, analysis of the raw spectra is practical and computationally feasible. Chemometric techniques, including variable selection, data pretreatment, and dimension reduction methods, are often required to minimize the noise and extract relevant information for quantitative analysis. The optimization of the NIR and Raman models is critical because the prediction needs to be accurate, precise, and robust. Under or over-fitting of the spectral data can result in poor future model performance.

The framework of this chapter was built upon the experimental design described in Chapter 3. The blocks of yellow dashed lines in Figure 4-1 illustrate how the development of NIR and Raman models was related to the experimental design for process modeling. In-line NIR predictive models that monitored LoD values (in-process moisture level) and coating weight gain were established using the data collected during the calibration batches of the process models. The LoD model was utilized to facilitate a feedback control loop that proportionally adjusted the spray rate based on the deviation of moisture level from the target value for the test set. The coating weight gain model was developed to indicate the time when the target coating weight gain was obtained so that the spraying of the coating process could be terminated. The performance of the coating weight gain model was evaluated using the data of the test runs; model statistics (R^2 and RMSEP) being

calculated. In contrast to the NIR model calibration, the design of calibration for the Raman model that predicts theophylline monohydrate (w/w) in the dried granules is independent of the experiments for process modeling. The predicted theophylline monohydrate concentration (w/w) was used to determine the endpoints of the drying phases.

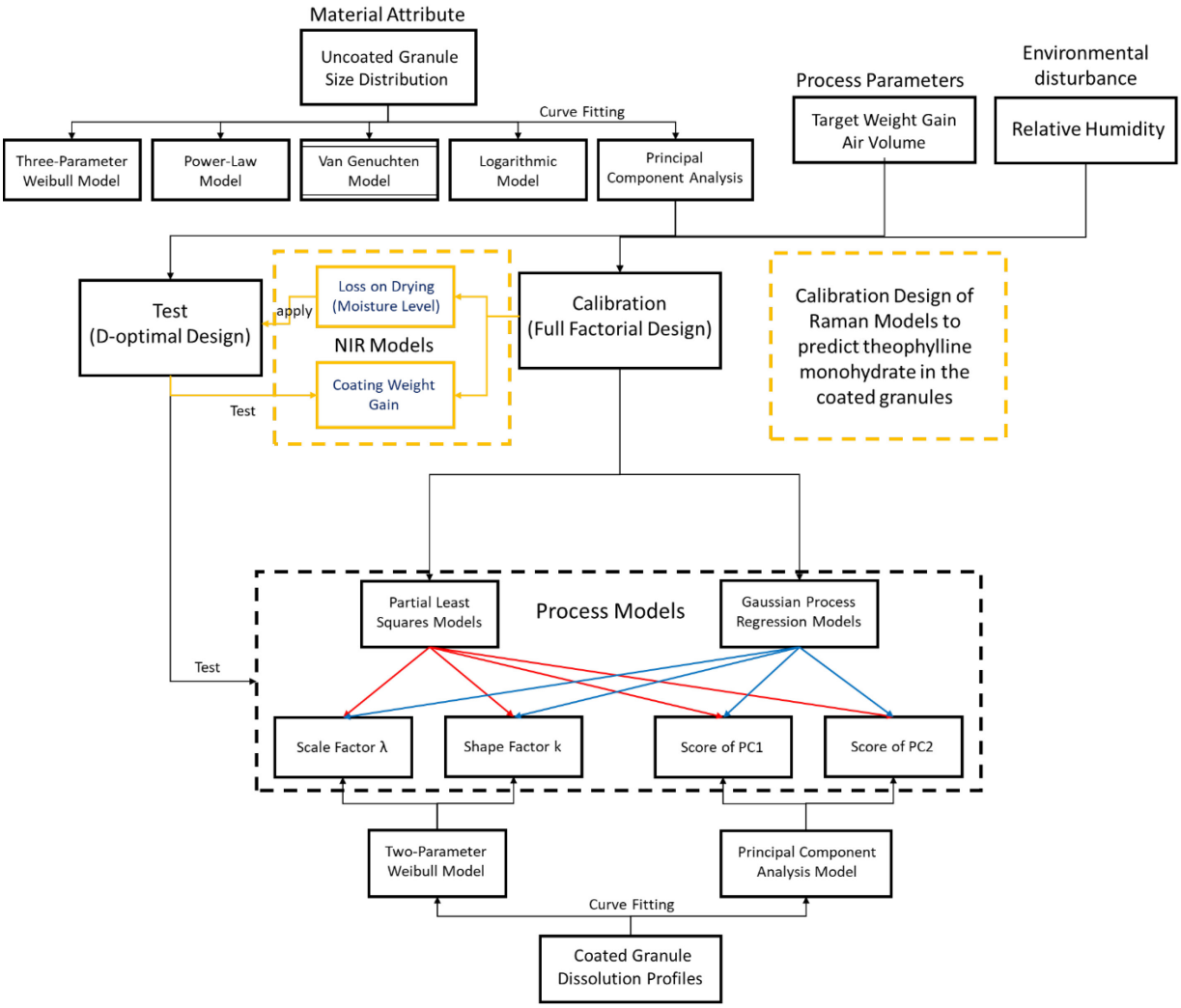

Figure 4-1: Illustration of the experimental plan and data analysis for the process modeling and the development of PAT models (shown in blocks of yellow dashed lines). The NIR models were developed using the data collected during the response surface design described in Chapter 3. The Raman model was established based on an independent design of calibration.

4.2 Materials and Methods

4.2.1 Materials and Equipment

The details of the materials, coating equipment, and NIR sensor set-up were described in Chapter 3. The off-line Raman spectra of the coated granules were collected during the drying phase using an RXN2 Hybrid analyzer (Kaiser Optical Systems, Ann Arbor, MI) with a thermoelectrically cooled charge-coupled detector. The raw data of NIR and Raman spectroscopy were processed using Matlab software (with Optimization Toolbox, version R2017a, Mathworks Inc., Natick, MA) and PLS Toolbox (version 8.2.1) by Eigenvector Research (Manson, WA).

4.2.2 Design of Calibration

NIR models

The DoE for process modeling was described in Section 3.2.2. This study developed two in-line NIR models to monitor in-process moisture level and coating weight gain using the data collected in the previously described calibration and test coating batches. It should be noted the loss on drying (LoD) value was used as a surrogate indicator for in-process moisture level since no volatile component other than water was presented in the formulation of both coated core and coating dispersion.

Raman model

The Raman model was developed to predict theophylline monohydrate concentration during the drying process. As a complex system containing a core and a coating layer, the coated granules were ground to powder using mortar and pestle to obtain representative Raman spectra. The calibration of the Raman model used a powder mixture of the pure API and excipients. The API and excipients were also ground using mortar and pestle for the same amount of time as the

granules to estimate the effect of grinding on the theophylline solid-state form. The calibration set was designed to decorrelate theophylline anhydrous and monohydrate signals, shown in Figure 4-2A. The coefficient of determination in the calibration design between the concentrations of the hydrate and anhydrate was 0.0221. Theophylline monohydrate was prepared by recrystallization from supersaturated theophylline solution and stored at the 95% RH condition maintained by a saturated solution of potassium nitrate.

In addition to the theophylline, the coated core also contained 1% w/w Hypromellose (HPMC), 18.5% w/w microcrystalline cellulose (MCC), and 19.5% w/w lactose monohydrate. The seven design points on the diagonal from the top left to the bottom right of Figure 4-2A were augmented with additional design conditions that included the excipient variability to enhance the robustness of the model. Shown as Figure 4-2B, the augmented design kept the 1% w/w HPMC consistent, varied the concentration of lactose monohydrate in three levels (10%, 19.5%, 29% w/w), and adjusted the concentration of MCC to a total of 100%. The powder mixtures were blended with an additional 20% w/w of the coating, of which the film was cast on a petri dish and then ground to powder using mortar and pestle.

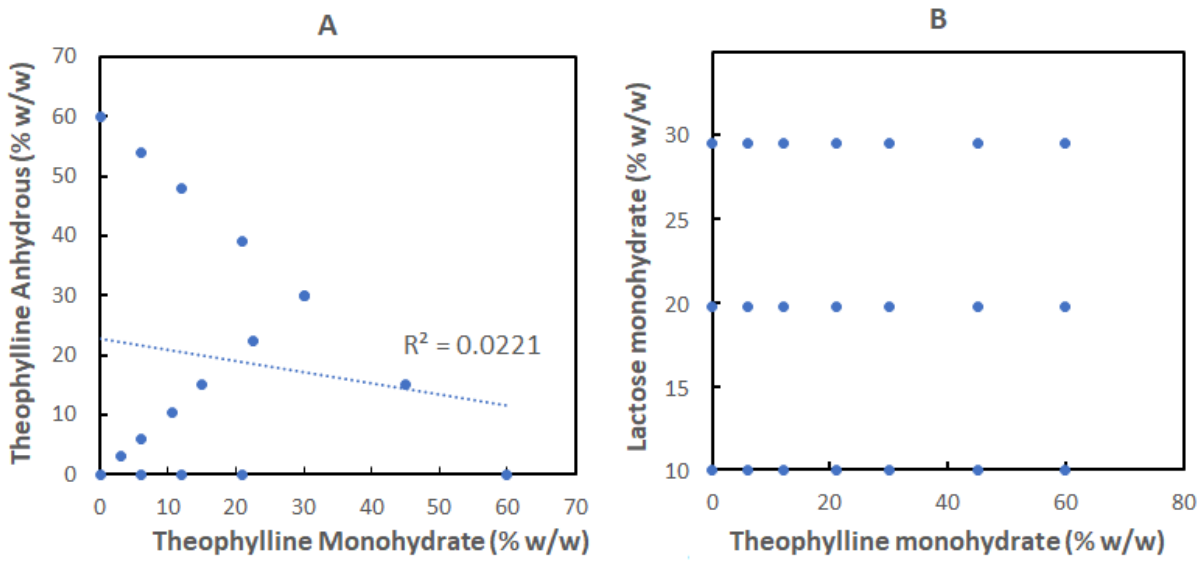

Figure 4-2: (A) the design of the ratio between theophylline anhydrous and theophylline monohydrate. (B) The three lactose concentration levels augment the seven design points on the leading diagonal of (A).

4.2.3 Near-infrared Spectra (NIRS) and Raman Spectra Collection

A NIR spectrometer (model: NIR-256-2, Control Development Inc., South Bend, IN) and halogen light source with a bifurcated fiber optic probe (Ocean Optics, Dunedin, FL) were used to collect spectra during the coating process. The probe was inserted through the side port of the fluid bed bowl, directly contacting the coated material. Each spectrum was acquired in real-time by averaging 16 scans over the range of 1077 – 2226 nm with a resolution of 1 nm. The integration time for one scan was determined using a Teflon reference sample to optimize the integration time (approximately 0.015 ms, varying by 0.002 ms for different batches). A near-infrared spectrum was recorded every 5 seconds, as the average of 16 spectra. The NIR Models were established by regressing the responses (LoD and coating weight gain) on the spectra using PLS algorithm. The primary methods to measure the responses were described in Section 2.2.4.3.

The Raman spectra were collected offline using a non-contact optic device (PhAT probe) after the coated granule samples were ground. The calibration samples were powder mixtures that did not require grinding but were still ground as if they were granule samples to reproduce the variability caused by grinding. The ground powders were stored in a 20 mL Thermo Scientific sample storage glass vial and scanned in a dark environment. The excitation laser was projected onto the top surface of the powder bed in the vial, forming a circular illuminated area of 6 mm diameter. The Raman spectra were collected with an exposure time of 5 seconds. The range of the Raman spectrum was 150 -1890 cm^{-1} wavenumbers, with a resolution of 1 cm^{-1}. The model response was the concentration of theophylline monohydrate, for which the values were gravimetrically determined.

4.2.4 Model Calibration and Evaluation

The predictive models were established following a procedure (Figure 4-3) to optimize the model performance. The calibration data were subjected to two pretreatments, including data preprocessing and variable selection. The preprocessing included a combination of mathematical methods to reduce the random noise and structured interference (*i.e.*, scattering effects in NIR spectra and fluorescence in Raman spectra). The variable selection was performed to focus on the signal from the analyte of interest by excluding irrelevant and noisy variables. The regression algorithm was PLS, of which the number of latent variables was optimized using a five-fold, five-iteration cross-validation. The cross-validation was performed using a random subset method which randomly partitioned the calibration data into five subsets. One of the five subsets was retained as the test set, and the rest four subsets were used as training data. The procedure was repeated five times so that all samples were used in both training and test, and each sample was

used as a test exactly once. The randomization process of data partition was done five times to obtain an average error value from multiple cross-validation runs.

The NIR-LoD model was implemented to control the in-process moisture level by adjusting the spray rate for the test batches. The model performance was evaluated by randomly sampling in-process products for actual LoD measurements. The measured LoD values were then compared to the model predicted LoD values. In contrast, the performance of the NIR model for coating weight gain was evaluated by the test batches of which the coating weight gain values followed a D-optimal design (described in Section 3.2.2). Model statistics, including the coefficients of determinations (R^2) of calibration, cross-validation, and prediction, and the root-mean-square errors of calibration (RMSEC), cross-validation (RMSECV), and prediction (RMSEP), were calculated. The values of R^2 represented the precisions of the models, which focused on the pure errors. The root-mean-square error (RMSE) was a combined measure of both accuracy and precision. It was calculated using Eq. 4.1:

$$RMSE = \sqrt{\frac{\sum_1^n (y_i - \hat{y}_i)^2}{n}} \qquad \textit{Eq. 4.1}$$

where y_i and $\hat{y}_i$ are measured and predicted responses, respectively, and n is the number of samples in calibration, cross-validation, or prediction. It should be noted the model parameters share the total degrees of freedom with the calibration and cross-validation errors but do not influence the degrees of freedom of the prediction errors from the test set. Thus, the formula used the sample size instead of the degrees of freedom for normalization to allow fair comparisons of RMSEC, RMSECV, and RMSEP.

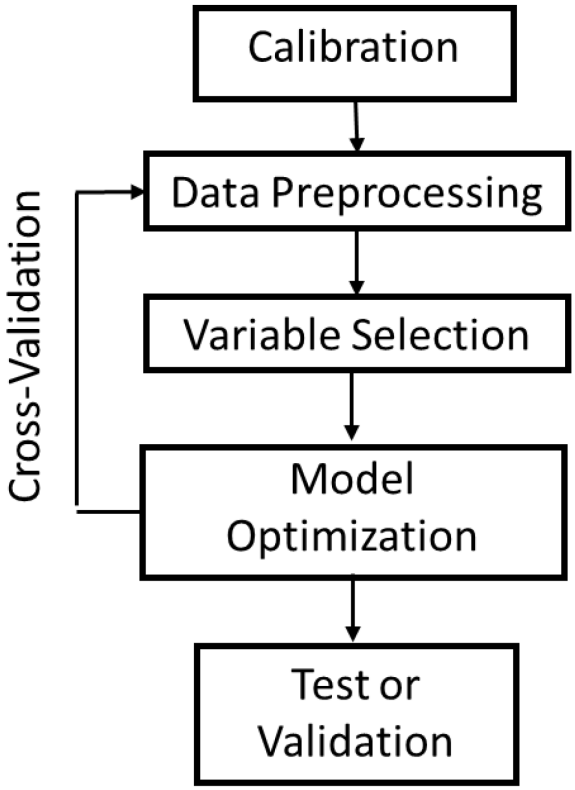

Figure 4-3: Modeling procedure for both NIR and Raman predictive models.

Both NIR and Raman spectra had thousands of highly correlated variables. The major variability related to the analyte of interest was buried in a few dimensions, leaving the remaining dimensions representative of noise. The linear combination of these noise sources sometimes matched well with the variance structure of the analyte of interest, which caused overfitting. The overfitted model explained the calibration data well but failed to predict new samples accurately. Therefore, the NIR and Raman predictive models were subjected to permutation tests to evaluate overfitting risks.

The permutation test randomly shuffled the order of the response (Y) and built the model by regressing the mismatched responses (Y) on the predictors (X): each sample was assigned to incorrect Y values, while the distribution of Y was retained. The permutation test was repeated to

generate the distributions of RMSEC, RMSECV, and RMSEP from the incorrect models. The distributions were then compared to RMSEC, RMSECV, and RMSEP from the correct model. The probability that the error statistics of the correct model were from the same error distribution as the incorrect models indicated the overfitting risk.

4.3 Results and Discussion

4.3.1 NIR Models Predicting Coating Weight Gain

NIR and Raman spectroscopies are complementary methods. Both detect the vibrational modes in molecules. In general, compounds with strong bands in the NIR spectrum have weak peaks in the Raman spectrum and vice versa. There are many chemical components in the coated granules that are NIR or Raman sensitive. The coating film is a complex polymeric system consisted of PVAc, PVP, SLS, TEC, Talc, and blue lake. The drug-loaded core is a mixture of theophylline, lactose monohydrate, MCC, and HPMC. The correlation between the NIR spectral change and the coating weight gain came from the increased signal of the coating film on the surface and the decreased signal of the drug-loaded core. Figure 4-4 shows the spectral responses to the change in coating weight gain (13%, 17%, and 20% w/w) of fluidized coated granules for both NIR (Figure 4-4A) and Raman spectroscopies (Figure 4-4B). In addition to the chemical variability, the NIR spectra are influenced by the scattering effect due to the fluidization in the fluid bed processor, which is observed primarily as a baseline shift. Thus, NIR spectra are impacted by both coating weight gain and the baseline shift. Unlike the broad peaks of the NIR spectra, the Raman spectra showed distinctive peaks. Changes in slope and offset of the baseline were observed in the Raman spectra, probably caused by the fluorescence of the coating film.

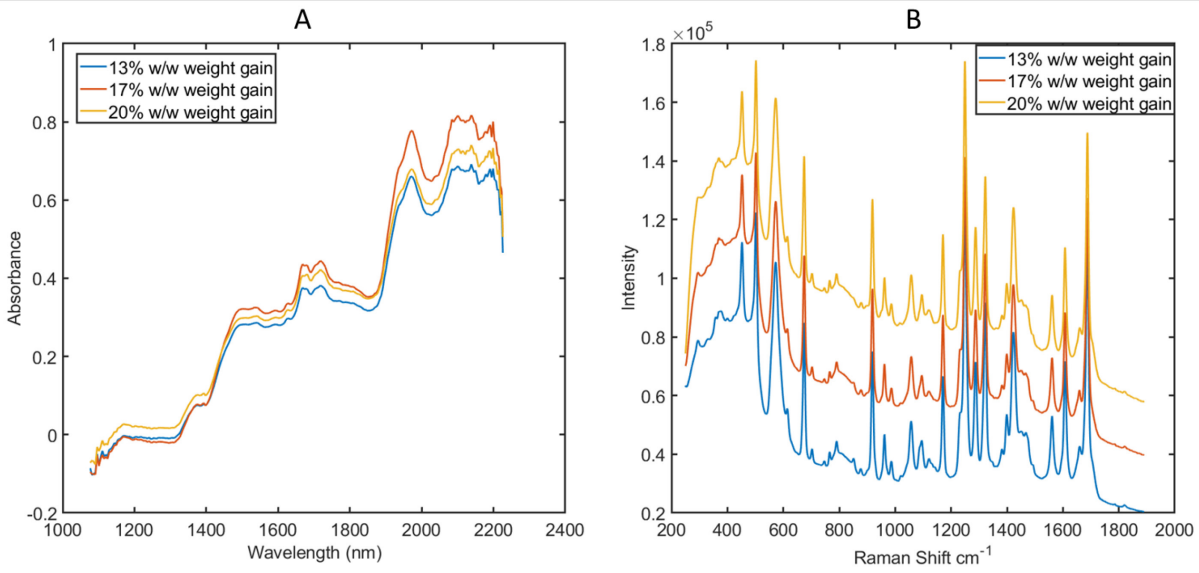

Figure 4-4: the NIR spectra (A) and Raman spectra (B) of fluidized coated granules at three different weight gain.

Although both NIR and Raman spectra have signals related to the change of coating weight gain, the NIR spectroscopy has the advantage of moisture sensitivity, while Raman spectroscopy is known to have weak signals from water molecules. Fluid bed coating is a wet process, and the dynamical change of the moisture level in the system potentially influences the batch stability and the product quality. The NIR spectra are used for the prediction of both coating weight gain and LoD.

The coating weight gain model was calibrated on the 30 samples from the calibration set and tested on the 27 samples from the test set. Ten spectra were collected within a 50-second interval at each designed time point when the granule samples were drawn for coating weight gain measurements. The noisy spectral regions of 1077 – 1150 nm and 2100 – 2226 nm were excluded from the model. The NIR predictive model was developed using partial least squares (PLS) regression. Since the major interference in the raw NIR spectra (Figure 4-5A) was the baseline shift, several preprocessing methods were evaluated to optimize the model performance. The

number of latent variables was chosen along with the selection of preprocessing method using cross-validation. The optimal preprocessing method for the spectra (X-block) was standard normal variate (SNV) followed by mean centering. Auto-scaling was applied to the coating weight gain data (Y-block). The model using four latent variables (Figure 4-5B) yielded the best results, where the values RMSEC, RMSECV, and RMSEP stopped decreasing with the increase of the number of latent variables. The calibration and prediction statistics (all values are absolute error) are in Figure 4-5C: RMSEC of 0.003, RMSECV of 0.003, and RMSEP of 0.005. The reduced Q residuals vs. Hoteling T^2 plot (Figure 4-4D) indicates that most of the test samples are within the 95% confidence interval of the calibration, suggesting that they are insignificantly different from the calibration data. The calibration utilizes the 99.68% variance from the spectral data to explain over 99% of the variance in coating weight gain. The total calibration range is from 0.10 to 0.29 fraction weight gain; the R^2 is 0.98, and an error of 0.005 (absolute) for the test set is observed.

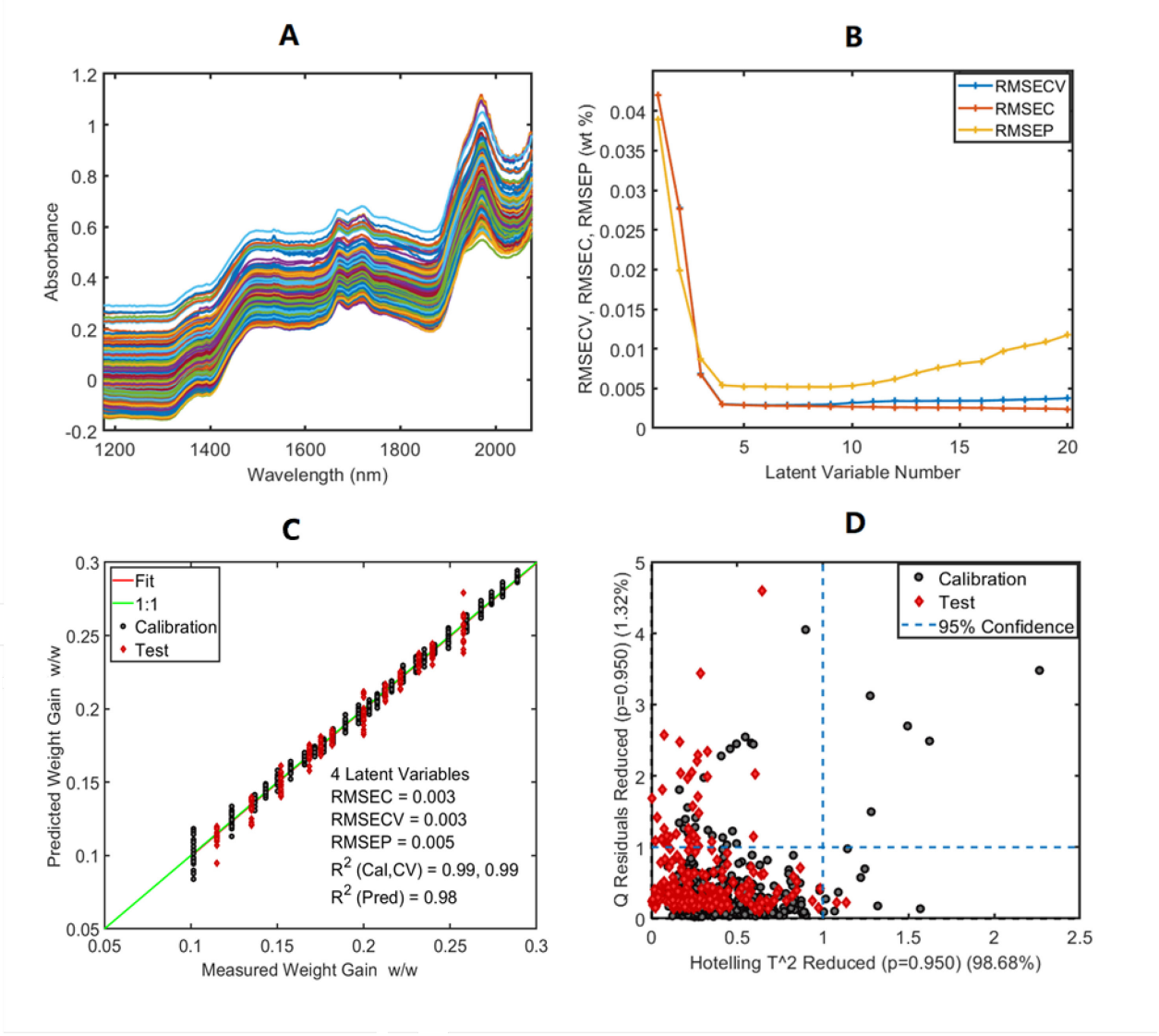

Figure 4-5: The NIRS predictive model for coating weight gain: (A) Raw NIR spectra of the calibration set; (B) Scree plot for the optimized preprocessing method: SNV + mean centering; (C) Predicted vs. measured weight gain; (D) Q residual vs. Hotelling T^2 plot.

The permutation test was repeated 100 times to get representative distributions of RMSECs, RMSECVs, and RMSEPs from the models using "incorrectly assigned" responses. Four latent variables were selected for all the models. The results of the permutation test are shown in Figure 4-6. The means of the RMSECs (0.049) and RMSEPs (0.042) are the same as the standard deviations of the responses (Y) in the calibration (0.049) and test sets (0.042). The introduction of

modeling uncertainty probably causes the higher mean (0.055) of the RMSECVs than the RMSECs. It is interesting to observe that the distributions of RMSEC and RMSECV are much narrower than RMSEP. It is probably because some of the incorrect models coincidently explain some variability in the responses of the test set, resulting in relatively low RMSEPs. However, the RMSEC (0.003), RMSECV (0.003), and RMSEP (0.005) of the original model predicting correct responses are one order of magnitude lower than the three distributions. The probability is less than 0.0001 that the original model is from the same population as the randomly shuffled models regarding either RMSEC, RMSECV, or RMSEP.

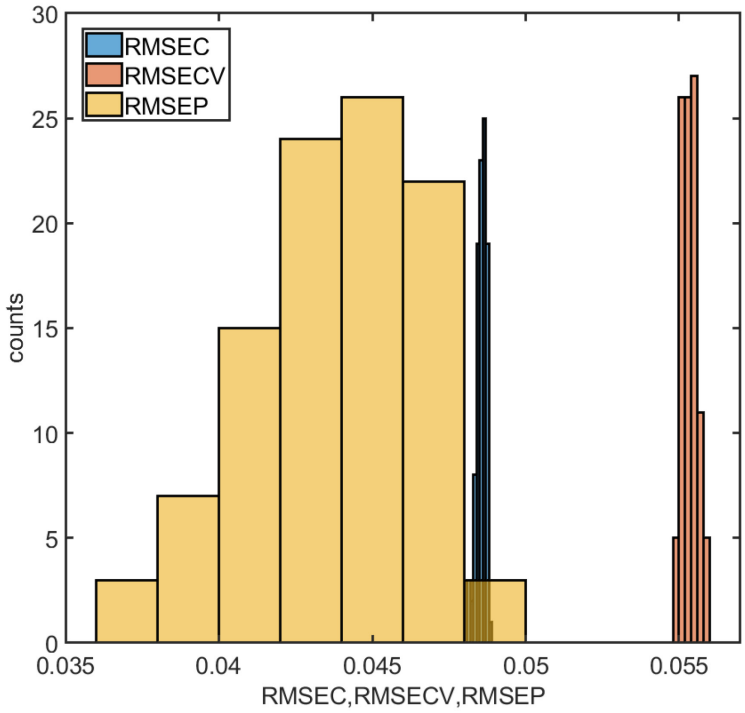

Figure 4-6: Distribution of RMSEC, RMSECV, and RMSEP from the permutation test of coating weight gain models.

The NIR model was utilized to enable the real-time monitoring of coating weight gain and determine the spraying endpoint. Figure 4-7 shows one example of a predicted coating weight gain

trajectory during the preheating and spraying phases. The blue line is the predicted weight gain of which the NIR model generated every five seconds. The fluctuation of the weight gain predictions is probably caused by granule fluidization, moisture variability, and instrumental noise. The baseline shift due to the fluidization has the highest leverage among the three probable causes because it changes the sample presentation for every scan. The initial flat region in Figure 4-7 indicates no coating weight gain during the preheating phase, and the increasing region shows that the increase of coating weight gain is steady and linearly correlated to time. The spraying automatically ended when the mean of 15 consecutive predictions reached the target, 20% w/w in this plot. The orange circles in Figure 4-7 indicate the time points when samples were drawn from the coating process for reference testing. Three samples were subjected to the assay and LoD measurements for every sampled time point. The actual coating weight gains were calculated using Eq. 2.2. The orange circles align well with the blue line (Figure 4-7), suggesting the NIR model predicts the coating weight gain with the desired accuracy. The seeming bias of the first two orange circles is only exhibited in this example by chance. No systematic errors were observed in other NIR model monitored coating batches.

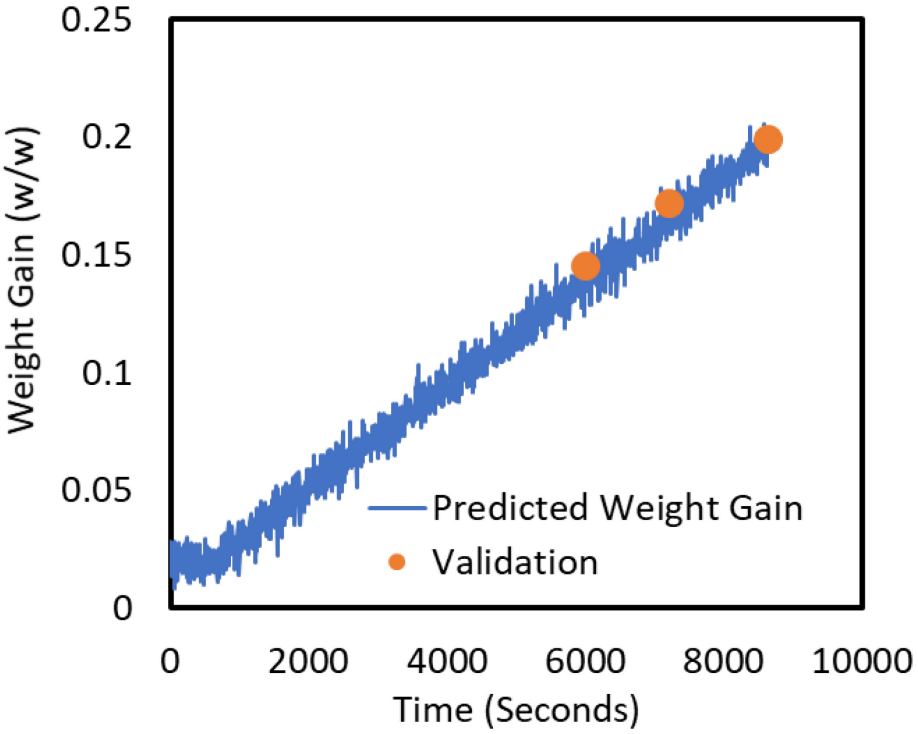

Figure 4-7: Process trajectory of the predicted coating weight gain using the NIR model.

4.3.2 NIR Models Predicting Loss on Drying

The moisture equilibrium in the coating system has a substantial effect on process stability and product quality.[143] Excessive moisture leads to the liquid bridge formation between the particles, which induces agglomeration and defluidization. Excessive drying can reduce the coating efficiency due to the premature of coating droplets. Water evaporation from the particle surface is a driving force of film formation. The surface tension of water residual in the coating promotes the ordering and deformation of the polymer particles, leading to particle coalescence to form a continuous film.[186, 187] Thus, maintaining the moisture level during the c0ating process is essential to prevent batch failure and consistently deliver quality products.

The screening study (Chapter 2) revealed the in-process moisture level was critical for maximizing coating efficiency, minimizing agglomeration, and preventing batch failure. Loss on drying (LoD) was used as a surrogate marker for the in-process moisture level, and the LoD value was found to be optimal at 5.5% w/w. A real-time monitoring tool was desired to prevent batch collapse and consistently deliver extended-release granules with efficient coating efficiency. In contrast to the humidity sensor, which measured the in-process air relative humidity, NIR spectroscopy had the advantage of directly measuring the moisture level of the granules. The in-line prediction of product LoD allowed a feedback loop to control product moisture level directly. The samples that were used for the calibration of the NIR model for LoD were drawn at random time points during the 30 calibration runs in the response surface study. The LoD values of the samples were primarily in the range of 2% - 7% w/w. There were only three samples of the higher LoD values than 7% w/w and four lower LoD values than 2% w/w. Thus, we randomly selected samples with LoD in the 2% - 7% w/w range to make a relatively uniform distribution of the responses (Y-block) in the range of 1% - 10% w/w. The average of five NIR spectra collected at a 25-second time interval of each sampling time point was used as the predictors (X-block) to minimize random variability in spectral scans. The NIR wavelength range of 1350 – 2125 nm was selected for the modeling, and two latent variables were used. The optimal preprocessing methods were standard normal variate (SNV) followed by mean centering for the X-block and auto-scaling for the Y-block. Figure 4-8A shows the correlation plot of the cross-validation predicted LoD vs. the measured LoD. The error statistics were calculated from the calibration and cross-validation with RMSEC of 0.254 and RMSECV of 0.324. The total calibration range was 1% - 10% w/w LoD; the R^2s were 0.988 for the calibration and 0.980 for the cross-validation. Figure 4-8B depicts the loading shape of the first latent variable in which 82.35% variance in the X-block explains

94.51% variance in the Y-block. The two major peaks were at 1400 -1450 nm and 1900 – 1950nm, both relevant to the O-H bond. It reflects the model specificity to the moisture level.

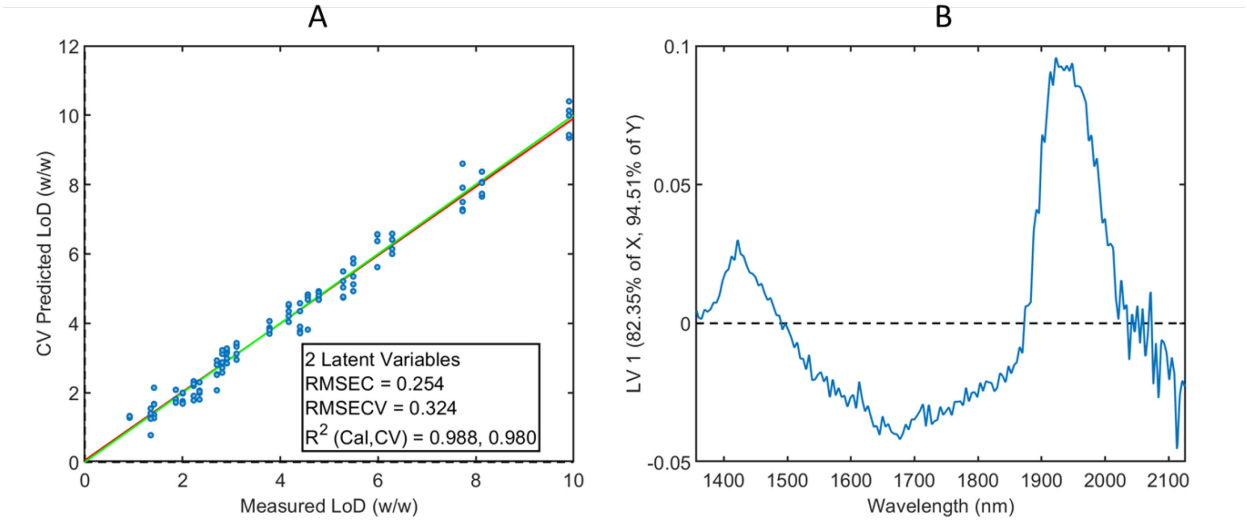

Figure 4-8: The NIRS predictive model for coating weight gain. (A) cross-validation (CV) predicted vs. measured LoDs, (B) the loading of the first latent variable.

The permutation test was repeated 100 times for the NIR-LoD models. The distributions of RMSECs and RMSECVs from the models using "incorrectly assigned" responses were generated using two latent variables, shown in Figure 4-9A. The standard deviation of the LoDs in the calibration was 2.2%, matched with the mean of RMSECs (2.2%) from the incorrect models. The distribution of RMSECVs has a higher mean (2.75%) and a broader range than those of RMSECs. This is probably caused by the extrapolation during random subset in the cross-validation process. The RMSEC (0.25%) and RMSECV (0.32%) of the original correct LoD model were one order of magnitude lower than the values of the two distributions from incorrect models. The risk of overfitting is deemed low because the probability of the original model being from the same population as the incorrect models is less than 0.0001.

The LoD model was subsequently applied as a surrogate sensor to monitor and control the moisture level of the test coating runs. In order to maintain a steady moisture level, the spray rate was adjusted proportionally to the deviation of the target in-process LoD value (5.5%) using Eq. 4.2:

$$\Delta Spray\ Rate = -20 \times (Predicted\ LoD\ - 5.5\%)\ g/min \qquad \textit{Eq. 4.2}$$

where $\Delta Spray\ Rate$ is the adjustment of the spray rate, and $Predicted\ LoD$ is the NIR model predicted LoD value. The proportional control coefficient was optimized at 20 based on the stability of the observed LoD predictions. The target LoD value was set at 5.5% based on the screening study results (Chapter 2), where the balance between maximizing process efficiency and minimizing agglomeration was reached.

Figure 4-9B shows an example of the model-controlled LoD trajectory in the preheating and spraying phases in one of the test runs. The blue line is the predicted LoD, and the orange circles represent the time points when samples were taken during the coating process and subjected to offline LoD measurements for verification. During the pre-heating phase, the LoD decreased due to the evaporation of pre-existing moisture in the uncoated granules. The LoD values start to increase in the initial stage of the spraying phase and became stable at around 5.5% w/w LoD. The standard deviation of the LoD predictions during the steady-state is 0.3%, and thus the 95% confidence interval of the LoD prediction is 4.9% - 6.1% w/w. The offline LoD values (orange circle) also reveal the actual moisture fluctuation in the steady-state is with the range of 5% - 6% w/w. It suggests the feedback loop controls the coating process with a relatively stable moisture level of the steady state.

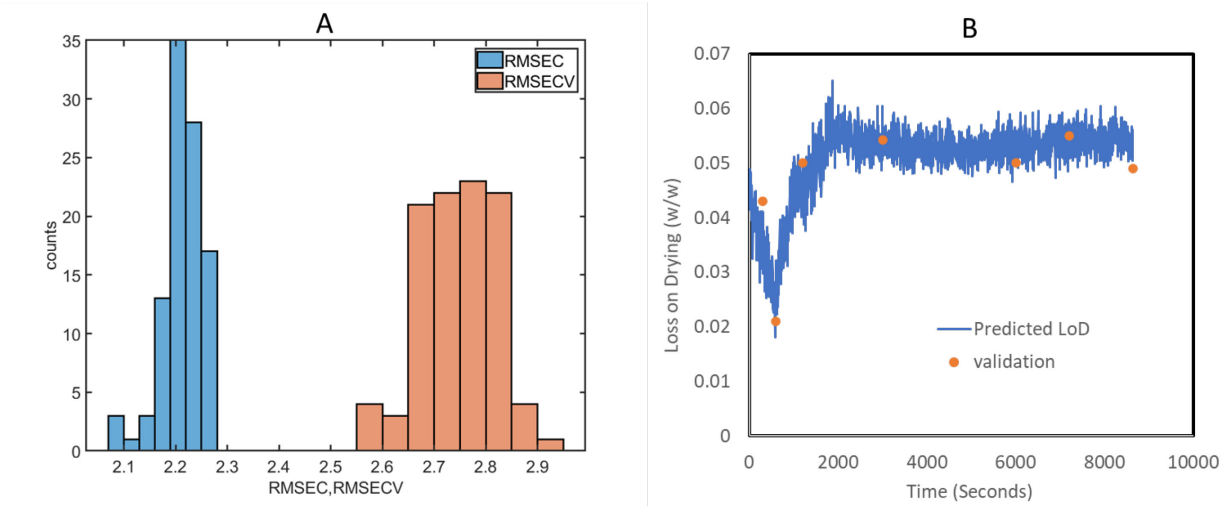

Figure 4-9: (A) Distribution of the values of RMSEC and RMSECV from the permutation test of the LoD models; (B) controlled process trajectory of the predicted LoD using the NIR model.

4.3.3 Raman Model Predicting Theophylline Monohydrate

Chapter 3 revealed the presence of theophylline monohydrate retarded the dissolution of coated granules. Since the aqueous coating process introduced water to the drug-loaded granules, the moisture levels of the coated granules, indicated by their model predicted LoD values, fluctuated around 5.5% w/w. Theophylline anhydrous Form II (CSD ref. code BAPLOT01) was partially converted to a monoclinic channel hydrate (CSD ref. code THEOPH01) upon contact with water during the spraying phase, but in the subsequent drying phase, the hydrate form lost the bound water at low relative humidity and elevated temperature. The Raman model was developed to monitor the partial conversion of theophylline monohydrate to the anhydrous form during the drying phase. The fluid bed chamber size limited the in-line application simultaneously using Raman and NIR spectrometers because the excitation laser Raman interfered with the NIR measurements. The Raman spectra were taken at-line after the samples were taken out from the fluid bed chamber and ground to powder form. Figure 4-10 suggests grinding did not cause peak

position change on the Raman spectra of the theophylline anhydrous (Form II) and theophylline monohydrate. However, the ground theophylline has lower Raman intensity than the unground, observed in both hydrate and anhydrous forms, probably due to the particle size reduction. This phenomenon was also reported by Gómez *et al.*[188] that Raman intensity increased with the increase of API particle size.

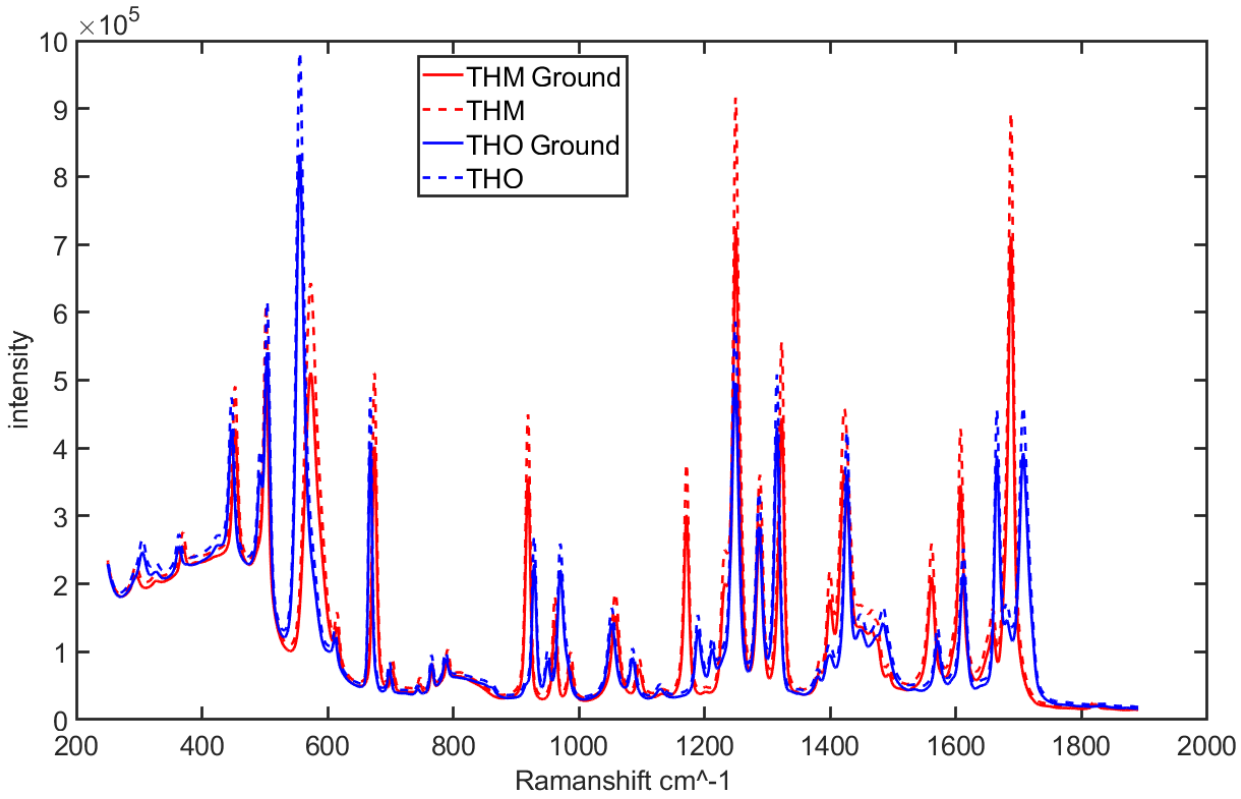

Figure 4-10: the Raman shift of the unground and ground theophylline anhydrous (THO) and monohydrate (THM).

The Raman model was developed using the mixture of ground dish-casted polymer film, theophylline monohydrate, theophylline anhydrous, lactose monohydrate, MCC, and HPMC. The raw spectra of the calibration set are shown in Figure 4-11A. The baseline offset and slope change were probably caused by the fluorescence of MCC and the coating film. Normalization to the unit area followed by mean centering was applied on the Raman spectra (X-block) to minimize the

impact of the baseline effect on model prediction, and autoscaling was used for the concentration of theophylline monohydrate (Y-block). Figure 4-11B is the scree plot of the Raman models where the RMSEC and RMSECV are plotted against the number of latent variables. Two latent variables were used to establish the theophylline monohydrate model since the decrease of RMSECV became trivial when the third latent variable was added into the model. Figure 4-11C is the correlation plot of cross-validation predicted vs. measured theophylline, with an RMSEC of 0.017 and an RMSECV of 0.025. The R^2 values of calibration and cross-validation are 0.991 and 0.984, suggesting that Raman spectra have a linear correlation with theophylline monohydrate concentration. The 95% confidence interval of 5% w/w theophylline monohydrate of the cross-validation is 0 - 10% w/w, which means any prediction below 5% w/w is statistically the same as 0% w/w at a 95% confidence level. Figure 4-11D shows the results from the permutation test, revealing the Raman model has a low probability (<0.0001) being from the same population as the models using "incorrect values" of theophylline monohydrate concentration as the responses.

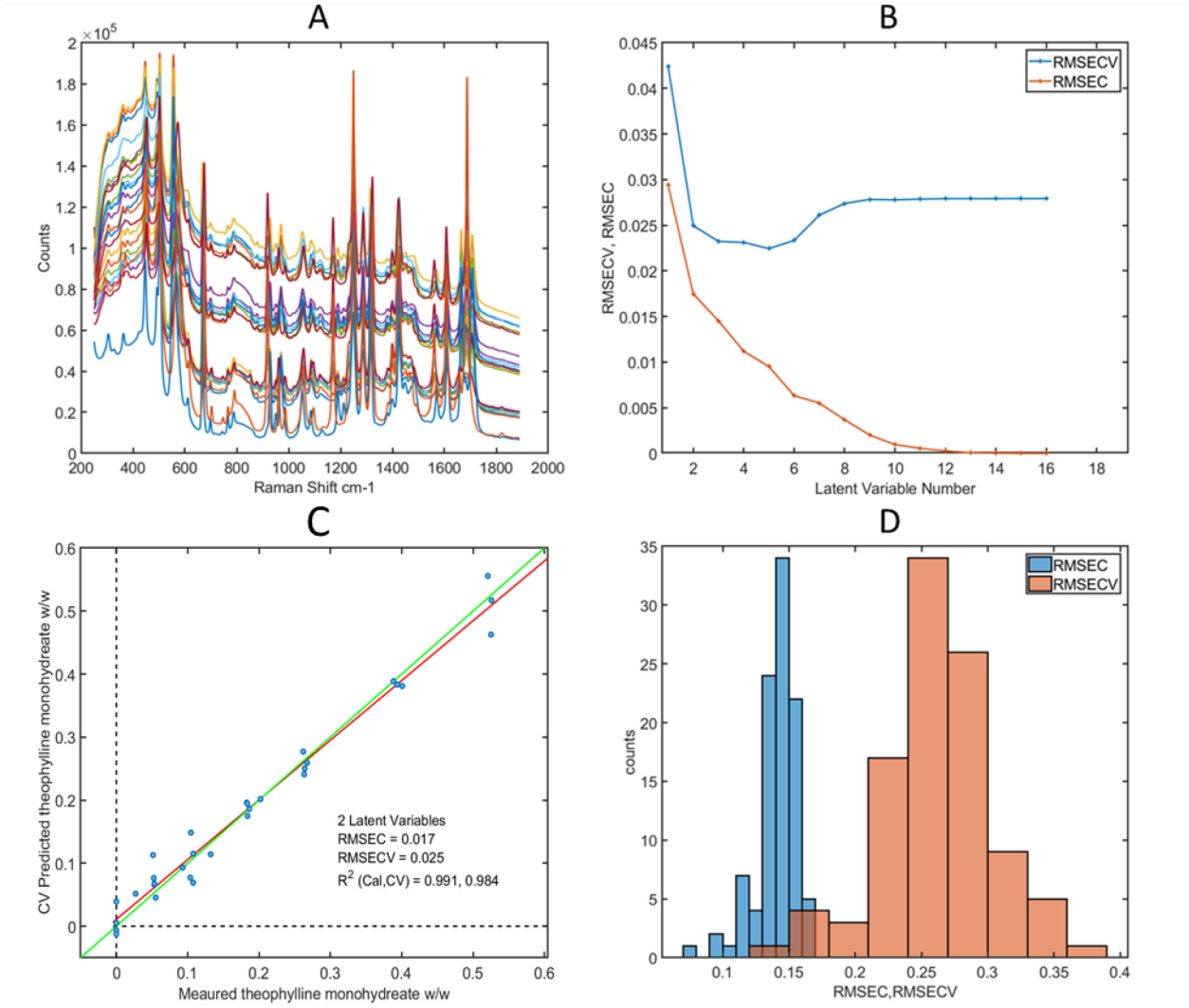

Figure 4-11: The Raman predictive model for the concentration of theophylline monohydrate: (A) Raw Raman spectra of the calibration set; (B) Scree plot for the optimized preprocessing method: normalization to the unit area + mean centering; (C) Predicted vs. measured concentration of theophylline monohydrate; (D) Distribution of the values of RMSEC and RMSECV from the permutation test of the theophylline monohydrate models. CV: cross-validation

The Raman model was tested on a sample of coated granules taken before the drying phase of the coating process. The granules were stored in a desiccator (room temperature: 20-22 °C) for 14 days, and four sets of samples were taken on Days 0, 3, 7, and 14. Each sample set was allocated to three parts, one for the Raman scan, one for the LoD measurement, and the last for the in vitro

dissolution test. Figure 4-12 shows the dissolution profiles of the samples taken on the four different days. The Raman model was applied to predict the concentrations of theophylline monohydrate. The sample from Day 0 was the granules taken from the fluid bed immediately after the spraying phase, in which there were 10.2% w/w theophylline monohydrate and 5.8% w/w loss on drying. The sample of Day 3 had a reduced concentration of theophylline monohydrate (6.0% w/w) and reduced LoD (4.2% w/w). Day 7 had 3.1 % w/w theophylline monohydrate concentration and 1.9% w/w LoD, while Day 10 had 0.6% w/w LoD with undetected theophylline monohydrate concentration (the Raman prediction was a negative value). Day 0 and 3 had slower dissolution rates than Day 7 and Day 14. The dissolution profiles of Day 0 and 3 were statistically similar, the f2 value being 87 (greater than 50). The results suggest the coated product can tolerate at least 3.1% w/w theophylline monohydrate and produce similar dissolution profiles. However, as previously discussed, the Raman model cannot statistically distinguish 0% w/w from 5% w/w theophylline monohydrate at a 95% confidence level, suggesting the model uncertainly made it unsuitable for the drying endpoint determination.

In contrast, the LoD measurement was an offline method of less uncertainty than the Raman predictive model. The limit of 1.9% w/w offline LoD measurement is probably a better target for drying termination than 3.1% w/w at-line predicted theophylline monohydrate concentration to produce coated granules with consistent dissolution profiles. As an alternative to the offline LoD measurements, the model using NIR spectroscopy was used in real-time to predict the LoD value. With the RMSEP of 0.5% w/w, the NIR model using a limit of 0.9% w/w LoD for drying termination was used to ensure the consistency of the dissolution profile at a confidence level of 95%.

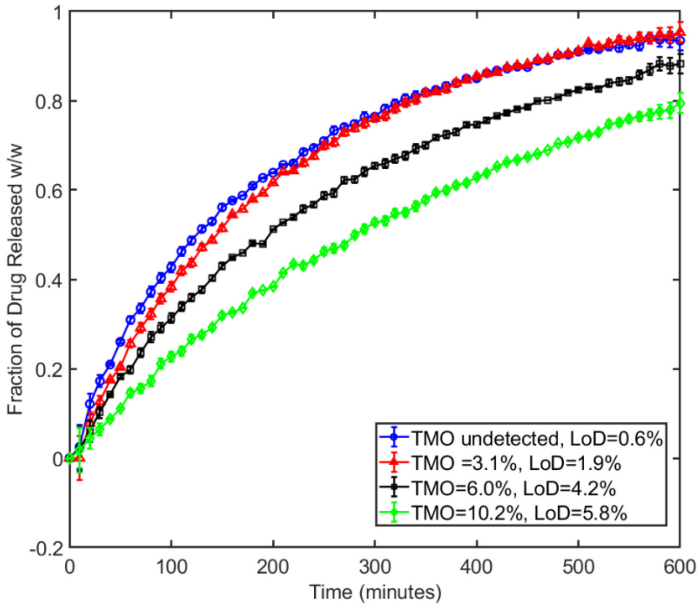

Figure 4-12: the dissolution profiles of four samples at different stages of the drying process. TMO: theophylline monohydrate, LoD: loss on drying.

4.4 Conclusion

This chapter discussed the PAT applications of NIR and Raman spectroscopies to monitor the fluid bed coating process and facilitate the development of feedback control loops.

Two NIR models were successfully established using PLS regression algorithm to predict coating weight gain and LoD values of granules as an indicator of moisture level, respectively. The performance of the NIR model for coating weight gain was evaluated using a test set, with an RMSEP of 0.5% w/w and an R^2 of 0.98. The NIR model for LoD values was used to help control the moisture level of the test runs, adjustments being made to maintain the LoD values of the in-process granules within the 5 – 6% w/w range.

A Raman model was developed to predict the concentration of theophylline monohydrate. A good correlation was found between the Raman spectra and theophylline monohydrate

concentration, with an R^2 of 0.99. However, based on the dissolution results of granules at different drying phases, the uncertainty of the Raman model made it unsuitable for the determination of the drying endpoint. Instead, the in-line NIR-LoD model was used as an indicator to produce the dried coated granules with consistent dissolution profiles.

This work demonstrated that the process analytical technologies were powerful tools for real-time monitoring of the fluid bed coating process. It also suggested the selection of PAT tools should be based on practical considerations and model uncertainty. The rapid and robust feedback control loops enabled by the NIR models accomplished Specific Aim 3.

Chapter 5 : Construction, Evaluation, and Validation of the Combined Feedforward-Feedback Control System Using Monte Carlo Simulation and Test Batches.

Abstract

This work demonstrates the use of combined feedforward and feedback loops to control (1) the in-process moisture and (2) the product *in vitro* dissolution profiles. In the moisture-control system, the feedback loop described in Chapter 4 was used to maintain a steady-state moisture level. In the dissolution-control system, the feedforward loops adjust the setpoints of the fluidization air volume and the target coat weight in the fluid bed processor to accommodate the variabilities of the inlet air relative humidity and the size distribution of input granules. NIR spectroscopy was utilized to monitor the coating weight gain and determine the spraying endpoint to achieve the desired dissolution profile. The control performance was evaluated by comparing the outcome of a Monte-Carlo simulation with and without the feedforward components. Twelve additional test batches were conducted to verify the simulated tolerance space. The simulation results revealed the feedforward controller reduced the probability of a dissolution failure, and the test batches verified the integrated control system produced quality products with desired dissolution profiles at extreme conditions.

5.1 Introduction

Pharmaceutical manufacturing relies on feedback controls to maintain the prescribed conditions necessary to manufacture quality products.[189] However, standard feedback control loops are

susceptible to input disturbances and uncertainties.[190] Thus, a control system must be designed to accommodate foreseeable variation in the input to the process.[107] Examples of typical disturbances in a pharmaceutical process include changes in raw material properties.[1, 4] Such disturbances can arise from the chemical and physical properties of APIs and excipients. In response to such disturbances, feedback systems must wait until the disturbance has an observable effect on the control system, produce reduced quality product, or create an instability in the loop.[191] In each of these scenarios, the product quality is at risk until the disturbance has been mitigated. The feedforward structure has the potential[15, 16] to mitigate all of these risks to product quality in a pharmaceutical manufacturing process.

Feedforward/feedback loops are used in this work in a control system to apply an extended-release coating to granules in a fluid bed processing system. Theophylline anhydrous was used as a model drug, and the extended-release layer was formed by a pH-independent aqueous-insoluble film,[131] using polyvinyl acetate. The minimum film formation temperature was reported as 18 °C without plasticizer,[128, 130] and curing was found unnecessary in previous studies (Chapter 2). The coating was applied to modulate the API dissolution to match a twice-daily dosing regimen for theophylline[151]. The ultimate goal of the coating process is to produce granules with a consistent release profile that meets appropriate specifications.

A significant challenge to this process is the batch-to-batch variation in granule size distribution and relative humidity, impacting both the process stability and product quality. The *in vitro* dissolution models, described in Chapter 3, are built based on the four parameters: inlet air relative humidity, the particle size distribution of the granules, inlet air volume, and target coating weight gain. As illustrated in Figure 5-1, the feedforward control was built based on the process models to account for the variability in granule size distribution and inlet air relative humidity. It provided

the coating process (and the feedback loops associated with it) set points that converted a given batch of granules to a coated system that met the required dissolution specifications. The specific set points from the feedforward loops were the fluidization air volume and the total quantity of coating (weight gain) to be applied. In essence, the feedforward loops established setpoints for the process, and the feedback loops achieve those set points. In this system, the feedback loops are inherently static, while the feedforward loop created a dynamic response to changes in the input material and environment. Near-infrared spectroscopy (NIR) as a process analytical technology was integrated into the feedback loop to monitor the coating process and terminate it when the feedforward loop determined target coat weight was achieved. The combination of feedforward and feedback loops created a control system capable of mitigating variation in the input materials and producing a product with consistent *in vitro* dissolution profiles.

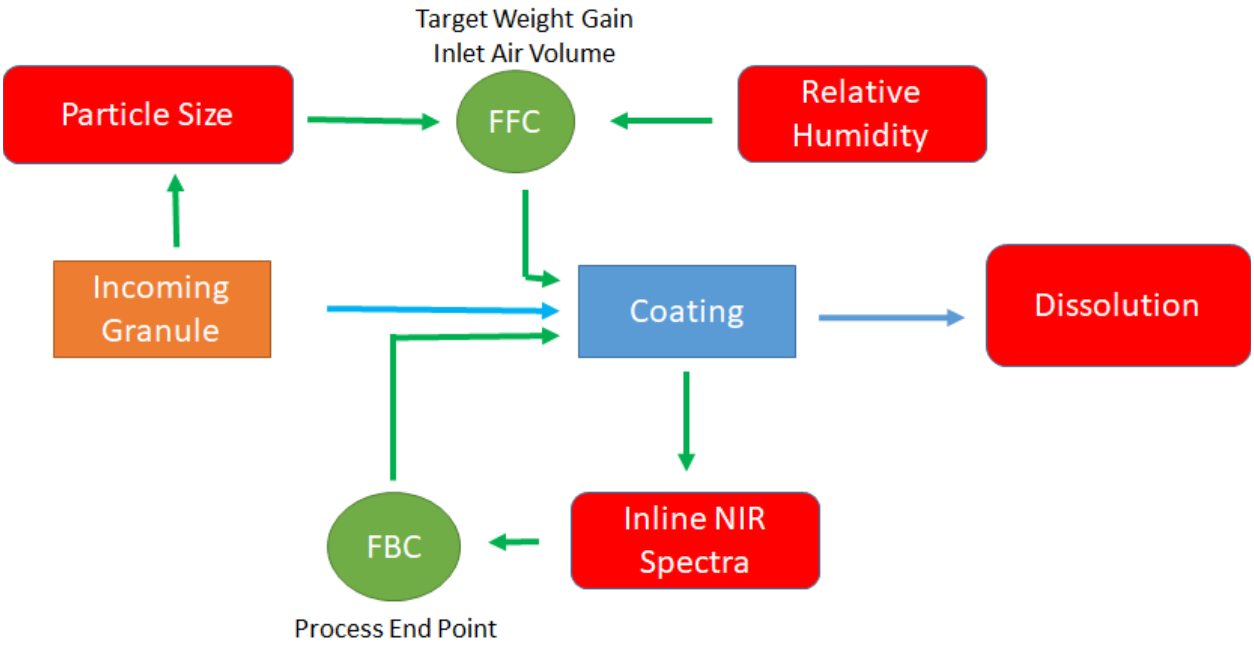

Figure 5-1: The schematic of the control system. FFC: feedforward control, FBC: feedback control.

This chapter aimed to fulfill the requirements of Specific Aim 4, which was also the ultimate testing of the hypothesis. The work included (1) the integration of the feedforward and feedback loops in a real-time data management system (SynTQ), (2) Monte Carlo simulations of the fluid bed coating process with and without the feedforward components, and (3) test batches conducted near the edge of failure of the simulated design space.

5.2 Materials and Methods

The materials and equipment used for the test batches were described in Chapter 2. The real-time analytical models and process models were developed in previous studies, and the details were discussed in Chapters 3 and 4. This chapter focused on developing a combined feedforward-feedback control system for a fluid bed coating to control product dissolution and prevent agglomeration. A Monte Carlo simulation was applied to explore the tolerance space of the coating process with and without the feedforward component for the dissolution control. The improvement of the control system on product consistency was analyzed using process capability.

5.2.1 Control System

The feedforward component to control product dissolution was established using the PLS and GPR-based process models (Chapter 3). The two curve-fitting methods (Weibull function fitting and PCA) generated different fitting-error profiles (Section 3.3.2), while the two regression methods (PLS and GPR) showed similar performance on the Weibull parameters or PCA scores prediction (Section 3.3.4). The PLS algorithm had the advantage of generating a known regression vector which was readily transformed into an optimization function over the GPR algorithm. Thus,

The PLS-based process models were chosen over GPR to develop feedforward loops. Figure 5-2 shows how a process model was used in a feedforward loop. The disturbances were inlet air relative humidity and size distribution of input granules, the process parameters included fluidization air volume and target coating weight gain, and the response (Y-block) is Weibull parameter or PCA score. The regression vector of the PLS-based process models was calculated using the calibration batches. For new batches, the regression vector, the desired responses (Y), and the measured disturbances were used as known input.

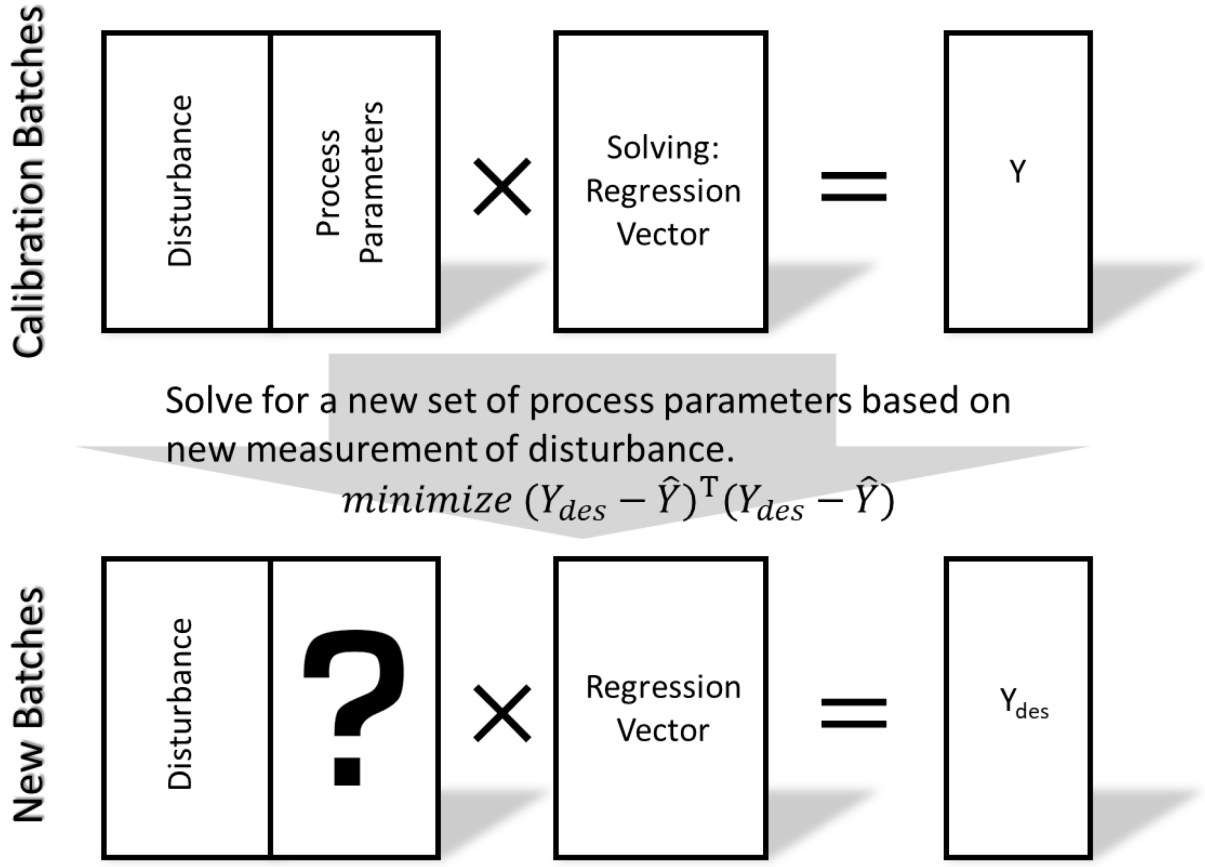

Figure 5-2: illustration of the feedforward controllers that solve for the process parameters: air volume and target weight gain, based on measured disturbance (inlet air relative humidity and size distribution of input granules), desired and target dissolution parameters (Y), and the PLS regression vectors.

The feedforward controller solved the process parameters by minimizing the cost function (J), which is the sum of squared error between the predicted and desired responses (Y). A constrained global searching algorithm ("*fmincon*" function coded in Matlab)[12, 13] was utilized. The feedforward controllers for Weibull parameters and PCA score had different cost functions (J), shown as Eq. 5.1 and Eq. 5.2, respectively:

$$J = (\hat{\lambda} - \lambda_{target})^2 + (\hat{k} - k_{target})^2 \qquad Eq.\ 5.1$$

where $\hat{\lambda}$ and λ_{target} were the predicted and target scale factors; $\hat{k}$ and k_{target} were the predicted and target shape factors from the Weibull function fitting.

$$J = (\widehat{PC1} - PC1_{target})^2 \qquad Eq.\ 5.2$$

where $\widehat{PC1}$ and $PC1_{target}$ were the model predicted and target scores of PC1 from the PCA decomposition. Since the process models were empirical, constraints were applied to both equations Eq. 5.1 and Eq. 5.2 to limit the solution of the process parameters to the model explored ranges: 25 - 35 m^3/h for fluidization air volume and 12% - 26% for weight gain.

The feedback controllers were described in Chapter 4, where near-infrared spectroscopy was employed to control the moisture level, determine coating weight gain during the spraying phase, and terminate the drying phase when the desired LoD (<0.9%) was achieved. The feedforward and feedback controllers were integrated into an automated control system, incorporating the fluid bed processor, an open platform communication system (OPC, DeltaV), and a real-time data management system (SynTQ). The fluid bed processor received and sent analog signals, while SynTQ managed discrete digital signals. The DeltaV system helped SynTQ access the fluid bed data by transferring the analog signals to the digital tags. In the SynTQ process orchestration, The fluid bed coating process was divided into three distinct phases:

(1) preheating phase, in which the uncoated granules were heated to an elevated temperature,

(2) spraying phase, in which the polymer suspension was deposited onto the granules,

(3) drying phase, in which the excess solvent was dried and the drug (theophylline) transferred from hydrate form to anhydrous form.

The process control commands and the PAT models were programmed as shown in Figure 5-3. The adjustment of process parameters and the collection of NIR spectra were synchronized to a 5 s cycle. The initiation of automation required manual input of the size distribution of the input granule cores measured by an offline canty particle size analyzer. The process model calculated the inlet air volume and the target coating weight gain in the first circle of the preheating phase. In the spraying phase, the coating process weight gain was first predicted by the NIR model to determine the phase transition point, and then if staying in the spraying phase, the spray rate was adjusted with the assistance of the LoD NIR model. The drying phase started when the target weight gain was reached and ended when the predicted LoD value reached the end process criterion (0.9% w/w LoD). The coated products were discharged and stored in a desiccator at room temperature after the coating process automatically ended.

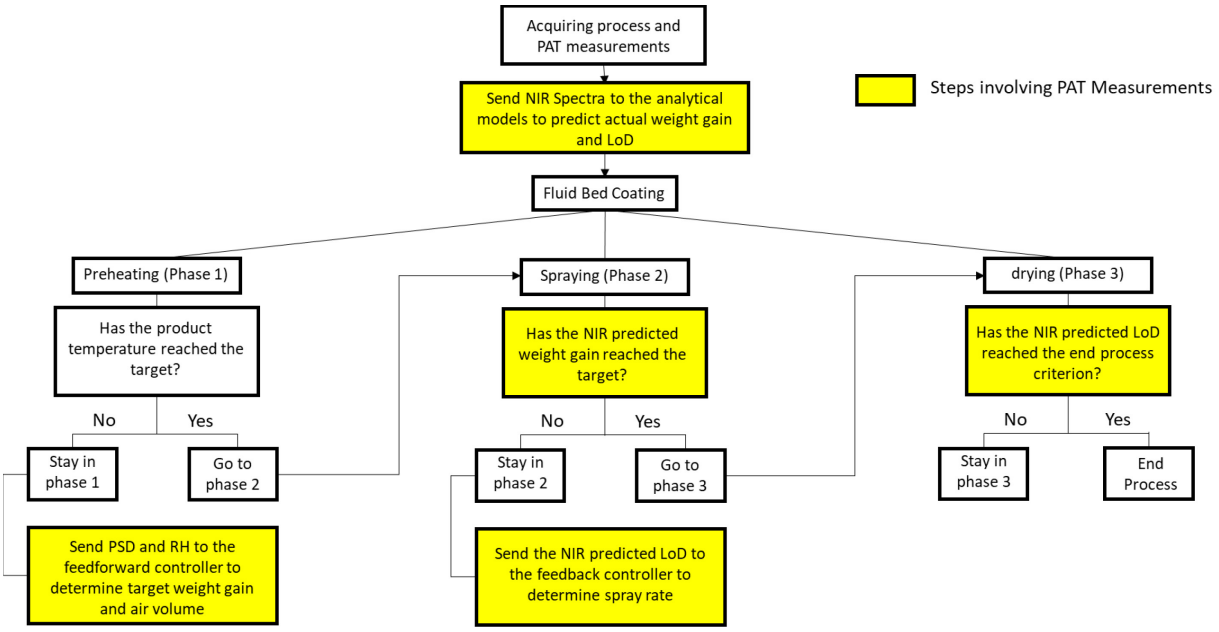

Figure 5-3: SynTQ orchestration implemented with the process and PAT models. PSD: particle size distribution of input granule; RH: inlet air relative humidity; LoD: loss on drying.

5.2.2 Monte Carlo Simulation methods

Monte Carlo simulation was applied to estimate the dissolution variability of the final products when the coating process was with or without the control of the integrated feedforward-feedback control system. The dissolution variability of the products manufactured without feedforward control mainly came from three sources:

(1) the variability of relative humidity (RH) and granule size distribution (GSD),

(2) the prediction error of the NIR model on coating weight gain,

(3) the inherent variability of the coating process.

In contrast, the process with feedforward control loops minimized the variability of the first source (RH and GSD) but introduced additional variabilities related to the process models, contributing to the control uncertainty. In order to test the center hypothesis: “a combined feedforward-feedback control system (1) improves the product quality and consistency, and (2)

grants flexibility to the process in terms of input material attributes and environmental disturbances", two Monte Carlo simulations were conducted to compute the dissolution profiles. The hypothesis is true only if the impact of the model uncertainty on the *in vitro* dissolution is smaller than the impact of RH and GSD.

Simulation 1

The first simulation (Simulation 1) was executed using the conditions near the center level of the response surface study to demonstrate that the feedforward component helped improve product quality and consistency. The granule size distribution (GSD, D50 = 480 nm) and the inlet air relative humidity (40 – 50%) were used as the initial input with their natural variabilities. The variability of the GSDs was calculated from the canty measurements of five samples from the center batch, simulating a coating process with tightly controlled GSD of input material. Five repeated GSD measurements of the same batch were projected to the PCA model, which was previously established from three different batches (Details of the model calibration were described in Section 3.3.1). The PC1 scores of the five replicates were assumed to follow a normal distribution, and thus the mean and the standard deviation were calculated. The normal distribution was then used to represent the natural variability of the input granule size. The natural variability of the inlet air relative humidity was assumed as a uniform distribution in the 40 – 50% interval. Different PC1 scores for GSDs and inlet air relative humidities were randomly sampled from the normal distribution and the uniform distribution, respectively.

Simulation 2

The second simulation (Simulation 2) expanded the simulated range of the GSD and RH to the boundary conditions of the previous response surface study. The GSD was represented using its PC1 score. Since the PCA model had one degree of freedom, each D50 value of the GSDs, 392,

419, 460, 480, and 504 µm in the calibration set, only corresponded to one PC1 score. The simulation process utilized 49 combinations (Figure 5-4) of D50 in the range of 390 - 510 µm and inlet air relative humidity in 20 – 80% as inputs. The resolutions of D50 (X-axis) and relative humidity (Y-axis) were 20 µm and 10%, respectively. Simulation 2 was performed to test whether the feedforward component caused the coating process to respond correctly to the size distribution of input granules and inlet air relative humidity.

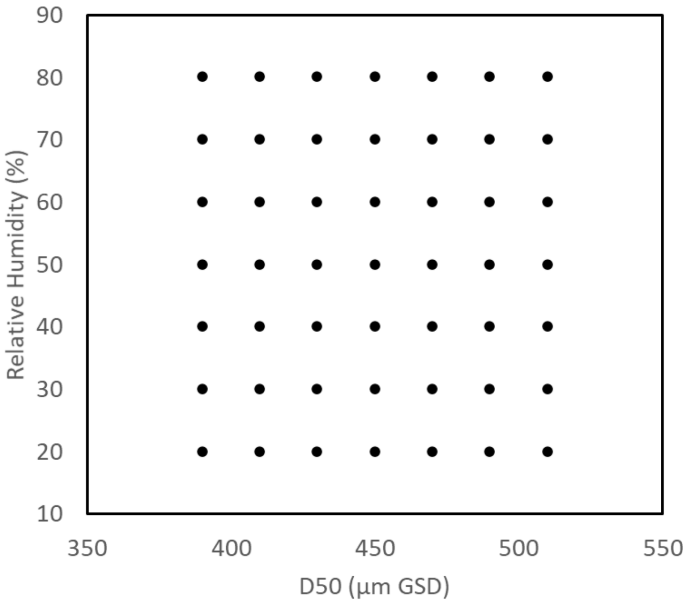

Figure 5-4: the array plot of the 49 combinations of D50 and relative humidity.

Simulation Procedure

The schematic of the Monte Carlo simulation is illustrated in Figure 5-5. The target dissolution profile was generated based on the in-house specification (Table 3-2), which had four acceptance intervals at each of the four specified time points ((1, 2, 4, and 8 hours). The centers of the acceptance intervals were 20%, 42.5%, 67.5%, and 90%. The target Weibull parameters were calculated by fitting the Weibull function to the four centers, using percentage drug dissolved as

dependent variables and dissolution time as independent variables. The PC1 score of the target dissolution profile was solved by minimizing the sum of the least squared errors between the PC1-score-reconstructed dissolution and the target dissolution profile. The Weibull parameters (λ and k) and the PC1 scores were used as the target response (Y_{target}) in the searching algorithm of the feedforward controllers. In Simulation 1, the input values of RH and GSD were randomly sampled from the defined distributions. The distributions of pure error from curve-fitting, the process models, and the NIRS model were assumed to have Gaussian shapes. The simulation algorithm ran in the following sequence:

1. the feedforward controller determined the fluidization air volume and target weight gain based on the input GSD and RH.
2. one error value was randomly selected from the error distribution of the NIRS model ($\sigma(NIRS)$) and applied to the target weight gain,
3. the error incorporated weight gain value was employed for the calculation of the scale and shape factors (Weibull function) or the score of PC1 (PCA model) using the process models,
4. error values were randomly chosen from the error distributions of process models ($\sigma(\lambda)$ and $\sigma(k)$, or $\sigma(score\ of\ PC1)$,) and applied to the scale and shape factors or the score of PC1, respectively,
5. the dissolution curve was reconstructed using the error incorporated scale and shape factors or the score of PC1,
6. bias and a randomly selected pure error profile were applied to the dissolution curve to complete one simulation loop.

The out-of-specification rate was calculated after every generation of 100 simulated dissolution profiles. In Simulation 1, the algorithm was repeated until the out-of-specification rate converged:

the difference between the new and previous rate was smaller than 0.1%. Multiple runs were conducted and the algorithm stopped after generating 8,000-9,000 dissolution profiles. Therefore, 10,000 dissolution profiles were generated to get a representative simulation result, and the 95% tolerance intervals were calculated for the time points (1, 2, 4, and 8 hours) of the in-house specification. A mathematic expression of the dissolution profiles, with error terms, is described in Eq. 5.3 and Eq. 5.4:

$$\varphi = 1 - e^{-\left(\frac{t}{\lambda+\sigma(NIRS)+\sigma(\lambda)}\right)^{(k+\sigma(NIRS)+\sigma(k))}} + bias + pure\ error \qquad Eq.\ 5.3$$

where φ is the fraction of drug released, $\sigma(NIRS)$ is from the error of weight gain from the NIRS model, $\sigma(\lambda)$ and $\sigma(k)$ are the errors of dissolution parameters from the process models, bias and pure error are from the Weibull function fitting.

$$Dissolution = (T_{pc1} + \sigma(NIRS) + \sigma(T_{pc1})) \times PC1 + offset + pure\ error \qquad Eq.\ 5.4$$

where $offset$ is the mean dissolution profile of the calibration set in the response surface study, T_{pc1} is the score of PC1, $\sigma(NIRS)$ and $\sigma(T_{pc1})$ are the errors from the NIR model and process model, respectively. The pure error is from the PCA modeling of dissolution profiles.

Simulation 2 used 49 initial known conditions of relative humidity and GSD instead of randomly sampling. Each initial condition was simulated using the same procedure as Simulation 1, and the procedure was repeated 10,000 times. The probability of the simulated dissolution profile that failed to meet the specification was calculated for each initial condition.

Simulation 1 and 2 were also performed without the feedforward control (step 1) to understand the contribution of the feedforward component to the control system. In Simulation 1, the mean values of the process parameters (target fluidization air volume and target coating weight gain) from the simulation with feedforward control were used as the setpoints for the simulation of feedback control alone, and the same setpoints were used in the 10,000 runs. In Simulation 2, the

setpoints of process parameters were kept constant for all runs, using the mean values of the 49 individual fluidization air volumes and weight gains generated by the simulation with feedforward control. The failure rates and the tolerance spaces were calculated using the same amount (10,000) of simulated dissolution profiles.

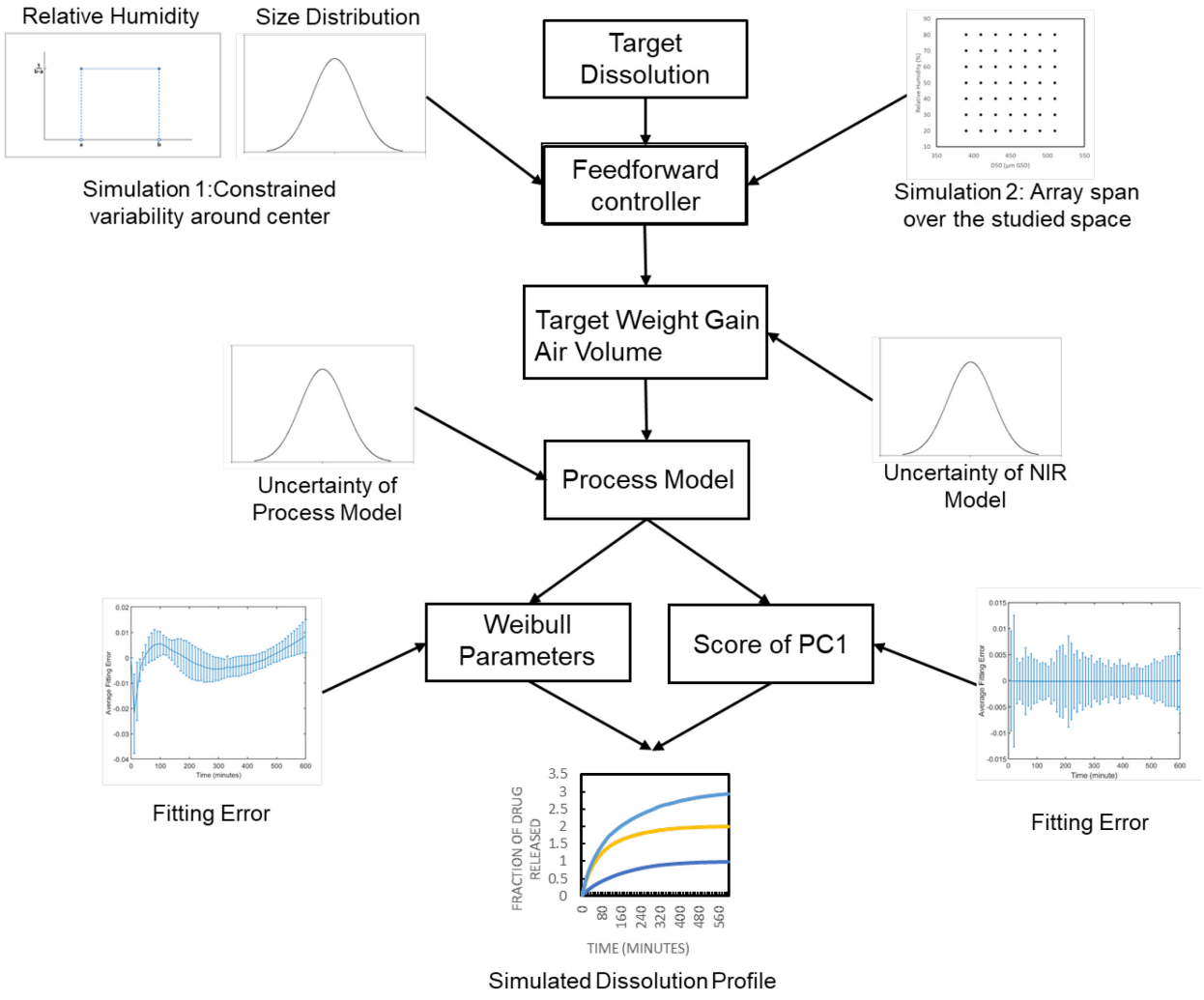

Figure 5-5: illustration of the procedure for the Monte Carlo simulation.

5.2.3 Control Performance Evaluation

The simulation results were used to evaluate the performance of the integrated feedforward-feedback control system. Simulation 1 was used to understand the fluctuation of final product

dissolution profiles, which could be assessed using process capability. Two process capability indices, C_p and C_{pk}, were used as indicators. The calculations were shown as Eqs. 5.5 and 5.6:

$$C_p = \frac{USL - LSL}{6s} \qquad \textit{Eq. 5.5}$$

and

$$C_{pk} = min[\frac{USL - \mu}{3s}, \frac{\mu - LSL}{3s}] \qquad \textit{Eq. 5.6}$$

where USL and LSL are upper and lower limits of CQA specifications, μ and s are the mean and standard deviation of six test runs. The value of C_p measures the natural variability of the process, and the value of C_{pk} indicates the risk of failure. The drug fraction released at the four time points: 1, 2, 4, 8 h, were the CQAs. The specifications were defined based on the USP standard drug release test 2 for theophylline extended-release capsules, where LSL and USL are 10% and 30% for Hour 1, 30% and 55% for Hour 2, 55% and 80% for Hour 4, and 80% and 100% for Hour 8. Therefore, four $C_p s$ and four $C_{pk} s$ were calculated to evaluate the stability of one CQA: *in vitro* dissolution. Due to the correlation between the fraction of drug released at the four time points, multivariate process capability indices (MPCIs) were adapted to reduce the number of indices from 8 to 2. Various researchers have proposed alternative approaches to calculate the MPCIs, including the volume ratio method by Taam *et al.*[192], the three vectors method by Shahriari *et al.*[193], and the multiple bilateral tolerance zones method by Chen.[194] In this study, we applied a relatively simple approach suggested by Raeisi[195], which used the weighted mean of the individual C_ps and C_{pk}s. This approach assumed the dissolution value at any of the four time points followed a normal distribution, and thus the joint distribution of the four dissolution values followed a multivariate distribution. The MPCIs were defined by Eqs. 5.7 and 5.8:

$$MC_p = \sum_{i=1}^{4} W_i \, C_{p(i)} \qquad \textit{Eq. 5.7}$$

and

$$MC_{pk} = \sum_{i=1}^{4} W_i \, C_{pk(i)} \qquad \textit{Eq. 5.8}$$

where MC_p and MC_{pk} act as equivalents for $C_{p(i)}$ and $C_{pk(i)}$ in multivariate circumstance and W_i is the normalized importance weight of the drug dissolution at the ith time point based on the user's decision. It should be noted the sum of W_i equals 1.

Simulation 2 explored the tolerance of the controlled fluid bed coating process to the variability in relative humidity and size distribution of input granules. A response surface, namely tolerance space, was derived from the simulation results of the 49 conditions to interpolate the failure rate of the product dissolution within the studied range. The response surface was established for the coating processes using the combined control system or the feedback control alone.

Twelve test runs were conducted to verify the tolerance space from the simulation. Six different combined conditions of inlet air relative humidity and GSD were selected on the edge of the tolerance space. Six test runs of those conditions were conducted using the combined control system, while another six test runs of the same six conditions were carried out using feedback control alone. The feedforward controller used in the test runs employed the Weibull parameters as the model response because its simulated tolerance space had higher success rates than PCA. The actual dissolution profiles of 12 test runs were measured and compared to verify the contribution of the feedforward control.

5.3 Results and Discussion

In this section, the results of the two Monte Carlos simulations were discussed. The indices of process capability were calculated based on the result of Simulation 1. In Simulation 2, the tolerance spaces were established in the studied ranges of relative humidity and GSD. The impact of the dissolution curve-fitting methods (Weibull function or PCA) on the control performance were investigated. The tolerance space was verified using 12 test coating runs near the edge of failure, generated using the Weibull-function-facilitated control system.

5.3.1 Simulation 1 for Process Capability

The results of Simulation 1 are illustrated in Figure 5-6, including four subplots. Each subplot shows a joint distribution of fractions of drug released at two specified time points (Hour 2 vs. Hour 1, or Hour 8 vs. Hour 4) of the dissolution profile with or without the feedforward control. The specifications are illustrated in the subplots, and the 95% confidence intervals of the joint distributions are calculated. Since the GSD and the inlet air relative humidity are constrained to a narrow range in Simulation 1, most simulated dissolutions met the in-house specification (the black squares). The process regulated by the combined feedforward-feedback control generates narrower 95% confidence intervals (the blue squares) than the feedback control alone (the red squares). It is noteworthy the 95% confidence intervals of the Weibull function fitted dissolution results are narrower than the PCA model fitted dissolution in all four specified time points (1, 2, 4, and 8 h), in both cases with and without feedforward control. The combined feedforward-feedback control coupled with Weibull function fitting generates a smaller area of the 95% confidence interval, comparing Figure 5-6A to Figure 5-6C or comparing Figure 5-6B to Figure 5-6D. It is probably because the PCA-facilitated process model has only one degree of freedom

(the PC1 score), resulting in greater prediction errors in the reconstructed dissolutions than the Weibull-function-facilitated process model which has two degrees of freedom (λ and k). The greater errors in the PCA-facilitated process model propagate to the feedforward controller and lead to higher uncertainty in the simulated dissolution profiles.

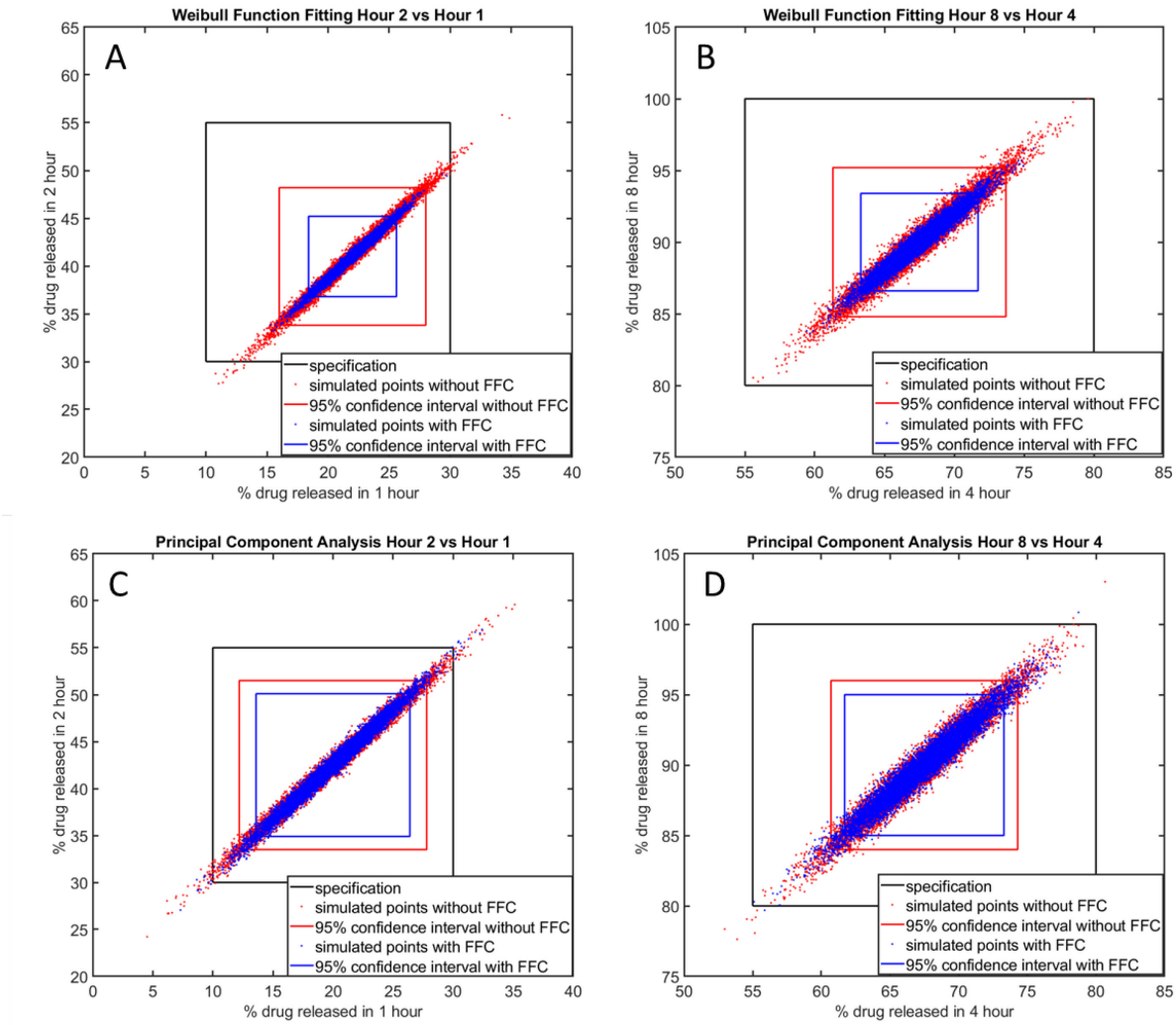

Figure 5-6: Results of Simulation 1: (A) simulated % drug released at Hour 1 and 2 using the Weibull function to fit dissolution profiles; (B) simulated % drug released at Hour 4 and 8 using the Weibull function to fit dissolution profiles; (C) simulated % drug released at Hour 1 and 2 using the PCA model to fit dissolution profiles; (D) simulated % drug released at Hour 4 and 8 using the PCA model to fit dissolution profiles. FFC: feedforward controller.

The 95% confidence intervals in Figure 5-6 B, C, and D have the same center as the center of the specification squares, while Figure 5-6A depicts a bias of the simulated dissolution profiles from the center of the specifications in the first two specified time points (1 and 2 hours). The bias is caused by the biased error profiles (Figure 3-7) due to Weibull function fitting, in which the reconstructed dissolution profiles are lower at Hour 1 and higher at Hour 2 than the actual dissolution profiles.

The calculated indices of process capability (Table 5-1) support the observations (Figure 5-5) of the dissolution profiles from Simulation 1. The C_ps and C_{pk}s were calculated for each specified time point in the four control systems:

(1) Weibull-function-facilitated feedback control alone,

(2) Weibull-function-facilitated combined feedforward-feedback control,

(3) PCA model facilitated feedback control alone,

(4) PCA model facilitated combined feedforward-feedback control.

The four specified time points of the specification were deemed equally critical to the drug release profile. Therefore, the MCPIs, short for multivariate process capability indices, were calculated using the average of the four process capability indices. The values of C_p and C_{pk} increased when the combined feedforward-feedback control was used instead of the feedback control alone, regardless of the dissolution curve-fitting methods. It suggests the feedforward control advances the product quality by reducing the variability in the *in vitro* dissolution profiles, thus improving product consistency. The Weibull function fitting outperformed the PCA fitting, the C_{pk} value of the Weibull-function-facilitated control being greater than the PCA-facilitated control at every specified time point of either feedback control alone or the combined control, even with the bias presented in the Weibull function fitted dissolution profiles at Hour 1 and 2. The

combined feedforward-feedback control system coupled with the Weibull function fitting method had the highest MCPIs, 1.945 for C_p and 1.773 for C_{pk}.

Table 5-1: indices for process capability in four cases: (1) feedback-controlled coating process using the Weibull function to fit dissolution profiles; (2) feedback-controlled coating process using the PCA model to fit dissolution profiles; (3) combined feedforward-feedback coating controlled process using the Weibull function to fit dissolution profiles; (4) combined feedforward-feedback controlled coating process using the PCA model to fit dissolution profiles. MCPI: multivariate process capability index, calculated by taking the average of the process capability indices at the four specified time points (1, 2, 4, and 8 hours).

Time	Feedback control alone				Combined feedforward-feedback control			
	Weibull		PCA		Weibull		PCA	
	C_p	C_{pk}	C_p	C_{pk}	C_p	C_{pk}	C_p	C_{pk}
Hour 1	1.111	0.889	0.855	0.684	1.852	1.481	1.042	0.833
Hour 2	1.157	1.019	0.926	0.815	1.984	1.746	1.096	0.965
Hour 4	1.344	1.317	1.225	1.201	1.984	1.944	1.437	1.408
Hour 8	1.282	1.256	1.111	1.089	1.961	1.922	1.333	1.307
MCPI	1.224	1.120	1.029	0.947	1.945	1.773	1.227	1.128

5.3.2 Simulation 2 for Design Space

Simulation 2 had 49 initial conditions and generated 490,000 simulated dissolution profiles, 10,000 simulations for each initial condition. The simulated dissolution profiles were compared to the in-house specification, and the tolerance space was established based on the rate of failure. The contour plots (Figure 5-6) depict the tolerance spaces of the four control systems. The four control systems were the same four as described in Simulation 1. The tolerance spaces were built to reflect the probabilities of successful batches at different combinations of initial conditions. The X-axis of the plots is D50, an indicator of the GSD. The Y-axis is inlet air relative humidity. The colors

indicate the probabilities of successful batches (meeting specification). The yellow regions are the conditions of product dissolution profiles with a greater than 95% chance to meet the specifications. The 95% tolerance space is the design space of the coating process when the corresponding control strategy is applied to assure the product quality. The area of the yellow region increased substantially when the Weibull-function-facilitated combined feedforward-feedback control system (Figure 5-6B) was applied to replace the feedback control alone (Figure 5-6A). The same trend was observed in the PCA-facilitated control systems, comparing Figure 5-6D to Figure 5-6C. It suggested adjusting the process parameters using the feedforward controller increased the chance of success for the initial conditions where the product qualities were at risk (tolerance level <95%) using feedback control alone.

Comparing the two pairs of subplots, Figure 5-6A to Figure 5-6C, and Figure 5-6B to Figure 5-6D, the 95% tolerance space (design space) generated from the Weibull function fitted dissolution profile has a larger area than the PCA fitting, regardless of the control systems. It suggests the Weibull function outperforms the PCA fitting in terms of establishing a larger tolerance space. This observation aligns with the finding in Simulation 1. Therefore, the Weibull-function-facilitated control system was used to define the six initial conditions of GSD (D50) and relative humidity (RH) for the test runs 1-6:

(1) D50 = 392μm, RH = 23%,

(2) D50 = 392μm, RH = 75%,

(3) D50 = 504μm, RH = 24%,

(4) D50 = 504μm, RH = 78%,

(5) D50 = 419μm, RH = 23%,

(6) D50 = 480μm, RH = 76%.

Each initial condition was subjected to two runs with and without the feedforward controller. Three out of the six products coated using feedback control alone fail to meet the specification, shown in Figure 5-7. Two batches (Test run 3 and 4) have slower dissolution profiles, and one batch (Test run 1) has faster dissolution than the specification. In comparison, the dissolution profiles of the coated granules produced from the combined feedforward-feedback control system meet the specification with no exceptions. The results suggest that intentional changes to the in-process parameters can mitigate batch-to-batch variation in the input if a well-designed feedforward loop is used.

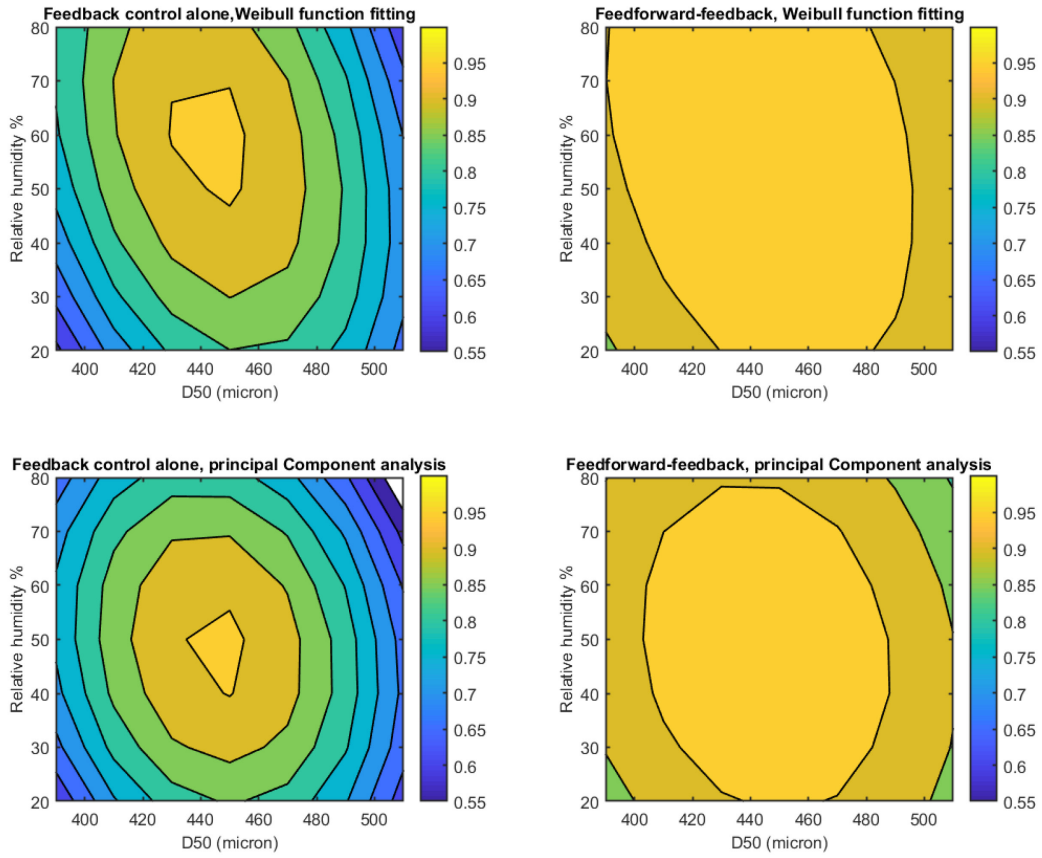

Figure 5-7: Results of Simulation 2. the tolerance space of coating process using (A) the feedback control alone coupled with Weibull function fitting for dissolution, (B) the combined feedforward-feedback control coupled with Weibull function fitting, (C) the feedback control alone coupled with the PCA model fitting, (D) the combined feedforward-feedback control coupled with the PCA

model fitting. The yellow regions indicate the process had the probability of meeting specifications greater than 95%.

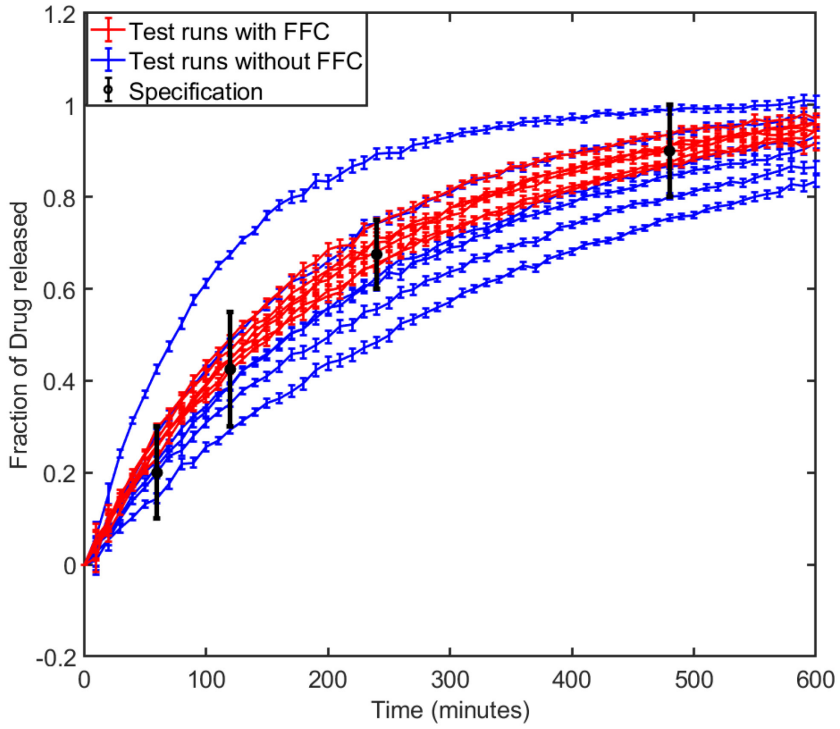

Figure 5-8: Dissolution profiles of the 12 test runs with or without the feedforward controller.

5.4 Conclusion

The feedforward control loops for the fluid bed granular coating were developed and integrated with the feedback control loops. The combined feedforward-feedback control system was deployed using the SynTQ rea-time data management system to control the fluid bed coating process by adjusting the fluidization air volume and coating weight gain to mitigate the undesired impact of variable granule size and inlet air relative humidity on the *in vitro* dissolution.

The performance of the combined feedforward-feedback control system was evaluated using two Monte Carlo simulations. Simulation 1 was designed to test whether the combined control system improved the product quality and consistency when the variabilities of GSDs and relative humidity were tightly controlled. Simulation 2 was used to test whether the combined control system adjusted the coating process to mitigate the impacts of different levels of GSDs and relative humidities.

The simulation results showed the coating process with the feedforward component had higher process capability and larger tolerance space than the process without the feedforward component. The twelve test batches showed the coating process controlled by the combined feedforward-feedback control system had a higher probability of succeeding near the edge of the failure of the tolerance space than the process controlled by feedback control alone. This study showed the employment of the combined feedforward-feedback control system on the coating process fulfilled the requirements in ICH Q8"…the control of the process such that the variability (*e.g.*, of raw materials) can be compensated for in an adaptable manner to deliver consistent product quality." [11]

Chapter 6 : Summary and Future Directions

The US Food and Drug Administration requires pharmaceutical companies to develop extensive process understanding and comprehensive control strategy for product manufacturing. The current pharmaceutical quality by design (QbD) is a systematic approach to enhance process understanding and identify an acceptable range of material and process variables for each unit operation to assure the product quality specification is consistently met. In contrast to the traditional quality by test, which only characterizes the final product, the QbD approach tries to identify the sources of variabilities and understand their impacts on product characteristics to implement a flexible and robust process to deliver consistent quality products, referred to as a design space. The common practice to establish the design space is to use a number of experiments to determine the association between process parameters and critical quality attributes (CQAs). Moving within the design space is not considered a change by the regulatory bodies and requires no supplementary submission for regulatory approvals. The process parameters can be modified in a feedback manner to control the product quality during the routine manufacturing process. Typically, limited studies are conducted during the development of design space to investigate the effects of environmental disturbance and material variations on process robustness. However, a major disturbance affecting drug product quality is the lot-to-lot variability of the incoming raw materials. Additionally, environmental changes can influence manufacturing processes and clinical performance of products. The ICH Q8 guideline[11] defined the highest control level as a system where the process parameters were adjusted to compensate for undesired disturbance and stabilize drug product quality. The critical challenges of enabling this level of control include effectively understanding the process and converting the process knowledge to an implementable system.

This dissertation presented a combined feedforward-feedback control system as a solution to enable the highest control level. An extended-release theophylline oral dosage form was employed as the model drug product, manufactured using a top-spray fluid bed processor. The QbD approach was adopted to gain process understanding and facilitate the development of the control system. In chapter 2, the quality target product profile of the extended-release multiparticulate dosage form was defined. The critical quality attributes, critical formulation variables, and critical process parameters of the fluid bed coating process were identified and confirmed using risk assessments and screening studies. In addition, the theophylline solid-state form change in the drug product was identified as a high-risk failure mode since it significantly altered the *in vitro* dissolution. Chapter 3 demonstrated a response surface design and related statistical data analysis. Process models using critical material attributes and process parameters to predict the *in vitro* dissolution profiles were established using two regression methods, including PLS and GPR. The two methods showed similar performances in predicting new samples from a test set. The process models serve as the basis of feedforward control loops.

Chapter 4 showed the development of feedback control loops using NIR and Raman spectroscopies as PAT tools to monitor the fluid bed coating process in real time. In Chapter 5, The feedforward control loops for the fluid bed granular coating were developed and integrated with the feedback control loops. The combined feedforward-feedback control system was deployed using the SynTQ rea-time data management system to control the fluid bed coating process. The performance of the combined control system was evaluated using Monte Carlo simulations and twelve test batches. The result showed the combined feedforward-feedback control system reduced the batch failures and improved product quality and consistency. The control system also increased the process robustness against the input material attributes and

environmental disturbance, which offered tremendous flexibility to pharmaceutical companies in selecting raw material from different sources.

Though this dissertation demonstrated the establishment and application of a combined feedforward-feedback control system as part of process development, there are still gaps to be filled. The future research directions are briefly summarized in three aspects:

1) The feedforward component relies on incoming material characterizations, which cost a substantial amount of time and prevent the material from entering the manufacturing process. The holding time can be minimized if rapid analytical methods are applied. Process analytical technologies, such as near-infrared spectroscopy, Raman spectroscopy, real-time particle size analyzer, and on-line X-ray diffraction analyzer, are promising candidates for in-line, on-line, or at-line material characterization. The development of such real-time characterization methods will enable automated feedforward-feedback controls in continuous manufacturing.
2) When pharmaceutical companies attempt to identify and study the sources of variability in their original DoE during the process development phase, it is almost impossible to include all of them. Over time unpredicted and uncontrollable changes, such as lot-to-lot variability of input material or equipment aging, can significantly and adversely impact the process and product quality. In such a situation, criteria (*e.g.*, Westgard rules) are required to set the performance limit so that undesired shifts and trends can be detected from the data of routine manufacturing runs. Risk management and experimental studies are needed to analyze the root cause of the undesired impact. Once the source of variability is identified, a cost-effective methodology is highly desired to expand the knowledge space of the

manufacturing process and mathematically adapt the combined control system to the new variability.

3) This dissertation focuses on the development of the control system and the evaluation of control performance. However, a vital point of deciding whether a feedforward component is necessary or not is the economic benefit. The system performance improvement in the output to the additional cost is the primary consideration of the pharmaceutical industry. There is a lack of study on the practicality of feedforward control in the current body of literature. More industrial applications and cost-effectiveness analysis are needed to understand the value of the combined feedforward-feedback control.

Reference

1. Yu, L. X.; Amidon, G.; Khan, M. A.; Hoag, S. W.; Polli, J.; Raju, G. K.; Woodcock, J., Understanding pharmaceutical quality by design. *The AAPS journal* **2014,** *16* (4), 771-83.

2. Igne, B.; Shi, Z.; Talwar, S.; Drennen, J. K.; Anderson, C. A., Adaptive design space as an integrated component of quality by design. *Journal of Pharmaceutical Innovation* **2012,** *7* (3-4), 119-126.

3. Higaki, M.; Kameyama, M.; Udagawa, M.; Ueno, Y.; Yamaguchi, Y.; Igarashi, R.; Ishihara, T.; Mizushima, Y., Transdermal delivery of CaCO3-nanoparticles containing insulin. *Diabetes technology & therapeutics* **2006,** *8* (3), 369-74.

4. Yu, L. X., Pharmaceutical quality by design: product and process development, understanding, and control. *Pharmaceutical research* **2008,** *25* (4), 781-91.

5. MacGregor, J. F.; Bruwer, M.-J., A framework for the development of design and control spaces. *Journal of Pharmaceutical Innovation* **2008,** *3* (1), 15-22.

6. Zacour, B. M. The application of first principle modeling in combination with empirical design of experiments and real-time data management for the automated control of pharmaceutical unit operations. Duquesne University, 2012.

7. Chamarthy, S. P.; Pinal, R.; Carvajal, M. T., Elucidating raw material variability—importance of surface properties and functionality in pharmaceutical powders. *AAPS PharmSciTech* **2009,** *10* (3), 780.

8. Hlinak, A. J.; Kuriyan, K.; Morris, K. R.; Reklaitis, G. V.; Basu, P. K., Understanding critical material properties for solid dosage form design. *Journal of Pharmaceutical Innovation* **2006,** *1* (1), 12-17.

9. Myerson, A. S.; Krumme, M.; Nasr, M.; Thomas, H.; Braatz, R. D., Control systems engineering in continuous pharmaceutical manufacturing. . *Journal of pharmaceutical sciences* **2015,** *104* (3), 832-9.

10. Singh, R.; Roman-Ospino, A. D.; Romanach, R. J.; Ierapetritou, M.; Ramachandran, R., Real time monitoring of powder blend bulk density for coupled feed-forward/feed-back control of a continuous direct compaction tablet manufacturing process. *International journal of pharmaceutics* **2015,** *495* (1), 612-25.

11. Harmonisation, T. I. C. o., Q8 (R2) Pharmaceutical Development. Harmonisation, T. I. C. o., Ed. In Anonymous Internation Conference on Harmonisation of Technical Requirements for Registration of Pharmaceuticals for Human Use, 2009.

12. Koji Muteki, K. Y., George L. Reid, Mahesh Krishnan, De-risking Scale-up of a High Shear Wet Granulation Process Using Latent Variable Modeling and Near-Infrared Spectroscopy. *J Pharm Innov* **2011,** *6*, 142-156.

13. Muteki, K.; Swaminathan, V.; Sekulic, S. S.; Reid, G. L., De-risking pharmaceutical tablet manufacture through process understanding, latent variable modeling, and optimization technologies. *AAPS PharmSciTech* **2011,** *12* (4), 1324-34.

14. Johan A. Westerhuis, P. M. J. C., Coenraad F. Lerk, Multivariate modelling of the tablet manufacturing process with wet granulation for tablet optimization and in-process control. *International journal of pharmaceutics* **1997,** *156*, 109-117.

15. Westerhuis, J. A.; Coenegracht, P. M. J.; Lerk, C. F., Multivariate modelling of the tablet manufacturing process with wet granulation for tablet optimization and in-process control. *International journal of pharmaceutics* **1997,** *156*, 109-117.

16. Hattori, Y.; Otsuka, M., Modeling of feed-forward control using the partial least squares regression method in the tablet compression process. *International journal of pharmaceutics* **2017,** *524* (1-2), 407-413.

17. Singh, R.; Ierapetritou, M.; Ramachandran, R., System-wide hybrid MPC–PID control of a continuous pharmaceutical tablet manufacturing process via direct compaction. *European Journal of Pharmaceutics and Biopharmaceutics* **2013,** *85* (3), 1164-1182.

18. Lawrence, X. Y.; Lionberger, R. A.; Raw, A. S.; D'Costa, R.; Wu, H.; Hussain, A. S., Applications of process analytical technology to crystallization processes. *Advanced drug delivery reviews* **2004,** *56* (3), 349-369.

19. Wu, H.; Tawakkul, M.; White, M.; Khan, M. A., Quality-by-Design (QbD): An integrated multivariate approach for the component quantification in powder blends. *International journal of pharmaceutics* **2009,** *372* (1-2), 39-48.

20. Wu, H.; White, M.; Khan, M. A., Quality-by-Design (QbD): An integrated process analytical technology (PAT) approach for a dynamic pharmaceutical co-precipitation process characterization and process design space development. *International journal of pharmaceutics* **2011,** *405* (1-2), 63-78.

21. Balmayor, E. R.; Azevedo, H. S.; Reis, R. L., Controlled delivery systems: from pharmaceuticals to cells and genes. *Pharmaceutical research* **2011,** *28* (6), 1241-58.

22. de Haan, P.; Lerk, C. F., Oral controlled release dosage forms. A review. *Pharmacy World & Science* **1984,** *6* (2), 57-67.

23. Roy, P.; Shahiwala, A., Multiparticulate formulation approach to pulsatile drug delivery: Current perspectives. *Journal of Controlled Release* **2009,** *134* (2), 74-80.

24. Dey, N.; Majumdar, S.; Rao, M., Multiparticulate drug delivery systems for controlled release. *Tropical Journal of Pharmaceutical Research* **2008,** *7* (3), 1067-1075.

25. Qiu, Y.; Chen, Y.; Zhang, G. G.; Yu, L.; Mantri, R. V., *Developing solid oral dosage forms: pharmaceutical theory and practice*. Academic press: 2016.

26. McGinley, E. J.; Tuason Jr, D. C., Enteric coating for pharmaceutical dosage forms. Google Patents: 1985.

27. Siepmann, F.; Siepmann, J.; Walther, M.; MacRae, R. J.; Bodmeier, R., Polymer blends for controlled release coatings. *Journal of controlled release : official journal of the Controlled Release Society* **2008,** *125* (1), 1-15.

28. Felton, L. A., Mechanisms of polymeric film formation. *International journal of pharmaceutics* **2013,** *457* (2), 423-427.

29. P.H. Sharma, S. N. K., R.A. Kamble, Review on Polymers Used for Film Coating. *Asian Journal of Pharmaceutical Technology & Innovation* **2013,** *1* (2), 1-16.

30. Yamak, H. B.; Yıldırım, H., Improvement of film properties of vinyl acetate based emulsion polymers by using different types of maleic acid diesters. *Progress in Organic Coatings* **2013,** *76* (12), 1874-1878.

31. Steward, P.; Hearn, J.; Wilkinson, M., An overview of polymer latex film formation and properties. *Advances in colloid and interface science* **2000,** *86* (3), 195-267.

32. Kothari, B. H.; Fahmy, R.; Claycamp, H. G.; Moore, C. M.; Chatterjee, S.; Hoag, S. W., A systematic approach of employing quality by design principles: risk assessment and design of experiments to demonstrate process understanding and identify the critical process parameters for coating of the ethylcellulose pseudolatex dispersion using non-conventional fluid bed process. *AAPS PharmSciTech* **2017,** *18* (4), 1135-1157.

33. Pillai, O.; Panchagnula, R., Polymers in drug delivery. *Current Opinion in Chemical Biology* **2001,** *5* (4), 447-451.

34. Lecomte, F.; Siepmann, J.; Walther, M.; MacRae, R. J.; Bodmeier, R., Polymer blends used for the aqueous coating of solid dosage forms: importance of the type of plasticizer. *Journal of controlled release : official journal of the Controlled Release Society* **2004,** *99* (1), 1-13.

35. Edgren, D. E.; Theeuwes, F., Aqueous based pharmaceutical coating composition for dosage forms. Google Patents: 1990.

36. Gordon, J.; Rouse, G.; Gibbs, J.; Risen Jr, W. M., The composition dependence of glass transition properties. *The Journal of Chemical Physics* **1977,** *66* (11), 4971-4976.

37. Nollenberger, K.; Albers, J., Poly (meth) acrylate-based coatings. *International journal of pharmaceutics* **2013,** *457* (2), 461-469.

38. Ammar, H. O.; Ghorab, M. M.; Felton, L. A.; Gad, S.; Fouly, A. A., Effect of antiadherents on the physical and drug release properties of acrylic polymeric films. *AAPS PharmSciTech* **2016,** *17* (3), 682-692.

39. Kranz, H.; Jürgens, K.; Pinier, M.; Siepmann, J., Drug release from MCC-and carrageenan-based pellets: experiment and theory. *European journal of pharmaceutics and biopharmaceutics* **2009,** *73* (2), 302-309.

40. Mehta, R. Y.; Missaghi, S.; Tiwari, S. B.; Rajabi-Siahboomi, A. R., Application of ethylcellulose coating to hydrophilic matrices: a strategy to modulate drug release profile and reduce drug release variability. *AAPS PharmSciTech* **2014,** *15* (5), 1049-1059.

41. Felton, L. A.; Porter, S. C., An update on pharmaceutical film coating for drug delivery. *Expert opinion on drug delivery* **2013,** *10* (4), 421-435.

42. Keddie, J., Film Formation of latex. *Materials Science and Engineering* **1997,** *21*, 101-170.

43. Schultz, P.; Tho, I.; Kleinebudde, P., A new multiparticulate delayed release system.: Part II: coating formulation and properties of free films. *Journal of controlled release* **1997,** *47* (2), 191-199.

44. Vanderhoff, J.; Bradford, E.; Carrington, W. In *The transport of water through latex films*, Journal of Polymer Science: Polymer Symposia, Wiley Online Library: 1973; pp 155-174.

45. Frenkel, J., Viscous flow of crystalline bodies under the action of surface tension. *J. phys.* **1945,** *9*, 385.

46. Dillon, R.; Matheson, L.; Bradford, E., Sintering of synthetic latex particles. *Journal of Colloid Science* **1951,** *6* (2), 108-117.

47. Brown, G. L., Formation of films from polymer dispersions. *Journal of Polymer science* **1956,** *22* (102), 423-434.

48. Voyutskǐ, S., Amendment to the papers by bradford, brown, and co-workers:"Concerning mechanism of film formation from high polymer dispersions". *Journal of Polymer Science* **1958,** *32* (125), 528-530.

49. Bradford, E.; Vanderhoff, J., Additional studies of morphological changes in latex films. *Journal of Macromolecular Science, Part B: Physics* **1972,** *6* (4), 671-693.

50. Bradford, E.; Vanderhoff, J., Morphological changes in latex films. *Rubber Chemistry and Technology* **1968,** *41* (2), 514-526.

51. Cocco, R.; Karri, S. R.; Knowlton, T., Introduction to fluidization. *Chem. Eng. Prog* **2014,** *110* (11), 21-29.

52. Teunou, E.; Poncelet, D., Batch and continuous fluid bed coating–review and state of the art. *Journal of food engineering* **2002,** *53* (4), 325-340.

53. Geldart, D., Single particles, fixed and quiescent beds. *Gas fluidization technology* **1986,** *2*, 11-32.

54. Prata, A. S.; Maudhuit, A.; Boillereaux, L.; Poncelet, D., Development of a control system to anticipate agglomeration in fluidised bed coating. *Powder technology* **2012,** *224*, 168-174.

55. Fries, L.; Antonyuk, S.; Heinrich, S.; Palzer, S., DEM–CFD modeling of a fluidized bed spray granulator. *Chemical Engineering Science* **2011,** *66* (11), 2340-2355.

56. Wen, H.; Park, K., *Oral controlled release formulation design and drug delivery: theory to practice*. John Wiley & Sons: 2011.

57. Jones, D., Development, optimization, and scale-up of process parameters: Wurster coating. In *Developing Solid Oral Dosage Forms*, Elsevier: 2009; pp 807-825.

58. Turton, R.; Cheng, X. X., The scale-up of spray coating processes for granular solids and tablets. *Powder Technology* **2005,** *150* (2), 78-85.

59. Heinrich, S.; Dosta, M.; Antonyuk, S., Multiscale analysis of a coating process in a Wurster fluidized bed apparatus. In *Advances in Chemical Engineering*, Elsevier: 2015; Vol. 46, pp 83-135.

60. Hede, P. D.; Bach, P.; Jensen, A. D., Small-scale top-spray fluidised bed coating: Granule impact strength, agglomeration tendency and coating layer morphology. *Powder technology* **2007,** *176* (2-3), 156-167.

61. Ronsse, F.; Pieters, J.; Dewettinck, K., Modelling side-effect spray drying in top-spray fluidised bed coating processes. *Journal of Food Engineering* **2008,** *86* (4), 529-541.

62. Dewettinck, K.; Huyghebaert, A., Fluidized bed coating in food technology. *Trends in Food Science & Technology* **1999,** *10* (4-5), 163-168.

63. Srivastava, S.; Mishra, G., Fluid bed technology: overview and parameters for process selection. *International Journal of Pharmaceutical Sciences and Drug Research* **2010,** *2* (4), 236-246.

64. Hede, P. D.; Bach, P.; Jensen, A. D., Batch top-spray fluid bed coating: Scale-up insight using dynamic heat-and mass-transfer modelling. *Chemical Engineering Science* **2009,** *64* (6), 1293-1317.

65. Korakianiti, E.; Rekkas, D.; Dallas, P.; Choulis, N., Sequential optimization of a pelletization process in a fluid bed rotor granulator. *Journal of Drug Delivery Science and Technology* **2004,** *14* (3), 207-214.

66. Hutchings, D.; Kuzmak, B.; Sakr, A., Processing Considerations for an EC Latex Coating System: Influence of Curing Time and Temperature. *Pharmaceutical research* **1994,** *11* (10), 1474-1478.

67. Implementation, I. E. G. f. I. Q. Q. Q., ICH Quality Implementation Working Group Points to Consider (R2). *International Conference on Harmonisation Technical Document* **2011**.

68. Kelley, B. In *Quality by design risk assessments supporting approved antibody products*, MAbs, Taylor & Francis: 2016; p 1435.

69. Rathore, A. S., Roadmap for implementation of quality by design (QbD) for biotechnology products. *Trends in biotechnology* **2009,** *27* (9), 546-53.

70. Roy, S., Quality by design: A holistic concept of building quality in pharmaceuticals. *Int J Pharm Biomed Res* **2012,** *3* (2), 100-108.

71. Elder, D.; Teasdale, A., ICH Q9 quality risk management. *ICH quality guidelines: an implementation guide. Wiley, Hoboken* **2017**, 579-610.

72. Naelapaa, K.; Veski, P.; Kristensen, H. G.; Rantanen, J.; Bertelsen, P., Building quality into a coating process. *Pharmaceutical development and technology* **2010,** *15* (1), 35-45.

73. Fahmy, R.; Kona, R.; Dandu, R.; Xie, W.; Claycamp, G.; Hoag, S. W., Quality by design I: Application of failure mode effect analysis (FMEA) and Plackett-Burman design of experiments in the identification of "main factors" in the formulation and process design space for roller-compacted ciprofloxacin hydrochloride immediate-release tablets. *AAPS PharmSciTech* **2012,** *13* (4), 1243-54.

74. Ericson, C. A., *Hazard analysis techniques for system safety*. John Wiley & Sons: 2015.

75. Dhillon, B. S., *Engineering Maintainability:: How to Design for Reliability and Easy Maintenance*. Gulf Professional Publishing: 1999.

76. Huang, J.; Kaul, G.; Cai, C.; Chatlapalli, R.; Hernandez-Abad, P.; Ghosh, K.; Nagi, A., Quality by design case study: an integrated multivariate approach to drug product and process development. *International journal of pharmaceutics* **2009,** *382* (1-2), 23-32.

77. Stowe, R. A.; Mayer, R. P., Efficient screening of process variables. *Industrial & Engineering Chemistry* **1966,** *58* (2), 36-40.

78. Glodek, M.; Liebowitz, S.; McCarthy, R.; McNally, G.; Oksanen, C.; Schultz, T.; Sundararajan, M.; Vorkapich, R.; Vukovinsky, K.; Watts, C., Process robustness—A PQRI white paper. *Pharm. Eng* **2006,** *26* (6), 1-11.

79. Food, U.; Administration, D., Guidance for industry: Q8 (2) pharmaceutical development. 2009. *Google Scholar There is no corresponding record for this reference* **2018**.

80. Gendre, C.; Boiret, M.; Genty, M.; Chaminade, P.; Pean, J. M., Real-time predictions of drug release and end point detection of a coating operation by in-line near infrared measurements. *International journal of pharmaceutics* **2011,** *421* (2), 237-43.

81. Gupta, A.; Peck, G. E.; Miller, R. W.; Morris, K. R., Real-time near-infrared monitoring of content uniformity, moisture content, compact density, tensile strength, and Young's modulus of roller compacted powder blends. *Journal of pharmaceutical sciences* **2005,** *94* (7), 1589-97.

82. Moltgen, C. V.; Puchert, T.; Menezes, J. C.; Lochmann, D.; Reich, G., A novel in-line NIR spectroscopy application for the monitoring of tablet film coating in an industrial scale process. *Talanta* **2012,** *92*, 26-37.

83. Hansuld, E. M.; Briens, L.; Sayani, A.; McCann, J. A. B., An investigation of the relationship between acoustic emissions and particle size. *Powder Technology* **2012,** *219*, 111-117.

84. Lee, M. J.; Seo, D. Y.; Lee, H. E.; Wang, I. C.; Kim, W. S.; Jeong, M. Y.; Choi, G. J., In line NIR quantification of film thickness on pharmaceutical pellets during a fluid bed coating process. *International journal of pharmaceutics* **2011,** *403* (1-2), 66-72.

85. De Beer, T.; Burggraeve, A.; Fonteyne, M.; Saerens, L.; Remon, J. P.; Vervaet, C., Near infrared and Raman spectroscopy for the in-process monitoring of pharmaceutical production processes. *International journal of pharmaceutics* **2011,** *417* (1-2), 32-47.

86. El-Hagrasy, A. S.; Drennen, J. K., 3rd, A Process Analytical Technology approach to near-infrared process control of pharmaceutical powder blending. Part III: Quantitative near-infrared calibration for prediction of blend homogeneity and characterization of powder mixing kinetics. *Journal of pharmaceutical sciences* **2006,** *95* (2), 422-34.

87. D'Souza, S., A review of in vitro drug release test methods for nano-sized dosage forms. *Advances in Pharmaceutics* **2014,** *2014*.

88. Ibrahim, A.; Kothari, B. H.; Fahmy, R.; Hoag, S. W., Prediction of dissolution of sustained release coated ciprofloxacin beads using near-infrared spectroscopy and process parameters: a data fusion approach. *AAPS PharmSciTech* **2019,** *20* (6), 222.

89. Zaborenko, N.; Shi, Z.; Corredor, C. C.; Smith-Goettler, B. M.; Zhang, L.; Hermans, A.; Neu, C. M.; Alam, M. A.; Cohen, M. J.; Lu, X., First-principles and empirical approaches to predicting in vitro dissolution for pharmaceutical formulation and process development and for product release testing. *The AAPS journal* **2019,** *21* (3), 32.

90. Wu, H.; Lyon, R. C.; Khan, M. A.; Voytilla, R. J.; Drennen III, J. K., Integration of near-infrared spectroscopy and mechanistic modeling for predicting film-coating and dissolution of modified release tablets. *Industrial & Engineering Chemistry Research* **2015,** *54* (22), 6012-6023.

91. Noyes, A. A.; Whitney, W. R., The rate of solution of solid substances in their own solutions. *Journal of the American Chemical Society* **1897,** *19* (12), 930-934.

92. Dokoumetzidis, A.; Macheras, P., A century of dissolution research: from Noyes and Whitney to the biopharmaceutics classification system. *International journal of pharmaceutics* **2006,** *321* (1-2), 1-11.

93. Zhao, Y.; Li, W.; Shi, Z.; Drennen III, J. K.; Anderson, C. A., Prediction of Dissolution Profiles From Process Parameters, Formulation, and Spectroscopic Measurements. *Journal of pharmaceutical sciences* **2019,** *108* (6), 2119-2127.

94. Andersson, M.; Josefson, M.; Langkilde, F.; Wahlund, K.-G., Monitoring of a film coating process for tablets using near infrared reflectance spectrometry. *Journal of pharmaceutical and biomedical analysis* **1999,** *20* (1-2), 27-37.

95. Cogdill, R. P.; Forcht, R. N.; Shen, Y.; Taday, P. F.; Creekmore, J. R.; Anderson, C. A.; Drennen, J. K., Comparison of terahertz pulse imaging and near-infrared spectroscopy for rapid, non-destructive analysis of tablet coating thickness and uniformity. *Journal of Pharmaceutical Innovation* **2007,** *2* (1-2), 29-36.

96. Lee, M.-J.; Seo, D.-Y.; Lee, H.-E.; Wang, I.-C.; Kim, W.-S.; Jeong, M.-Y.; Choi, G. J., In line NIR quantification of film thickness on pharmaceutical pellets during a fluid bed coating process. *International journal of pharmaceutics* **2011,** *403* (1-2), 66-72.

97. Moes, J. J.; Ruijken, M. M.; Gout, E.; Frijlink, H. W.; Ugwoke, M. I., Application of process analytical technology in tablet process development using NIR spectroscopy: Blend uniformity, content uniformity and coating thickness measurements. *International journal of pharmaceutics* **2008,** *357* (1-2), 108-118.

98. Weyer, L. G., Near-infrared spectroscopy of organic substances. *Applied Spectroscopy Reviews* **1985,** *21* (1-2), 1-43.

99. Andersson, M.; Folestad, S.; Gottfries, J.; Johansson, M. O.; Josefson, M.; Wahlund, K.-G., Quantitative analysis of film coating in a fluidized bed process by in-line NIR spectrometry and multivariate batch calibration. *Analytical Chemistry* **2000,** *72* (9), 2099-2108.

100. Kirsch, J. D.; Drennen, J. K., Determination of film-coated tablet parameters by near-infrared spectroscopy. *Journal of Pharmaceutical and Biomedical Analysis* **1995,** *13* (10), 1273-1281.

101. Bogomolov, A.; Engler, M.; Melichar, M.; Wigmore, A., In-line analysis of a fluid bed pellet coating process using a combination of near infrared and Raman spectroscopy. *Journal of chemometrics* **2010,** *24* (7-8), 544-557.

102. Fevotte, G., In situ Raman spectroscopy for in-line control of pharmaceutical crystallization and solids elaboration processes: A review. *Chemical Engineering Research and Design* **2007,** *85* (7), 906-920.

103. Skoog, D. A.; Holler, F. J.; Crouch, S. R., *Principles of instrumental analysis*. Cengage learning: 2017.

104. Taylor, L. S.; Langkilde, F. W., Evaluation of solid-state forms present in tablets by Raman spectroscopy. *Journal of pharmaceutical sciences* **2000,** *89* (10), 1342-1353.

105. Wikström, H.; Marsac, P. J.; Taylor, L. S., In-line monitoring of hydrate formation during wet granulation using Raman spectroscopy. *Journal of pharmaceutical sciences* **2005,** *94* (1), 209-219.

106. Johansson, J.; Pettersson, S.; Taylor, L. S., Infrared imaging of laser-induced heating during Raman spectroscopy of pharmaceutical solids. *Journal of pharmaceutical and biomedical analysis* **2002,** *30* (4), 1223-1231.

107. Johansson, B. Feedforward control in dynamic situations. Linköping University Sweden, 2003.

108. Q8 (R2) Pharmaceutical Dvelopment. In Anonymous Internation Conference on Harmonisation of Technical Requirements for Registration of Pharmaceuticals for Human Use, 2009.

109. De Leersnyder, F.; Peeters, E.; Djalabi, H.; Vanhoorne, V.; Van Snick, B.; Hong, K.; Hammond, S.; Liu, A. Y.; Ziemons, E.; Vervaet, C., Development and validation of an in-line NIR spectroscopic method for continuous blend potency determination in the feed frame of a tablet press. *Journal of pharmaceutical and biomedical analysis* **2018,** *151*, 274-283.

110. Close, E.; Bracewell, D. G.; Sorensen, E., A model based approach to an adaptive design space in chromatography. In *Computer Aided Chemical Engineering*, Elsevier: 2013; Vol. 32, pp 115-120.

111. Watano, S.; Numa, T.; Miyanami, K.; Osako, Y., A fuzzy control system of high shear granulation using image processing. *Powder technology* **2001,** *115* (2), 124-130.

112. Skibsted, E.; Westerhuis, J.; Smilde, A.; Witte, D., Examples of NIR based real time release in tablet manufacturing. *Journal of pharmaceutical and biomedical analysis* **2007,** *43* (4), 1297-1305.

113. Yu, W.; Muteki, K.; Zhang, L.; Kim, G., Prediction of bulk powder flow performance using comprehensive particle size and particle shape distributions. *Journal of pharmaceutical sciences* **2011,** *100* (1), 284-93.

114. Palamanit, A.; Prachayawarakorn, S.; Tungtrakul, P.; Soponronnarit, S., Performance evaluation of top-spray fluidized bed coating for healthy coated rice production. *Food and bioprocess technology* **2016,** *9* (8), 1317-1326.

115. Link, K. C.; Schlünder, E.-U., Fluidized bed spray granulation: investigation of the coating process on a single sphere. *Chemical Engineering and Processing: Process Intensification* **1997,** *36* (6), 443-457.

116. Palamanit, A.; Soponronnarit, S.; Prachayawarakorn, S.; Tungtrakul, P., Effects of inlet air temperature and spray rate of coating solution on quality attributes of turmeric extract coated rice using top-spray fluidized bed coating technique. *Journal of food engineering* **2013,** *114* (1), 132-138.

117. Dewettinck, K.; Huyghebaert, A., Top-spray fluidized bed coating: Effect of process variables on coating efficiency. *LWT-Food Science and Technology* **1998,** *31* (6), 568-575.

118. Ronsse, F. Modelling heat and mass transfer in fluidised bed coating processes. Ghent University, 2006.

119. Seton, L.; Khamar, D.; Bradshaw, I. J.; Hutcheon, G. A., Solid state forms of theophylline: presenting a new anhydrous polymorph. *Crystal growth & design* **2010,** *10* (9), 3879-3886.

120. Amado, A. M.; Nolasco, M. M.; Ribeiro-Claro, P. J., Probing pseudopolymorphic transitions in pharmaceutical solids using Raman spectroscopy: Hydration and dehydration of theophylline. *Journal of pharmaceutical sciences* **2007,** *96* (5), 1366-1379.

121. Phadnis, N. V.; Suryanarayanan, R., Polymorphism in anhydrous theophylline—implications on the dissolution rate of theophylline tablets. *Journal of pharmaceutical sciences* **1997,** *86* (11), 1256-1263.

122. Airaksinen, S.; Karjalainen, M.; Räsänen, E.; Rantanen, J.; Yliruusi, J., Comparison of the effects of two drying methods on polymorphism of theophylline. *International Journal of Pharmaceutics* **2004,** *276* (1-2), 129-141.

123. Nunes, C.; Mahendrasingam, A.; Suryanarayanan, R., Investigation of the multi-step dehydration reaction of theophylline monohydrate using 2-dimensional powder X-ray diffractometry. *Pharmaceutical research* **2006,** *23* (10), 2393-2404.

124. Pharmacipeia, U. S., Theophylline Extended-Release Capsules. *Pharmacopeial Forum* **2006,** *21* (1), 185.

125. Asman, G.; Akçay, E., Effect of membrane preparation methods on the release of theophylline through CA membranes at in-vitro conditions. *Journal of Macromolecular Science, Part A* **2014,** *51* (4), 326-338.

126. Dashevsky, A.; Ahmed, A. R.; Mota, J.; Irfan, M.; Kolter, K.; Bodmeier, R. A., Effect of water-soluble polymers on the physical stability of aqueous polymeric dispersions and their implications on the drug release from coated pellets. *Drug Dev Ind Pharm* **2010,** *36* (2), 152-60.

127. Dashevsky, A.; Kolter, K.; Bodmeier, R., Compression of pellets coated with various aqueous polymer dispersions. *International journal of pharmaceutics* **2004,** *279* (1-2), 19-26.

128. Dashevsky, A.; Wagner, K.; Kolter, K.; Bodmeier, R., Physicochemical and release properties of pellets coated with Kollicoat SR 30 D, a new aqueous polyvinyl acetate dispersion for extended release. *International journal of pharmaceutics* **2005,** *290* (1-2), 15-23.

129. USFDA, Quality by design for ANDAs: an example for immediate-release dosage forms. *US Department of Health and Human Service (FDA, Rockville, MD, 2012)* **2012**.

130. Kolter, K.; Dashevsky, A.; Irfan, M.; Bodmeier, R., Polyvinyl acetate-based film coatings. *International journal of pharmaceutics* **2013,** *457* (2), 470-9.

131. Mota, J. Matrix- and reservoir- type oral multiparticulate drug delivery systems. Freien Universität Berlin, Berlin, 2010.

132. Okarter, T.; Singla, K., The effects of plasticizers on the release of metoprolol tartrate from granules coated with a polymethacrylate film. *Drug development and industrial pharmacy* **2000,** *26* (3), 323-329.

133. Pillay, V.; Fassihi, R., Evaluation and comparison of dissolution data derived from different modified release dosage forms: an alternative method. *Journal of Controlled Release* **1998,** *55* (1), 45-55.

134. Simionato, L. D.; Petrone, L.; Baldut, M.; Bonafede, S. L.; Segall, A. I., Comparison between the dissolution profiles of nine meloxicam tablet brands commercially available in Buenos Aires, Argentina. *Saudi pharmaceutical journal* **2018,** *26* (4), 578-584.

135. Yuksel, N.; Kanık, A. E.; Baykara, T., Comparison of in vitro dissolution profiles by ANOVA-based, model-dependent and-independent methods. *International journal of pharmaceutics* **2000,** *209* (1-2), 57-67.

136. Shao, Z. J.; Morales, L.; Diaz, S.; Muhammad, N. A., Drug release from Kollicoat SR 30D-coated nonpareil beads: evaluation of coating level, plasticizer type, and curing condition. *AAPS PharmSciTech* **2002,** *3* (2), 87-96.

137. Chen, Y.; Ding, Y.; Papadopoulos, D.; Ghadiri, M., Energy-based analysis of milling α-lactose monohydrate. *Journal of pharmaceutical sciences* **2004,** *93* (4), 886-895.

138. Brydson, J. A., 14 - Poly(vinyl acetate) and its Derivatives. In *Plastics Materials (Seventh Edition)*, 1999; pp 386-397.

139. Aaltonen, J.; Heinänen, P.; Peltonen, L.; Kortejärvi, H.; Tanninen, V. P.; Christiansen, L.; Hirvonen, J.; Yliruusi, J.; Rantanen, J., In situ measurement of solvent-mediated phase transformations during dissolution testing. *Journal of pharmaceutical sciences* **2006,** *95* (12), 2730-2737.

140. Rodríguez-Hornedo, N.; Lechuga-Ballesteros, D.; Wu, H.-J., Phase transition and heterogeneous/epitaxial nucleation of hydrated and anhydrous theophylline crystals. *International journal of pharmaceutics* **1992,** *85* (1-3), 149-162.

141. Ahuja, S.; Scypinski, S., *Handbook of modern pharmaceutical analysis*. Academic press: 2001; Vol. 3.

142. Wikström, H.; Carroll, W. J.; Taylor, L. S., Manipulating theophylline monohydrate formation during high-shear wet granulation through improved understanding of the role of pharmaceutical excipients. *Pharmaceutical research* **2008,** *25* (4), 923-935.

143. Devanga-Chinta, D.; Graves, R. A.; Pamujula, S.; Mandal, T. K., Controlled release multiple layer coatings. *Drug development and industrial pharmacy* **2010,** *36* (2), 200-208.

144. Wesseling, M.; Bodmeier, R., Drug release from beads coated with an aqueous colloidal ethylcellulose dispersion, Aquacoat®, or an organic ethylcellulose solution. *European journal of pharmaceutics and biopharmaceutics* **1999,** *47* (1), 33-38.

145. Siepmann, J.; Lecomte, F.; Bodmeier, R., Diffusion-controlled drug delivery systems: calculation of the required composition to achieve desired release profiles. *Journal of Controlled Release* **1999,** *60* (2-3), 379-389.

146. Kothari, B. H.; Fahmy, R.; Claycamp, H. G.; Moore, C. M.; Chatterjee, S.; Hoag, S. W., Comparing a statistical model and bayesian approach to establish the design space for the coating of ciprofloxacin HCl beads at different scales of production. *AAPS PharmSciTech* **2018,** *19* (8), 3809-3828.

147. Kukec, S.; Vrečer, F., A study of in situ fluid bed melt granulation using response surface methodology/Uporaba metodologije odgovornih površin za študij in situ granulacije s talinami v zvrtinčenih plasteh. *Acta Pharmaceutica* **2012,** *62* (4), 497-513.

148. Vanaja, K.; Shobha Rani, R., Design of experiments: concept and applications of Plackett Burman design. *Clinical research and regulatory affairs* **2007,** *24* (1), 1-23.

149. Mukkula, A. R. G.; Paulen, R., Model-based design of optimal experiments for nonlinear systems in the context of guaranteed parameter estimation. *Computers & Chemical Engineering* **2017,** *99*, 198-213.

150. Goldberger, A. S., Econometric theory. *Econometric theory.* **1964**.

151. Abdi, H., Partial least square regression (PLS regression). *Encyclopedia for research methods for the social sciences* **2003,** *6* (4), 792-795.

152. Djuris, J.; Ibric, S.; Djuric, Z., Chemometric methods application in pharmaceutical products and processes analysis and control. In *Computer-Aided Applications in Pharmaceutical Technology*, Elsevier: 2013; pp 57-90.

153. Si, X.-S.; Hu, C.-H.; Zio, E.; Li, G., Modeling for prognostics and health management: methods and applications. Hindawi: 2015.

154. Chen, T.; Morris, J.; Martin, E., Gaussian process regression for multivariate spectroscopic calibration. *Chemometrics and Intelligent Laboratory Systems* **2007,** *87* (1), 59-71.

155. Cui, C.; Fearn, T., Comparison of partial least squares regression, least squares support vector machines, and Gaussian process regression for a near infrared calibration. *Journal of Near Infrared Spectroscopy* **2017,** *25* (1), 5-14.

156. Ojha, V. K.; Schiano, S.; Wu, C.-Y.; Snášel, V.; Abraham, A., Predictive modeling of die filling of the pharmaceutical granules using the flexible neural tree. *Neural Computing and Applications* **2018,** *29* (7), 467-481.

157. Weibull, W., A statistical distribution function of wide applicability. *Journal of applied mechanics* **1951,** *18* (3), 293-297.

158. Gimenez, D.; Rawls, W.; Pachepsky, Y.; Watt, J., Prediction of a pore distribution factor from soil textural and mechanical parameters. *Soil science* **2001,** *166* (2), 79-88.

159. Haverkamp, R. t.; Parlange, J.-Y., Predicting the water-retention curve from particle-size distribution: 1. Sandy soils without organic matter1. *Soil Science* **1986,** *142* (6), 325-339.

160. Zhuang, J.; Jin, Y.; Miyazaki, T., Estimating water retention characteristic from soil particle-size distribution using a non-similar media concept. *Soil Science* **2001,** *166* (5), 308-321.

161. Wold, S.; Esbensen, K.; Geladi, P., Principal component analysis. *Chemometrics and intelligent laboratory systems* **1987,** *2* (1-3), 37-52.

162. Costa, P.; Lobo, J. M. S., Modeling and comparison of dissolution profiles. *European journal of pharmaceutical sciences* **2001,** *13* (2), 123-133.

163. Gao, Z., Mathematical modeling of variables involved in dissolution testing. *Journal of pharmaceutical sciences* **2011,** *100* (11), 4934-4942.

164. Rogers, A.; Ierapetritou, M., Challenges and opportunities in modeling pharmaceutical manufacturing processes. *Computers & Chemical Engineering* **2015,** *81*, 32-39.

165. García-Muñoz, S., Establishing multivariate specifications for incoming materials using data from multiple scales. *Chemometrics and Intelligent Laboratory Systems* **2009,** *98* (1), 51-57.

166. Sen, K.; Velez, N.; Anderson, C.; Drennen III, J. K.; Zidan, A. S.; Chaudhuri, B., Multicomponent granular mixing in a Bohle bin Blender-Experiments and simulation. *International journal of pharmaceutics* **2020,** *578*, 119131.

167. Lang, Y.-d.; Malacina, A.; Biegler, L. T.; Munteanu, S.; Madsen, J. I.; Zitney, S. E., Reduced order model based on principal component analysis for process simulation and optimization. *Energy & Fuels* **2009,** *23* (3), 1695-1706.

168. Peterson, J. J., A Bayesian approach to the ICH Q8 definition of design space. *Journal of biopharmaceutical statistics* **2008,** *18* (5), 959-975.

169. Kourti, T., Pharmaceutical manufacturing: the role of multivariate analysis in design space, control strategy, process understanding, troubleshooting, and optimization. *Chemical Engineering in the Pharmaceutical Industry: Drug Product Design, Development, and Modeling* **2019**, 601-629.

170. Zacour, B. M.; Drennen III, J. K.; Anderson, C. A., Development of a fluid bed granulation design space using critical quality attribute weighted tolerance intervals. *Journal of pharmaceutical sciences* **2012,** *101* (8), 2917-2929.

171. Culeddu, N.; Chessa, M.; Porcu, M. C.; Fresu, P.; Tonolo, G.; Virgilio, G.; Migaleddu, V., NMR-based metabolomic study of type 1 diabetes. *Metabolomics* **2012,** *8* (6), 1162-1169.

172. Pelikan, M.; Goldberg, D. E.; Cantú-Paz, E. In *BOA: The Bayesian optimization algorithm*, Proceedings of the genetic and evolutionary computation conference GECCO-99, Citeseer: 1999; pp 525-532.

173. Jones, D. R., A taxonomy of global optimization methods based on response surfaces. *Journal of global optimization* **2001,** *21* (4), 345-383.

174. Schonlau, M., Computer experiments and global optimization. **1997**.

175. Bull, A. D., Convergence rates of efficient global optimization algorithms. *Journal of Machine Learning Research* **2011,** *12* (10).

176. De Beer, T.; Burggraeve, A.; Fonteyne, M.; Saerens, L.; Remon, J. P.; Vervaet, C., Near infrared and Raman spectroscopy for the in-process monitoring of pharmaceutical production processes. *International journal of pharmaceutics* **2011,** *417* (1-2), 32-47.

177. Ciurczak, E. W.; Igne, B., *Pharmaceutical and medical applications of near-infrared spectroscopy*. CRC Press: 2014.

178. Morris, K. R.; Stowell, J. G.; Byrn, S. R.; Placette, A. W.; Davis, T. D.; Peck, G. E., Accelerated fluid bed drying using NIR monitoring and phenomenological modeling. *Drug development and industrial pharmacy* **2000,** *26* (9), 985-988.

179. Frake, P.; Greenhalgh, D.; Grierson, S.; Hempenstall, J.; Rudd, D., Process control and end-point determination of a fluid bed granulation by application of near infra-red spectroscopy. *International journal of pharmaceutics* **1997,** *151* (1), 75-80.

180. Cogdill, R. P.; Anderson, C. A.; Delgado, M.; Chisholm, R.; Bolton, R.; Herkert, T.; Afnan, A. M.; Drennen, J. K., Process analytical technology case study: part II. Development and

validation of quantitative near-infrared calibrations in support of a process analytical technology application for real-time release. *Aaps Pharmscitech* **2005,** *6* (2), E273-E283.

181. Reich, G., Near-infrared spectroscopy and imaging: basic principles and pharmaceutical applications. *Advanced drug delivery reviews* **2005,** *57* (8), 1109-1143.

182. Gupta, A.; Peck, G. E.; Miller, R. W.; Morris, K. R., Real-time near-infrared monitoring of content uniformity, moisture content, compact density, tensile strength, and Young's modulus of roller compacted powder blends. *Journal of pharmaceutical sciences* **2005,** *94* (7), 1589-1597.

183. Gendre, C.; Boiret, M.; Genty, M.; Chaminade, P.; Pean, J. M., Real-time predictions of drug release and end point detection of a coating operation by in-line near infrared measurements. *International journal of pharmaceutics* **2011,** *421* (2), 237-243.

184. Romero-Torres, S.; Pérez-Ramos, J. D.; Morris, K. R.; Grant, E. R., Raman spectroscopy for tablet coating thickness quantification and coating characterization in the presence of strong fluorescent interference. *Journal of pharmaceutical and biomedical analysis* **2006,** *41* (3), 811-819.

185. Radtke, J.; Kleinebudde, P., Real-time monitoring of multi-layered film coating processes using Raman spectroscopy. *European Journal of Pharmaceutics and Biopharmaceutics* **2020,** *153*, 43-51.

186. Keddie, J. L., Film formation of latex. *Materials Science and Engineering: R: Reports* **1997,** *21* (3), 101-170.

187. Bose, S.; Bogner, R. H., Solventless pharmaceutical coating processes: a review. *Pharmaceutical development and technology* **2007,** *12* (2), 115-131.

188. Gómez, D. A.; Coello, J.; Maspoch, S., The influence of particle size on the intensity and reproducibility of Raman spectra of compacted samples. *Vibrational spectroscopy* **2019,** *100*, 48-56.

189. Byrnes, C.; Isidori, A., Output regulation for nonlinear systems: an overview. *International Journal of Robust and Nonlinear Control: IFAC-Affiliated Journal* **2000,** *10* (5), 323-337.

190. Corripio, A. B., *Tuning of industrial control systems*. Isa: 2000.

191. Méndez-Acosta, H.; Campos-Delgado, D. U.; Femat, R.; González-Alvarez, V., A robust feedforward/feedback control for an anaerobic digester. *Computers & chemical engineering* **2005,** *29* (7), 1613-1623.

192. Taam, W.; Subbaiah, P.; Liddy, J. W., A note on multivariate capability indices. *Journal of applied statistics* **1993,** *20* (3), 339-351.

193. Shahriari, H.; Abdollahzadeh, M., A new multivariate process capability vector. *Quality Engineering* **2009,** *21* (3), 290-299.

194. Chen, H., A multivariate process capability index over a rectangular solid tolerance zone. *Statistica Sinica* **1994**, 749-758.

195. Raeisi, S., Multivariate process capability indices on the presence of priority for quality characteristics. **2009**.